

DEVELOPING AN ALZHEIMER'S DISEASE THERAPEUTIC: IDENTIFICATION
AND VALIDATION OF SIGNALING PATHWAYS INVOLVED IN SMALL
MOLECULE INDUCTION OF NERVE GROWTH FACTOR

by

Justin B. Davis
A Dissertation
Submitted to the
Graduate Faculty
of
George Mason University
in Partial Fulfillment of
The Requirements for the Degree
of
Doctor of Philosophy
Chemistry and Biochemistry

Committee:

_____	Dr. Robin Couch, Dissertation Director
_____	Dr. Douglas Armstrong, Committee Member
_____	Dr. Barney Bishop, Committee Member
_____	Dr. Virginia Espina, Committee Member
_____	Dr. Geraldine Grant, Committee Member
_____	Dr. John Schreifels, Department Chairperson
_____	Dr. Donna M. Fox, Associate Dean, Office of Student Affairs & Special Programs, College of Science
_____	Dr. Peggy Agouris, Dean, College of Science

Date: _____

Spring Semester 2016
George Mason University
Fairfax, VA

Developing an Alzheimer's Disease Therapeutic: Identification and Validation of Signaling Pathways Involved in Small Molecule Induction of Nerve Growth Factor

A Dissertation submitted in partial fulfillment of the requirements for the degree of Doctor of Philosophy at George Mason University

by

Justin B. Davis
Master of Science
George Mason University, 2011
Bachelor of Science
University of North Carolina at Chapel Hill, 2010

Director: Robin Couch, Professor
Department of Chemistry and Biochemistry

Spring Semester 2016
George Mason University
Fairfax, VA



THIS WORK IS LICENSED UNDER A [CREATIVE COMMONS
ATTRIBUTION-NONCOMMERICAL 3.0 UNPORTED LICENSE](https://creativecommons.org/licenses/by-nc/3.0/).

Dedication

To my parents, for always telling me to get back to work. To my sister, for giving me toughness and cat-like reflexes. To Princess, for making every good day a great day. To Relly, for being the ultimate sidekick. To Hampton, because we all start somewhere.

Acknowledgements

I would like to thank the many friends, relatives, and supporters who have made this happen. All the members of the Couch lab, especially Allyson, Amanda, Hameed, and Karl, who have been the greatest of teammates. None of this would have been possible without Dr. Robert Williams who inspired my scientific curiosity or Dr. Robin Couch who has been the greatest mentor any student could be privileged to have. Finally, a special thanks to Annie for shooting with me in the gym.

Table of Contents

	Page
List of Tables	ix
List of Figures	x
List of Abbreviations	xii
Abstract	xiv
Introduction.....	1
The Amyloid Hypothesis.....	1
Tau Hypothesis.....	7
Other potential contributors to neurodegeneration and AD	9
Neuronal cell death.....	11
Combating neurodegeneration with neuroprotection	12
Specific Aims and Project Overview	22
Project Overview	23
Specific Aim 1 – Establishing an Assay to Measure NGF Secretion from Cultured Human Glial Cells.....	25
Effects Relating to the Peptotech Assay Kit Components.....	27
Storage of ELISA components	27
Effects Relating to the Peptotech Assay Protocol.....	27
Solution pH.....	27
Achieving greater sensitivity utilizing an alternative colorimetric substrate (TMB)	28
Modification of block buffer to accommodate the TMB substrate	28
Modification to the ELISA wash protocol	29
Overcoming assay variation resulting from the avidin-HRP conjugate	30
Determine the duration of TMB incubation	33
Other miscellaneous contributors to poor assay performance.....	33
Effects Relating to Cell Culture Media.....	35
Effects of media components on the NGF ELISA	35

Stability of extracellular NGF	36
Effects of conditioned-media storage on the NGF ELISA	37
Using the optimized ELISA to determine the SMI dose-response	39
Overview	39
24-hour time course survey of PMA and Clenbuterol.....	40
Dose response for PMA, forskolin, and clenbuterol with a 12-hour incubation duration.....	41
Specific Aim 1 Conclusions.....	42
Specific Aim 2 – Quantitative PCR to Assess Small Molecule Induction of NGF Gene Expression.....	44
Gene Specific Primer Sequences.....	45
Transformation of E. coli with a plasmid containing an NGF cDNA.....	47
Agarose gel electrophoresis and qPCR melt curve analysis to confirm sequence specific amplification	49
Confirming primer efficiency.....	51
Real time PCR amplification of NGF mRNA in SMI treated samples – The Goal of Specific Aim 2.....	55
Effects of PMA, clenbuterol, and forskolin on NGF gene expression	60
Specific Aim 2 Conclusions	61
Specific Aim 3 – Mapping the Signal Transduction Pathway(s) for Select SMIs of NGF	63
Determining the glial cell pathways responsible for NGF induction	63
Confirming small molecule induction of NGF protein and transcript	63
Reverse phase protein microarray (RPPA) analysis	68
Reverse phase protein microarray methodology	68
Reverse phase protein microarray results	68
PMA	69
Clenbuterol	72
Forskolin.....	74
Note on other small molecules evaluated	75
Refined model of SMI Induction of NGF	76
Specific Aim 4 – Validation of the PKC Pathway in NGF Induction	78
Agonist and Antagonist Assays.....	78
The Agonists and Antagonists.....	80

Evaluating cytotoxicity of the agonists and antagonists.....	83
Validation study results.....	85
PKC Agonist: Bryostatin-I	85
Raf Agonist: ZM336372.....	86
MEK Antagonist: UO126.....	87
ERK Antagonist: FR180204.....	88
P90RSK Inhibitor: BI-D1870.....	89
CREB Antagonist: 217505	90
Revised signal transduction cascade	91
Pitfalls and Alternative Approaches.....	92
Methods and Materials.....	94
NGF ELISA and Related Experiments	94
NGF ELISA protocol.....	94
Effects of media components on NGF ELISA	96
Stability of NGF in cell environment	96
Effects of conditioned-media storage/freeze-thaw cycles on NGF ELISA.....	97
Effects of glycerol and SDS denaturing solution	97
Effects of urea.....	98
Cell culture and related experiments.....	98
Cell culture	98
24-hour time course survey of PMA and Clenbuterol.....	99
Dose response for PMA, forskolin, and clenbuterol at 12 hours.....	99
Evaluating small molecule induction of NGF secretion into conditioned media....	100
Preparation of SMI	101
Reverse phase protein microarrays and data analysis	103
Reverse phase protein microarrays.....	103
Quantitative reverse transcription PCR and related experiments.....	105
Transformation of XL1-Blue E. coli with pHumNGF_Internal plasmid.xdna	105
Agarose gel electrophoresis and qPCR melt curve analysis.....	106
Confirming primer efficiency	106
UV-Vis spectroscopy to quantify RNA extraction and identify protein contamination	107
Real time PCR and comparative C _T analysis	107

Agonist and Antagonist Assays and Related Experiments	108
Cytotoxicity Assay	108
Preparation of agonists and antagonists.....	108
Antagonist assays	109
Appendix 1 – Reverse phase protein microarray protein antibodies	110
Appendix 2 – Reverse phase protein microarray results for all tested SMI	113
Appendix 3 – Two tailed unpaired heteroscedastic t-test data and associated fold change	122
Appendix 4 – Transcription factors with multiple binding sites on the NGF gene	134
References	136

List of Tables

Table	Page
Table 1 - Interventional therapeutic agents currently being investigated in open phase 2, 3, or 4 clinical trials for Alzheimer's Disease	19
Table 2. Primer sequence information for NGF gene and control genes TATA box binding protein (TBP) and beta-Actin (Actb).	47
Table 3. UV-Vis spectroscopy evaluation of RNA	56
Table 4. Fold change in gene expression in PMA treated glial cells.	60

List of Figures

Figure	Page
Fig. 1. Processing of amyloid precursor protein (APP).....	2
Fig. 2. The progression of Alzheimer's disease.....	13
Fig. 3. SMIs of NGF	16
Fig. 4. Signal transduction pathways that may lead to the induction of NGF.	17
Fig. 5. NGF-ELISA.....	26
Fig. 6. Absorbance at 450 nM as a function of NGF concentration using ABTS substrate and TMB substrate.....	28
Fig. 7. Effects of block buffer composition (BSA concentration) on NGF ELISA.....	229
Fig. 8. Reusing pipette tips for washes has no significant effect on the resolution of the NGF ELISA	30
Fig. 9. GE Life Sciences vs Peprotech avidin-HRP conjugate comparison using Ultra OTMB substrate.....	32
Fig. 10. Effects of TMB Incubation Duration.....	33
Fig. 11. ELISA assay failure likely due to aged and/or contaminated 10X PBS stock solution.....	34
Fig. 12. Tween-20 and TMB both have significant effects on the ELISA baseline and resolution at low concentrations	35
Fig. 13. Effects of media components on the NGF ELISA	36
Fig. 14. Recovery of NGF from conditioned media	37
Fig. 15. Effects of freeze-thaw cycles on NGF titers, measured using an NGF-ELISA ..	38
Fig. 16. Effects of glycerol, SDS, and urea on NGF titers	39
Fig. 17. NGF induction as a function of incubation duration	41
Fig. 18. The SMI dose-response	42
Fig. 19. pHumNGF_Internal plasmid.....	48
Fig. 20. Agarose gel electrophoresis (2% w/v) confirming the presence of only one, size-specific amplicon for the Actb, Tbp, and NGF primer sets	50
Fig. 21. Melt curve analysis of PCR products using beta-Actin (Actb), TATA box binding protein (Tbp), and nerve growth factor (NGF) primer sets with cDNA template produced from reverse transcription of extracted total RNA obtained from cultured T98G cells	51
Fig. 22. NGF primer efficiency fluorescence results.....	53
Fig. 23. Actb primer efficiency fluorescence results	54
Fig. 24. Tbp primer efficiency fluorescence results	55
Fig. 25. Quantifying effects of PMA on NGF gene expression.....	59

Fig. 26. Fold change analysis of NGF gene expression after 4-hour treatment with SMI.	61
Fig. 27. Small molecules chosen for the study of NGF induction.	64
Fig. 28. NGF titers (vehicle-subtracted) as a result of exposure to small molecule	67
Fig. 29. Stained protein microarray slide.....	68
Fig. 30. The glial cell signal transduction pathway activated by PMA	69
Fig. 31. The PMA induced signal transduction as a function of time	72
Fig. 32. Clenbuterol and NGF gene induction.	73
Fig. 33. Forskolin and NGF gene induction	75
Fig. 34. Proposed signaling pathways of SMIs of NGF	76
Fig. 35. The PMA signal transduction pathway leading to NGF secretion.	80
Fig. 36. Resazurin cytotoxicity assay	84
Fig. 37. Effects of Bryostatin-1 on NGF gene expression and secretion.....	85
Fig. 38. NGF Induction by ZM336372.....	86
Fig. 39. Effects of the MEK Inhibitor UO126 on PMA Induction of NGF gene expression and secretion	87
Fig. 40. Effects of the ERK Inhibitor FR180204 on PMA Induction of NGF gene expression and secretion	88
Fig. 41. Effects of the P90RSK Inhibitor BI-D1870 on PMA Induction of NGF gene expression and secretion	89
Fig. 42. Effects of CREB Inhibitor 217505 on PMA induction of NGF gene expression.	90
Fig. 43. The revised PMA signal transduction pathway leading to NGF upregulation....	91

List of Abbreviations

Adenylate cyclase	AC
Alzheimer's Disease	AD
Alzheimer's Disease Assessment Scale-Cognitive.....	ADAS-Cog
Amyloid- β	A β
Amyloid precursor protein.....	APP
Apolipoprotein E.....	APOE
2,2'-Azinobis (3-ethylbenzothiazoline-6-sulfonic acid).....	ABTS
β -actin	Actb
β -adrenergic receptor	ADR
β -APP cleaving Enzyme	BACE
Bovine serum albumin	BSA
Brain derived neurotrophic factor	BDNF
C-Terminal fragment	CTF
cAMP response element binding protein.....	CREB
Concentration with half-maximal response	EC ₅₀
2-Cyano-3,12-dioxooleana-1,9(11)-dien-28-oyl.....	CDDO
Cyclic AMP	cAMP
Cyclin dependent kinase	CDK
CREB binding protein.....	CBP
Cycle threshold	C _T
Deoxyribonucleic acid	DNA
Diacylglycerol.....	DAG
Dimethyl sulfoxide.....	DMSO
Dulbecco's Modified Eagle Medium.....	DMEM
Endothelin converting enzyme	ECE
Enzyme linked immunosorbent assay.....	ELISA
Fetal bovine serum.....	FBS
Horseradish peroxidase.....	HRP
Insulin degrading enzyme	IDE
Interleukin	IL
Interferon.....	INF
Glycogen synthase kinase	GSK
Growth factor receptor-bound protein	Grb
Luria-Bertani	LB
Kinase-inducible domain	KID
Kinase-inducible domain interacting domain	KIX

Mechanistic (Mammalian) target of rapamycin.....	mTOR
Mini-Mental Status Examination.....	MMSE
Mitogen activated protein kinase.....	MAPK/ERK
Mitogen activated protein kinase kinase.....	MEK
Mild cognitive impairment.....	MCI
N-methyl-D-aspartate.....	NMDA
National Center for Biotechnology Information.....	NCBI
Neprilysin.....	NEP
Nerve Growth Factor.....	NGF
Neurotrophin 3.....	NT3
Paired helical filament.....	PHF
Phorbol 12-myristate 13-acetate.....	PMA
Phosphate buffered saline.....	PBS
Phosphoinositide 3-kinase.....	PI3K
Polymerase Chain Reaction.....	PCR
Positron emission tomography.....	PET
Presenilin.....	PSEN
Protein Kinase A.....	PKA
Protein Kinase B.....	PKB/Akt
Protein Kinase C.....	PKC
Reactive oxygen species.....	ROS
Recombinant human NGF.....	rhNGF
Reverse phase protein microarray.....	RPPA
Reverse transcription.....	RT
Ribonucleic acid.....	RNA
Ribosomal S6 Kinase.....	RSK
Sodium dodecyl sulfate.....	SDS
Son of sevenless protein.....	SOS
Small molecule inducer.....	SMI
3,3',5,5'-Tetramethylbenzidine.....	TMB
TATA-box binding protein.....	Tbp
Tropomyosin receptor kinase.....	Trk
Tuberous Sclerosis protein.....	TSC
Tumor necrosis factor.....	TNF

Abstract

DEVELOPING AN ALZHEIMER'S DISEASE THERAPEUTIC: IDENTIFICATION AND VALIDATION OF SIGNALING PATHWAYS INVOLVED IN SMALL MOLECULE INDUCTION OF NERVE GROWTH FACTOR

Justin B. Davis, Ph.D.

George Mason University, 2016

Dissertation Director: Dr. Robin Couch

Nerve growth factor (NGF) has been identified as a key protein involved in preventing neuronal cell death, a hallmark of neurodegeneration due to age and Alzheimer's Disease. Recent preclinical and clinical Alzheimer's Disease studies have noted a reduction in the rate of cognitive decline upon treatment with NGF. However, because NGF is unable to penetrate the blood-brain barrier, current means of delivering NGF to the brain are highly invasive and cost-prohibitive. An orally administered small molecule, capable of stimulating the upregulation of NGF in the brain, is preferred. Several small molecules that cause the upregulation of NGF have been discovered through serendipity, but their mechanisms of action are still poorly understood. A thorough investigation into the mechanisms of known inducers of NGF identified Protein Kinase C and the Mitogen Activated Protein Kinase pathway as critical to the upregulation of NGF protein. A series of protein specific agonists and antagonists was employed to validate select members of

this signaling pathway, revealing promising targets for the development of neuroprotective therapeutics.

Introduction

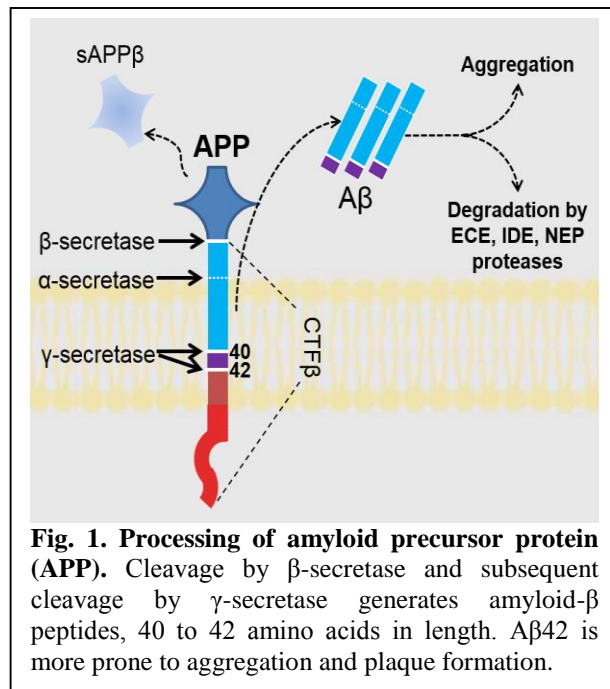
Alzheimer's disease (AD), currently the 6th leading cause of death in the United States, affects over 5.2 million Americans¹. The disease is projected to reach nearly 16 million by 2050¹, and there are currently no available treatment methods proven to prevent or halt disease progression. Pathologically, AD is hallmarked by the development of amyloid plaques, neurofibrillary tangles of tau protein, changes in neuronal glucose metabolism, and neurodegeneration. The breakdown of neural connections leads to dementia and loss of function. Approaches to treat Alzheimer's by targeting these specific issues individually have been unsuccessful thus far, and the development of Alzheimer's therapeutics has raised more questions than answers.

The following introduction will present the pathology behind Alzheimer's disease, identify the common targets for the development of interventional drugs, and illustrate the merit of a neuroprotective approach to combating the disease (the latter of which is the underlying premise of this thesis research).

The Amyloid Hypothesis

Alzheimer's disease, as it was first described by Dr. Alois Alzheimer in 1907, is most often characterized by the accumulation of beta-amyloid plaques derived from the aggregation of small amyloid- β ($A\beta$) peptides in the brain. The $A\beta$ peptide is generated by cleavage of membrane-bound amyloid precursor protein (APP). $A\beta$ peptide is excised

from APP holoprotein by a combination of β -APP cleaving enzyme (BACE or β -secretase) and the activity of γ -secretase^{2,3}. β -secretase acts extracellularly on APP, releasing a large fragment, soluble APP β (sAPP β , 671 aa, 76 kDa) to the extracellular environment (Fig. 1). Although few investigations have explored



the function of sAPP β in the healthy brain, the protein has been

implicated in neuroprotection against excitotoxicity and glucose deprivation and is believed to promote neurite outgrowth and neuronal differentiation⁴. The remaining 99 amino acid fragment (CTF β , 11 kDa) remains temporarily bound to the membrane^{3,5,6}.

The subsequent intracellular action of γ -secretase on CTF β is imprecise, generating fragments of two different sizes, A β ₄₀ and A β ₄₂, depending upon the site of cleavage^{3,6,7}.

The conformation of the longer fragment, A β ₄₂, differs dramatically from that of A β ₄₀, and is significantly more prone to aggregation, resulting in the formation of the amyloid plaques^{7,8}. Generally, γ -secretase generates A β ₄₀ 8 to 9 times more often than A β ₄₂^{3,9}, but neither species is the most prevalent final APP cleavage product found in the brain^{3,9,10}.

In healthy cells, 90% of the total APP is cleaved by α -secretase instead of β -secretase, generating sAPP α (687 aa, 78 kDa) extracellularly and an 83 amino acid fragment, CTF α (83 aa, 9 kDa)^{2,3,10}. The sAPP α cleavage product is believed to play roles in neuritogenesis, neuroprotection, proliferation of non-neuronal cells, long term potentiation of N-methyl-D-aspartate (NMDA) signaling, and immune response⁴. Subsequent intracellular cleavage of CTF α by γ -secretase generates p3 fragments, 24 or 26 residues in length, corresponding to the two γ -secretase cleavage sites³. Little is certain as to the biological function of p3. Several publications have proposed p3 induction of pro-inflammatory response in a fashion similar to A β ¹¹⁻¹³. Conflicting reports hypothesize a neuroprotective, anti-inflammation role for p3¹⁴ or suggest the fragment has no major biological role¹⁵. The remaining C-terminal portion of APP, p83 (colored red in Fig. 1), is quickly degraded and has no known biological function¹⁶. While the amount of A β ₄₂ present in healthy brains is minimal, AD is marked by a suppression of α -secretase activity and a gain in β -secretase activity, which drives an increase in amyloid- β production, thereby enhancing plaque formation¹⁰.

Aggregation of A β occurs in two phases, with soluble multimers preceding the development of fibrillar deposits^{17,18}. Soluble multimers and fibrillar deposits trigger different toxic responses and are recognized by different antibodies³. The exact mechanisms of action for A β induction of neurodegeneration is unknown, but smaller, soluble A β aggregates are believed to be the form most relevant to amyloid related toxicity in AD^{3,18}.

Natural prevention of amyloid- β accumulation requires the degradation or clearance of the A β peptide. The enzymes neprilysin (NEP), insulin degrading enzyme (IDE), and endothelin converting enzyme (ECE) have been implicated as proteins capable of degrading A β in the cell (Fig. 1)^{3,19-21}. However, none of these proteases are exclusive to A β ; IDE shows 20-fold greater binding affinity for insulin than for A β (thus, insulin is a competitive inhibitor of IDE degradation of A β , serving as a potential link between insulin-related diseases and AD)³, while NEP, a neutral endopeptidase, has broad substrate specificity and is best known for its role in degrading vasoactive and natriuretic proteins associated with heart failure^{22,23}. Endothelin converting enzymes ECE-1 and ECE-2 show 12-fold greater protease activity against endothelin ET-1 than A β ₄₀ and A β ₄₂²¹. Nevertheless, the proteases show significant hydrolysis activity against A β ²¹, and *ECE* (+/-) knockout mice show greater than 25% increases in cerebral A β accumulation compared to wild type²⁴. The proteins are strongly expressed in the human cerebral cortex, and certain ECE-1 genetic mutations are associated with late-onset AD²⁵. Undigested A β peptide can be transported across the blood-brain barrier, out of the brain via the activity of low-density lipoprotein receptor-related protein (LRP), and into the brain via the receptor for advanced glycation end products (RAGE)^{26,3}. Accordingly, a RAGE inhibitor (TTP448) is currently in phase 3 trials for the treatment of AD²⁷ (trial identifier NCT02080364; a list of AD therapeutics currently in development is provided in Table 1). It is noteworthy, however, that despite the known transport of A β peptide from the brain into the bloodstream, A β has been deemed poorly suited as a serum biomarker of AD, predominantly due to naturally occurring serum A β peptide originating

from skeletal muscle, organs, and peripheral cells of the body²⁸. A β peptide accumulation in the brain leads to the development of soluble multimers and fibrillar deposits, hallmarks of AD.

The perceived significance of amyloid- β to AD was heightened by the discovery of genetic mutations that related directly to A β and its clearance from the cell. Autosomal dominant mutations, implicated in familial, early onset AD, have been detected in the *presenilin 1* and *2* (*PSEN1* and *PSEN2*) genes^{2,29,30}. These two genes each encode polypeptides comprising the active site of the multimeric γ -secretase protein. The mutations of *PSEN1* and *PSEN2* alter the cleavage site specificity of γ -secretase, resulting in higher amounts of A β_{42} ^{2,3,29,109}.

Three different *apolipoprotein E* (*APOE*) alleles common in the population, *APOE2*, *APOE3*, and *APOE4*, have been correlated to AD. While *APOE3* is neutral, *APOE2* delays the onset of the disease, whereas *APOE4* enhances it (thereby decreasing the age of onset)². This phenomenon is believed to involve clearance of amyloid- β from the central nervous system, as apoE2, apoE3, and apoE4 proteins have decreasing effectiveness in amyloid- β removal^{2,32}. The mechanism behind this observation has yet to be clarified, but these proteins are known to act as ligands for receptor-mediated endocytosis of lipoproteins. Many have hypothesized that apoE plays a role in A β clearance by binding the protein directly and promoting its transport (with E2 being the most facilitative)^{33,34}. Others propose a mechanism in which apoE competes with A β for the same receptors for endocytosis (with E4 being the most competitive), blocking potential interactions between the receptors and A β ^{35,36}. As the only known genetic

mutations and risk alleles for AD relate directly to amyloid- β , and not to other known features of AD, inhibiting A β production and preventing its aggregation has received considerable attention in the development of AD therapeutics.

Several methods of preventing and reversing amyloid plaque formation have been examined. β -secretase inhibitors such as Minocycline³⁷ (NCT01463384), MK-8931³⁸ (NCT01953601), Thalidomide³⁹ (NCT01094340), and α -secretase enhancers such as Acitretin⁴⁰ (NCT01078168) are possible therapeutics currently being assessed in clinical trials. These compounds are intended to shift APP processing in favor of α -secretase action, thereby decreasing the amount of substrate for A β generation. Multiple γ -secretase inhibitors have also been assessed, however most have failed during clinical trials, most notably, semagacestat. Although semagacestat successfully reduced A β levels in both mice and in human phase III clinical trials, subsequent evaluation revealed that treatment with semagacestat results in increased deterioration in cognition when compared to placebo-treated controls². These disappointing results underscore the lack of success in treating AD via therapies targeting amyloid- β ^{41,42}.

It is noteworthy that A β and other β -secretase APP breakdown products indeed are present in healthy individuals. These peptides may have positive effects on neuronal cell viability when present at low concentrations in healthy brains. It is interesting to speculate then that the altered β -secretase activity observed in AD induces toxicity solely by increasing A β concentration to the point of aggregation. Alternatively, the resulting loss of neuroprotective α -secretase products such as sAPP α may be central to the development of AD. In support of the latter hypothesis, failure of amyloid-based

treatments has called into question the role of amyloid plaque formation as a causative agent of the disease. Clinically, loss of brain mass and the progression of dementia correlate only weakly to the quantity and distribution of A β in the brain^{3,43,44}. Instead of being the driving force behind the Alzheimer's phenotype, many have postulated that the formation of amyloid plaques is just one of many secondary events that occur in the progression of the disease. The Tau hypothesis seeks to provide an alternative rationale in attributing AD to the formation of neurofibrillary tangles composed of hyperphosphorylated tau^{2,7,3}.

Tau Hypothesis

The causes of excessive tau phosphorylation are still unverified, but toxicity induced by A β , oxidative stress, and inflammation may induce upregulation of tau kinases, downregulation of phosphatases, and modification to tau directly^{45,46}. Tau is a soluble microtubule-associated protein and has stabilizing effects on microtubulin assembly⁴⁷⁻⁴⁹. Six isoforms of tau are known to exist, with differences in the number and characteristics of their tubulin-binding domains and phosphorylation sites (KXGS motifs)⁴⁵. Changes in the proportions of each isoform relative to the others have been correlated with disease^{45,50,51}. Phosphorylation of tau has a destabilizing effect on microtubule binding, allowing dynamic changes in cell structure while still providing skeletal support. In healthy individuals, tau is phosphorylated at 2 to 3 of the four KXGS motifs within the protein by glycogen synthase kinase 3 β (GSK-3 β), cyclin dependent kinase (CDK5), and mitogen activated protein kinases. In AD, a 3- to 4- fold increase in

tau phosphorylation is observed, inhibiting the association of tau with the microtubules and inducing the formation of tau aggregates from dissociated tau protein⁵²⁻⁵⁴.

The microtubule network plays a critical role in neuronal morphology and the transport of signaling molecules, trophic factors, and organelles^{48,49}. Tau mutations and hyperphosphorylation have been correlated with a reduction in both microtubule density and fast axonal transport in mouse models⁴⁶. In a recent study, providing a microtubule-stabilizing drug to tau-transgenic mice with microtubule and motor deficits led to improvement in microtubule density and fast axonal transport as well as an improvement in motor function⁴⁶.

The effects of tau hyperphosphorylation on the microtubule network is only one of two potential causes of tau induced neurodegeneration. Neurofibrillary tangles occur when hyperphosphorylated tau forms aggregates with tau, microtubule associated proteins 1 and 2, and ubiquitin^{45,53}. Straight or paired helical forms of these aggregates exist with a notable toxic effect on the cellular environment⁴⁵. The abnormally phosphorylated tau, PHFtau, can aggregate to form paired helical filaments^{55,56}. However, only 10% of PHFtau is found in neurofibrillary tangles, with the remaining portion deposited in neuronal processes, appearing as dystrophic neuritis with swollen axons and dendrites⁵⁵. Recent animal model studies suggest that microtubule stability is sufficient for cognitive improvement, regardless of the continued presence of neurofibrillary tangles⁵⁵. This evidence points to microtubule dissociation, resulting from hyperphosphorylated tau, as a key component of disease progression. Currently, TRx0237⁵⁷ (NCT01626378), a tau aggregation inhibitor, is the only therapeutic targeting

tau in open phase 2+ clinical trials. However, multiple drugs involved in preventing tau aggregation and promoting microtubule stability are currently in development⁵⁷.

Other potential contributors to neurodegeneration and AD

While amyloid- β plaques and tau hyperphosphorylation are linked to the disease, recent research has begun to focus on inflammation, oxidative stress, and vascular degeneration as contributors of AD. The buildup of A β elicits an immune response from microglia and astrocytes. Microglia exhibit a limited phagocytic ability for amyloid. However, activated astrocytes and microglia may stimulate the release of specific cytokines and chemokines to recruit peripheral macrophages for the purpose of A β clearance⁵⁸. The overall response may initiate many cellular defense mechanisms such as the generation and localization of reactive oxygen species (ROS) and interleukins (IL-1 β , IL-6, TNF- α and INF- γ) that are pro-inflammatory⁵⁸. A β has also been shown to induce accumulation of major histocompatibility complex surface molecules and complement response⁵⁸. Astrocyte activation is a known pathological response to AD, and astrocytes can phagocytize amyloid directly, further contributing to the pro-inflammatory response⁵⁸. Additionally, activation of astrocytes disrupts their normal function in neuronal support, resulting in local neuron depolarization and cytotoxic damage. This phenomenon can lead to neuronal degradation and disease progression if astrocyte activation continues to persist⁵⁸. Recent trials have shown a decreased risk for AD in patients taking non-steroidal anti-inflammatory drugs⁵⁹, and multiple anti-oxidants and anti-inflammatory therapeutics are currently undergoing clinical trials as AD therapies.

Defects in brain glucose metabolism have also been identified as another characteristic of Alzheimer's disease. These faults are marked by reduced glucose utilization in early stages of AD and by corresponding downregulation of gene expression for proteins involved in oxidative phosphorylation⁶⁰. Originally believed to be the result of damage to the mitochondria accrued due to oxidative stress, several more recent analyses have revealed that these changes precede the mitochondrial damage associated with advanced AD and coincide with deficits in glucose transport and glucose availability in the brain that are evident in the early stages of the disease⁶¹⁻⁶³. The timeline suggests metabolic downregulation as a protective response, as proposed by Sun. *et al.*, following their observation that these genetic downregulation events occur before the onset of AD⁶¹. AC-1204 (NCT01741194), a potential therapeutic currently in open clinical trials⁶⁴, provides caprylic acid for ketone body (acetone, acetoacetic acid, and β -hydroxybutyric acid) production in the liver. These ketone bodies pass through the blood-brain barrier and into the brain, where they are converted to acetyl-CoA and used for energy metabolism when glucose levels are low⁶⁵.

Vascular dementia, another type of neurodegenerative disease, causes cognitive decline mainly through ischemia induced cortical microinfarcts and white matter lesions (i.e. cellular death or tissue necrosis in the brain caused by mini-strokes)^{66,67}. These vascular lesions are often apparent in cases of AD, but are not required for the cognitive decline associated with the disease⁶⁸. Vascular degeneration has also been theorized to play a role in hippocampal atrophy⁶⁸, a key contributor to cognitive decline in AD, and β -secretase activity is known to increase in response to hypoxia and oxidative stress⁶⁹. The

increased severity of AD-type dementia in comparison to vascular dementia creates difficulty in identifying the impact of vascular degeneration in AD; however, the cognitive effects of cortical microinfarcts in combination with AD are statistically pronounced beyond the cognitive decline in AD alone⁶⁶. When vascular dementia and Alzheimer's disease are both involved in causing dementia, the disease is referred to as mixed dementia (dementia multiforme). Whether these vascular abnormalities truly play a role in causing or accelerating the onset of AD is unclear, but diagnoses of mixed dementia are becoming more prevalent as more is understood about the interplay between these diseases⁶⁶.

Neuronal cell death

Amyloid- β , complement, and oxidative damage have all been linked to the lysing and apoptosis of neurons in the brain. Examinations of synaptic density have revealed significant decreases in synaptic number per unit volume in both lamina III (-42%) and lamina V (-29%) of the human frontal cortex of AD patients⁷⁰. A negative correlation between synapse abundance and synapse size is also observed, likely as a compensatory response⁷⁰. Significant decline in synaptic numbers in both the superior and middle temporal gyrus is also detected in AD⁷¹. Further, lower hippocampal baseline volumes and higher atrophy rates are seen in patients with AD compared to healthy controls, and whole brain atrophy rates are higher in patients with AD than in either healthy controls or persons afflicted with only mild cognitive impairment⁷².

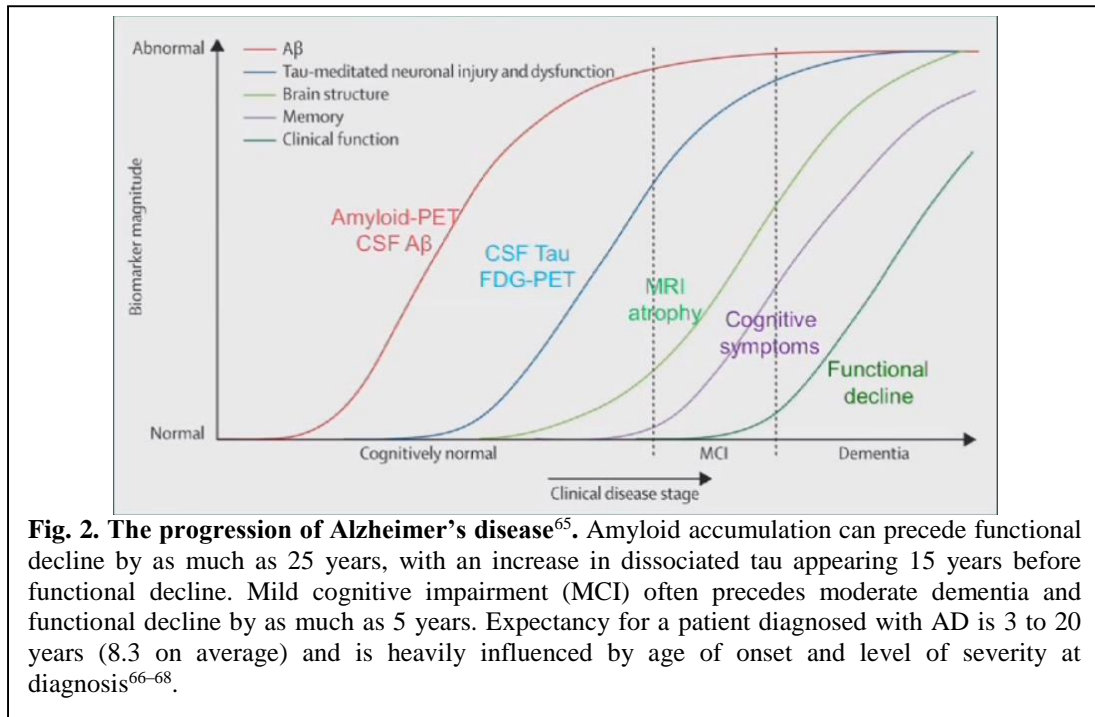
The selective loss of forebrain cholinergic neurons has been a known element of Alzheimer's pathology since the 1970s⁷³. The phenomenon correlates with the

breakdown of cholinergic pathways in the cerebral cortex and basal forebrain of persons afflicted with AD⁷⁴. Fittingly, 4 of the 5 FDA approved disease modifying therapies for Alzheimer's (Donepezil, Rivastigmine, Galantamine, and Tacrine) are cholinesterase inhibitors that prevent the degradation of acetylcholine in the neural synapse^{75,74}.

Although cholinesterase inhibitors can generate improvements in cognitive function, they do little to impact the physiological causes of neurodegeneration underlying the disease^{2,74}. Thus, as it stands, current methods of treating AD are ineffective in addressing the underlying pathologies of the disease. Greater success in treating AD will likely require therapeutics addressing multiple aspects of the disease's underlying etiology.

Combating neurodegeneration with neuroprotection

The decades of delay between the appearance of amyloid plaques and neurofibrillary tangles and the onset of AD type dementia suggests that the cells survive for a significant amount of time in the face of cytotoxicity (Fig. 2)⁷⁶. This phenomenon suggests the presence of neuroprotective agents that are pro-survival and suppress apoptotic cascades. One avenue of preventing the cognitive decline associated with AD may lie in promoting the mechanisms that allow neurons to survive in an environment of A β , hyperphosphorylated tau, and the inflammation that follows. Neurotrophins, neuroprotective peptides secreted by neurons and glia that promote neuronal growth and survival, may hold the key to such a therapy.



Neurotrophins such as brain derived neurotrophin factor (BDNF), neurotrophin-3 (NT3), and nerve growth factor (NGF) promote cell growth and cell survival upon binding to specific receptor tyrosine kinases on the neuron (TrkB, TrkC, and TrkA, respectively)⁷⁷. Binding of NGF to TrkA stimulates transphosphorylation of the receptor tyrosine kinase, initiating the recruitment and activation of proteins such as Grb-2, SOS, and Ras^{77,78}. Increases in Ras activity promote peripheral neuron survival, while inhibition of Trk-mediated Ras signaling has been correlated to decreased survival of sympathetic neuron populations⁷⁸. Ras affects multiple signaling pathways including the PI-3K/Akt pathway⁷⁹⁻⁸¹, which promotes survival by inhibiting the activity of apoptotic

proteins such as Bad, pro-caspase-9, forkhead, and through the inhibitor of apoptosis (IAP) family of caspase inhibitors^{78,82,83}. Also affected by Ras is the MEK/MAPK pathway which stimulates the activity and expression of anti-apoptotic (pro-survival) proteins^{78,84,85} and upregulates the transcription factor CREB^{78,85}, a key regulator of neurotrophin expression^{78,86,87}. The MEK/MAPK pathway has also been shown to protect sympathetic neurons from cytokine arabinoside induced apoptosis and cerebellar neurons from apoptosis due to oxidative stress^{78,88-90}.

Several studies have illustrated the protective effect of NGF in animal models of AD. Mouse-NGF⁹¹ and recombinant human NGF⁹² have been shown to almost completely prevent reductions in the number and size of cholinergic neurons. The neurotrophins also prevent atrophy in the medial septal nucleus in monkeys afflicted with degenerative changes due to fimbria-fornix lesions (untreated controls showed significant degeneration of these cell types). Recombinant human NGF (rhNGF) has also been shown to be active in the prevention of cholinergic neuron degradation in primates caused by age⁹³.

Administration of nerve growth factor is challenging because NGF cannot cross the blood-brain barrier⁹⁴. To overcome this obstacle, one successful primate study utilized NGF conjugated to an antibody directed against the transferrin receptor, OX-26, at the blood-brain barrier. This system permitted transport of NGF to the brain, preventing degeneration of NGF-responsive neurons⁹⁵. Alternatively, grafts of encapsulated cells secreting NGF have been used to successfully rescue basal forebrain neurons in primates⁹⁶ and in mice⁹⁷. In addition, viral expression systems have been used

to deliver NGF to the brain of rats, resulting in neurite extension upon treatment with rhNGF⁹⁸.

The positive effects of NGF:TrkA mediated signaling have brought upon a wave of proposals for NGF-based treatments for AD in humans. A phase 1 clinical trial attempted gene delivery of NGF to the nucleus basalis region of the brain in eight individuals with mild Alzheimer's disease⁹⁹. Two of the patients suffered cortical hemorrhaging due to abrupt movements during the surgical procedure, with one dying during the surgery and the other suffering death five months after the operation⁹⁹. Examination of the latter patient's brain post-mortem revealed that the gene therapy was successful, with cholinergic axon sprouting into the site of NGF delivery, indicating that degenerating neurons in AD patients are still responsive to the NGF protein⁹⁹. PET scans of the other treated individuals also revealed an increase in cortical glucose uptake in the affected region. Among these study participants, the rate of disease progression was reduced by 36-51% for a mean period of almost 2 years, as measured by Mean Mini-Mental Status Examination (MMSE) scores and Alzheimer Disease Assessment Scale-Cognitive subcomponent scores (ADAS-Cog). Cognition improved or was stabilized in five of the six patients. The promising results of this and other similar clinical trials¹⁰⁰ strongly support the development of NGF therapeutics for the treatment of AD. However, the risks and expense of such invasive therapeutic approaches are far too prohibitive for treating a disease as widespread as AD. Instead, an orally bioavailable therapeutic able to cross the blood-brain barrier and induce an endogenous NGF response is greatly preferred.

To date, several small molecule inducers (SMIs) of NGF have been identified (Fig. 3)¹⁰¹⁻¹⁰⁴. Generally, the NGF response by these SMIs has been discovered through serendipity, and thus, the mechanism of action behind their response is poorly understood. ***The aim of this***

research proposal is to

identify signal transduction pathways underlying the upregulation of NGF expression and secretion. The results will reveal new target proteins for the rational development of drugs to prevent and treat AD.

Our hypothesis: The Involvement of the PKC-mTOR and PKA Signal Transduction Pathways. We hypothesize that the PKC-mTOR and PKA pathways are central to the activity of select SMIs of NGF. Although a direct interaction remains to be shown, scabronine A-induced NGF secretion reportedly involves Protein Kinase C (PKC)¹⁰⁵ (Fig. 3 & 4). Similarly, we've reported that the structurally related cyathin A3 (Fig. 3) also induces NGF secretion, presumably via PKC¹⁰⁴. Phorbol-related diterpene esters, such as PMA (Fig. 3), are well-known PKC activators that function by mimicking its natural activator, diacylglycerol. Thus, the diterpenes scabronine A, cyathin A3, and

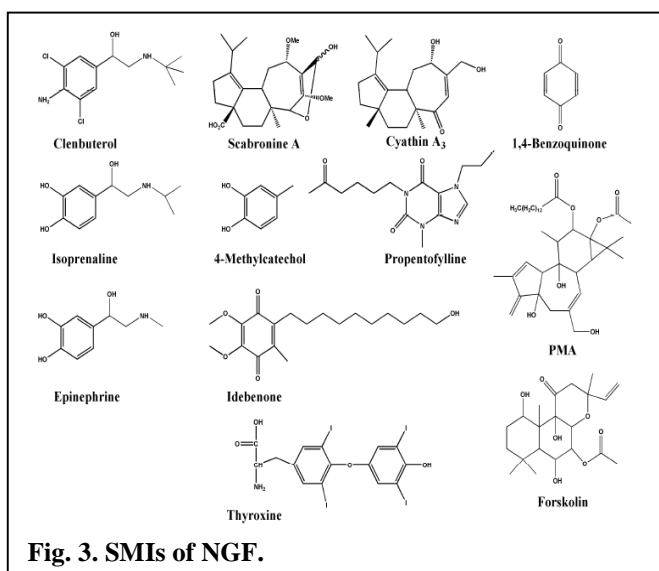


Fig. 3. SMIs of NGF.

PMA may share a similar mechanism of NGF induction by binding to and activating PKC. Activated PKC could subsequently phosphorylate and activate Ribosomal S6 Kinase (RSK), which in turn would phosphorylate Tuberos Sclerosis Protein 1 (TSC1), thereby disrupting the TSC1/TSC2 complex that inhibits Rheb (Ras Homolog

Enriched in Brain; Fig. 4). Uninhibited Rheb can bind and activate the Mammalian Target

of Rapamycin Complex 2 (mTORC2), resulting in the phosphorylation of several target proteins including Rho and Rac which participate in exocytosis (NGF secretion?), PKC which is known to regulate translation (proNGF biosynthesis?), and Akt which can phosphoregulate several additional downstream proteins, not the least of which is the transcription factor CREB. Phosphorylated CREB has been reported to be a requirement for transcription of the NGF gene¹⁰⁶, so the PKC-mTOR pathway appears to be a feasible

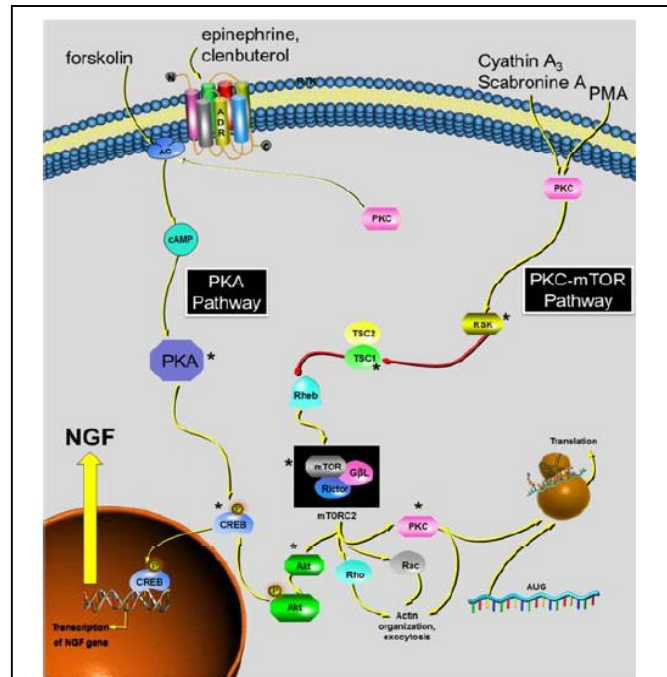


Fig. 4. Signal transduction pathways that may lead to the induction of NGF. The activation state of each pathway can be determined using phosphospecific antibodies to the signal.

route for the induction of NGF by scabronine A, cyathin A3, and PMA (and presumably other structurally similar SMIs of NGF).

In addition to the involvement of the PKC-mTOR pathway, we propose that the PKA pathway also leads to NGF induction. Clenbuterol and epinephrine are both SMIs of NGF (Fig.3). Clenbuterol, a bronchodilator used for the treatment of asthma, is known to confer its effects through binding to β -adrenergic receptors. Similarly, epinephrine (aka adrenaline) activates α - and β -adrenergic receptors. Thus, clenbuterol and epinephrine may induce NGF by activation of the β -adrenergic receptor (ADR), which in turn would result in the activation of Adenylate Cyclase (AC; Fig. 4). Active AC would increase intracellular cyclic AMP (cAMP) levels, thereby leading to the activation of Protein Kinase A (PKA; activation of PKA also involves phosphorylation by associated proteins). PKA is known to phosphorylate numerous downstream proteins, including CREB. Of additional relevance, forskolin (commonly used in cell biology research) raises intracellular levels of cAMP by binding to Adenylate Cyclase, thereby activating the enzyme. Forskolin is a SMI of NGF (Fig. 3 & 4). Furthermore, the phosphodiesterase (PDE) inhibitor propentofylline (Fig. 3) results in increased intracellular levels of cAMP, and is also a SMI of NGF (Fig. 4). Thus, we propose that the PKA pathway is another route for the upregulation of NGF biosynthesis. In fact, the PKC-mTOR pathway may crosstalk with the PKA pathway, since PKC can activate Adenylate Cyclase, thereby initiating the PKA cascade (Fig. 4). Thus, it's conceivable that the PKC-mTOR pathway could stimulate NGF induction via two branches leading to CREB activation.

Intriguingly, activation via PKC would therefore result in a larger dose-response, making the PKC-mTOR pathway the target of choice for drug development.

Table 1 - Interventional therapeutic agents currently being investigated in open phase 2, 3, or 4 clinical trials for Alzheimer's Disease

Agent	Mechanism of Action
AC-1204	Induces chronic ketosis in order to improve mitochondrial metabolism
ACC-001 3 µg/ QS-21 50 µg	Reduces beta amyloid by stimulating an immune response against the peptide
Acetyl-Choline Esterase Inhibitors and Choline supplements	Acetyl-choline esterase (AChE) inhibitors and choline supplements.
Acitretin	Enhancement of the α -secretase activity
Amisulpride	Blocks presynaptic dopamine D2/D3 receptors
Atomoxetine	Selective norepinephrine receptor inhibitor
AVP-923 (dextromethorphan/quinidine)	NMDA antagonist and sigma1 receptor agonist
BAN2401	Humanized IgG1 monoclonal antibody that binds beta-amyloid protofibrils
Brexipiprazole, OPC-34712	D2 dopamine partial agonist
Bryostatin	Protein kinase C modulator
Caprylic Triglyceride (Axona)	Coconut oil product used to provide energy source for brain under conditions of impaired glucose metabolism
Carum Cravi (Caraway)	Thyroid function effector (elevates TSH levels)
Carvedilol	Nonselective beta blocker/alpha-1 blocker
Cerebrolysin	Regulates glycogen synthase kinase 3-beta and cyclin-dependent kinase5 activity.
Cilostazol	Phosphodiesterase inhibitor (increases cAMP, causing increase in active form of PKA)
Crenezumab	Monoclonal antibody against human 1-40 and 1-42 beta amyloid
Curcumin	Natural product with antioxidant, anti-inflammatory, and lipophilic activity
DCB-AD1	Mechanism of action is unclear.
Donepezil (Aricept)	Acetylcholinesterase inhibitor
Doxycycline	Tetracycline antibiotic doxycycline that disrupts beta-amyloid fibrils
ELND005	Anti-aggregation regulation of beta-amyloid
Elontril	Dopamine and norepinephrine reuptake inhibitor, nicotinic acetylcholine receptor antagonist
ENA713	Acetylcholinesterase inhibitor
Encenicline (EVP-6124, MT-4666)	Alpha 7 nAChR inhibitor
Epigallocatechin-3-gallate (EGCG)	EGFR receptor antagonist and potent antioxidant
Escitalopram	Selective serotonin reuptake inhibitor
Etanercept	Cytokine inhibitor to treat inflammation in AD

Exendin-4 (Exanatide)	Glucagon-like-peptide-1 agonist
Fu fang dan shen	Acetylcholinesterase inhibitor
Galantamine	Cholinesterase inhibitor
Gantenerumab	Anti-beta-amyloid antibody
Gastrodin	Regulates free radicals, Bax/Bcl-2 mRNA, caspase-3, cleaved poly(ADP-ribose) polymerase (PARP)
Huperzine A	Acetylcholinesterase inhibitor and NMDA receptor antagonist
ITI-007	Serotonin 5-HT _{2A} receptor antagonist, dopamine receptor partial agonist/antagonist, glutamatergic modulation, serotonin reuptake inhibition.
Levetiracetam	Presynaptic calcium channel inhibitor (reduces neurotransmitter release)
Levodopa (L-DOPA)	Precursor for monoamine or catecholamine neurotransmitters dopamine, norepinephrine, and epinephrine.
Lipoic Acid plus Omega-3 Fatty Acids	Antioxidant effects
Liraglutide	Activator of GLP-1 receptor, a membrane-bound receptor coupled to adenylyl cyclase by G _s . Increases cAMP
Lu AE58054	5-HT ₆ receptor antagonist
Lutein / Zeaxanthin	Antioxidant effects
Masitinib	Tyrosine kinase inhibitor
Meganatural-Az Grapeseed Extract	Promotes disassociation of preformed tau aggregates
Melatonin	Antioxidant effects
Memantine	NMDA receptor blocker
Metformin	Ameliorates insulin action in the brain
Methylphenidate	Dopamine-norepinephrine reuptake inhibitor
Minocycline	Beta-secretase 1 (BACE1) inhibitor that reduces development of tau tangles
Mirtazapine	Noradrenergic and specific serotonergic antidepressant (NaSSA)
MK-7622	Mechanism of action is unclear.
MK-8931	BACE inhibitor, decreases production of amyloid beta peptide
Niacin	Cholesterol reducing agent
Nic5-15	Shown to prevent formation of beta-amyloid plaques in animal models
Nilvadipine	Calcium channel
Octohydroaminoacridine Succinate	Acetylcholinesterase inhibitor
Perindopil	Angiotensin Converting Enzyme inhibitor (ACEI). Used with Telmisartan.
PF-05212377 (SAM-760)	5-HT receptor effector
Pimavanserin tartrate	5-HT _{2A} inverse agonist
Pioglitazone	Agonist at peroxisome proliferator-activated gamma type receptors.
PM012	Mechanism of action is unclear.
Pomegranate Juice	Antioxidant effects
Rasagiline	Monamine oxidase B inhibitor
Riluzole	TTX-sensitive sodium channel blocker, glutamate

	release inhibitor
Rivastigmine	Acetylcholinesterase inhibitor
RO4602522	Monoamine oxidase type B inhibitor
RPh201	Mechanism of action is unclear.
Sagramostim (Leukine)	Recombinant granulocyte macrophage colony-stimulating factor
Simvastatin	HMG-CoA reductase inhibitor
Solanezumab	Monoclonal antibody that binds to amyloid-beta
T-817MA	Mechanism of action is unclear.
Tamibarotene	Retinoic acid receptor agonist
Telmisartan	Angiotensin receptor blocker. Used with Perindopil.
Tetrahydrobiopterin	Essential cofactor for dopamine and serotonin synthesis (cofactor for all isoforms of nitric oxide synthase)
Thalidomide	Decreases BACE1 activity
TRx0237	Tau aggregation inhibitor
TTP-448	Receptor for advanced glycation endproducts (RAGE) inhibitor

Specific Aims and Project Overview

The goal of this research project is to identify protein targets for the development of small molecule inducers (SMIs) of Nerve Growth Factor (NGF) expression and secretion. By elucidating the mechanism utilized by known SMIs of NGF, the key signaling proteins responsible for their activity will be identified, providing potential targets for the rational drug development of NGF-promoting therapeutics. The specific aims of this project are as follows:

Specific Aims

Specific Aim 1: Establishing an Assay to Measure NGF Secretion from Cultured Human Glial Cells. An NGF-specific enzyme linked immunosorbent assay (ELISA) will be optimized and then used to quantify NGF titers secreted from cultured human glial cells treated with select SMIs of NGF. Dose-response relationships will be established for the SMIs.

Specific Aim 2: Quantitative PCR to Assess Small Molecule Induction of NGF Gene Expression. In addition to causing NGF secretion, small molecules that also upregulate NGF gene expression are preferred for use in NGF-based AD therapies. In order to assess changes in NGF gene expression in response to each SMI, a real-time PCR-based assay will be developed and used to quantify NGF transcript levels.

Specific Aim 3: Mapping the Signal Transduction Pathway(s) for Select SMIs of NGF. Reverse phase protein microarrays will be used to map the signal transduction cascade that occurs in response to small molecule induction of cultured human glial cells. Diverse small molecules representing different chemical classes will be evaluated. Signal transduction mapping will be performed using each SMI at its EC₅₀, and the cells will be assessed at various time points to establish temporal maps of signal transduction.

Specific Aim 4: Validation of the Signal Transduction Pathway(s) for NGF Induction. To validate the involvement of the signal transduction pathway(s) identified in Specific Aim 3, the activity of select pathway proteins will be specifically modulated using commercially available agonists and antagonists. After ensuring pathway agonists/antagonists are nontoxic to cultured human glial cells, established NGF assay protocols (ELISA and quantitative PCR) will be employed to assess the targeted signal transduction pathway.

Project Overview

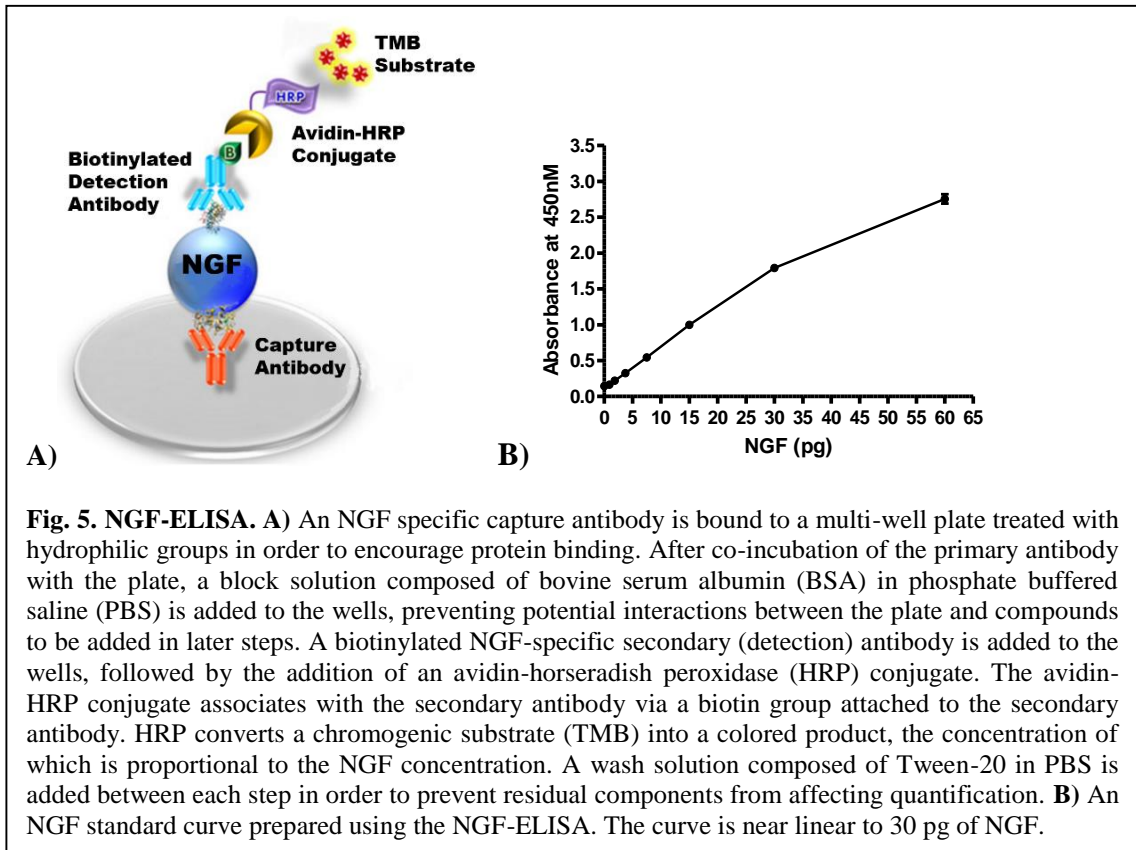
To measure small molecule induction of NGF secretion by glial cells, an NGF-specific enzyme linked immunosorbent assay (ELISA) was optimized to quantify NGF titers from conditioned media (*Specific Aim 1*). Two potential routes for small molecule induction of NGF (the PKA pathway and the PKC-mTOR pathway) were hypothesized (see Introduction), and three agonists of these pathways (clenbuterol, forskolin, and PMA), each a known SMI of NGF, were chosen for evaluation. As cultured glial cells are sensitive to a wide array of external stimuli, we had to confirm direct correlation between SMI concentration and NGF induction using standard sigmoidal dose-response plots

(NGF titer as a function of SMI concentration). The dose response plots were used to determine half-maximal effective concentrations (EC_{50}) for all three compounds. To assess if increased NGF gene expression accompanies an increase in secreted NGF titer, a quantitative RT-PCR assay was developed. This transcript-based assay was used to quantify NGF gene expression in SMI treated cells (at EC_{50} concentration) relative to cells treated with vehicle alone (*Specific Aim 2*). Reverse phase protein microarrays (RPPA) were used to determine the effect of small molecules on the glial cell proteome for the purpose of identifying pathways responsible for NGF induction (*Specific Aim 3*). Finally, pathways activated by SMI exposure (as revealed by RPPA) were validated by agonist and antagonist assays, confirming their role in the SMI response (*Specific Aim 4*).

Specific Aim 1 – Establishing an Assay to Measure NGF Secretion from Cultured Human Glial Cells

Specific Aim 1: Establishing an Assay to Measure NGF Secretion from Cultured Human Glial Cells. An NGF-specific enzyme linked immunosorbent assay (ELISA) was optimized and then used to quantify NGF titers secreted from cultured human glial cells treated with select SMIs of NGF. Dose-response relationships were established for the SMIs.

A commercially available NGF ELISA Development Kit (Peprotech) was purchased and optimized to suit our specific experimental conditions. The ELISA sandwich format is illustrated in Figure 5.



The ELISA development kit includes an NGF-specific polyclonal antibody (the capture antibody (Fig. 5); produced in rabbits), biotinylated anti-NGF detection antibody (also produced in rabbits then subsequently biotinylated), avidin conjugated horseradish peroxidase, and recombinant human NGF protein for use as a standard. Sufficient reagents are provided to perform ten 96-well assays per kit.

Despite being commercially available, the ELISA development kit was far from ‘plug and play’. The largest effects on sensitivity and reproducibility of the NGF ELISA

fell into three broad categories; 1) effects relating to the Peprotech assay kit components (proteins and solutions), 2) effects relating to the Peprotech assay protocol, and 3) assay effects relating to the cell culture media. Each of these were optimized to develop and tailor the NGF ELISA to best suit our needs, as described in detail below.

Effects Relating to the Peprotech Assay Kit Components

Storage of ELISA components

Peprotech recommends reconstituting the lyophilized capture antibody, detection antibody, and recombinant hNGF in water and storing all aliquots at -20°C. When following their direction, we found that the ELISA signal intensity decreased between successive assays and attributed the phenomenon to protein degradation during storage (results not shown). As it is well known that a pH buffered saline storage solution will typically improve the conformational stability and catalytic activity of proteins in solution¹⁰⁷, we addressed this issue by refining the protocol to resuspend the lyophilized proteins in freshly prepared, sterile-filtered phosphate buffered saline (PBS). This alteration led to a significant improvement in signal consistency from assay-to-assay.

Effects Relating to the Peprotech Assay Protocol

Solution pH

The Peprotech protocol calls for assay solutions (wash buffer (PBS + 0.05% Tween-20)) and diluent (wash buffer + 0.1% BSA) to be prepared using PBS with the pH adjusted within a range of 7.00 to 7.40. However, in our hands, the enzymatic activity of HRP is quite sensitive to the assay solution pH. Accordingly, a comparison of multiple ELISAs performed across a pH range of 7.00 to 7.40 confirmed that maximum signal

strength and reproducibility was achieved within a narrow pH range of 7.25 to 7.30 (data not shown). Thus, this range was adopted for all subsequent assays.

Achieving greater sensitivity utilizing an alternative colorimetric substrate (TMB)

Although Peprotech explicitly

indicates the use of ABTS substrate

(2,2'-Azinobis [3-ethylbenzothiazoline-

6-sulfonic acid]- diammonium salt) with

their HRP, to improve the sensitivity of

the assay we adapted their protocol to

incorporate the use of TMB (3,3',5,5'-

Tetramethylbenzidine; Pierce Ultra

TMB) instead. As illustrated in Figure 6,

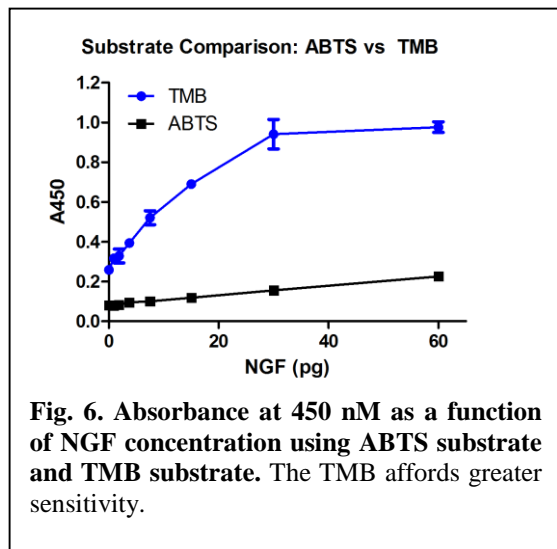
an appreciable improvement in signal

intensity is achieved with this

modification. It is noteworthy, however,

that the TMB signal saturates at

approximately 30 pg NGF.



Modification of block buffer to accommodate the TMB substrate

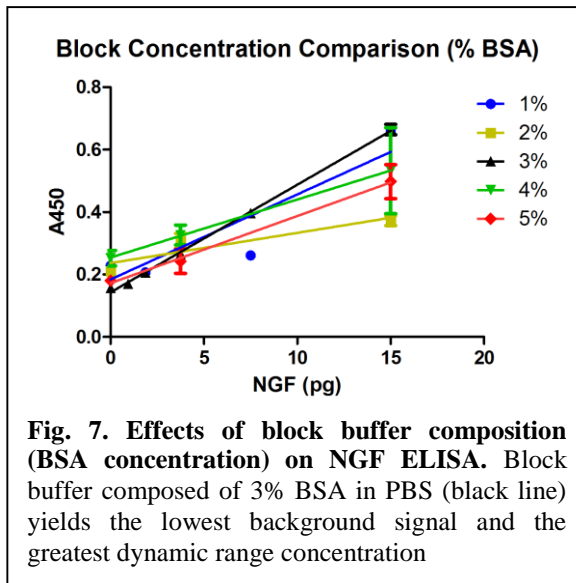
The provided Peprotech protocol recommends 1% BSA in PBS as block buffer.

We found this to produce sporadic results when the assay is performed with the sensitive

TMB substrate. Thus, to determine the ideal concentration of BSA to use with the

modified TMB-based protocol, NGF-protein standard curves were evaluated in assays

incorporating a range of BSA concentrations (1% to 5%) (Fig. 7). The blocking reagent plays a key role in sensitivity, as it directly impacts background absorbance and signal-to-noise ratio. If the concentration of BSA is too low, not all non-specific interactions between the 96-well plate and assay components will be prevented, leading to an increase in background signal. If the concentration of BSA is too high, non-specific interactions between assay components and BSA will occur, also leading to an increase in background and variation between replicates. The results indicate that 3% BSA achieves the lowest baseline and the greatest resolution between high and low concentrations of NGF.



Modification to the ELISA wash protocol

The recommended Peprotech protocol calls for four 300 μ L washes in PBS + 0.05% Tween-20 between each step of the assay. These washes are critical to minimizing carryover of ELISA components between stages, ensuring the final absorbance measurements are specific to the NGF titers from each individual sample. Standard laboratory protocol would utilize fresh pipette tips for each well for every wash, in order

to minimize cross-contamination and sample carryover. Due to the amount of samples and required washes, adhering to this technique would be cost prohibitive. To limit the cost per assay, we evaluated the effects of reusing the same pipette tips for all wells for a given wash. Figure 8 illustrates the effects of reusing pipette tips. The data suggests that the altered protocol has no significant detrimental effects on well-to-well variation, indicating minimal cross-contamination. For reasons not yet understood, the altered protocol does have a slight deleterious effect on overall signal intensity.

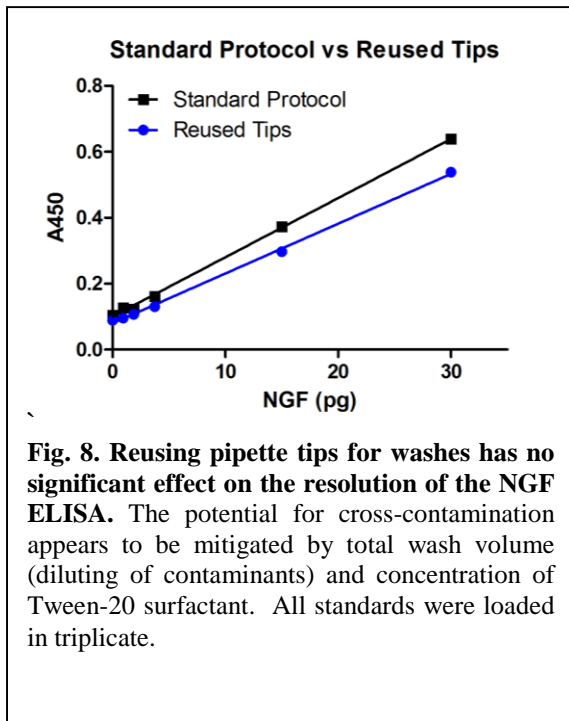


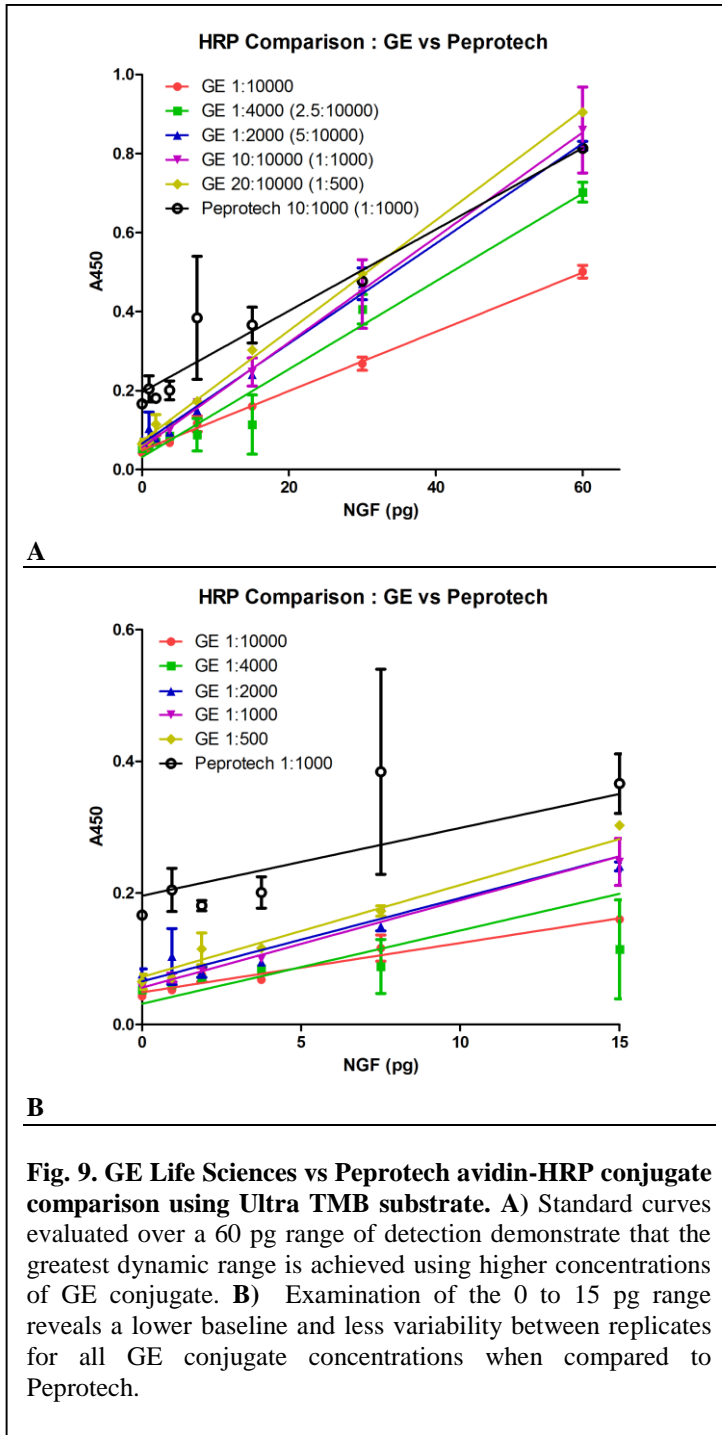
Fig. 8. Reusing pipette tips for washes has no significant effect on the resolution of the NGF ELISA. The potential for cross-contamination appears to be mitigated by total wash volume (diluting of contaminants) and concentration of Tween-20 surfactant. All standards were loaded in triplicate.

Overcoming assay variation resulting from the avidin-HRP conjugate

Peptotech supplies the avidin-HRP conjugate for the NGF ELISA development kit but does not provide information as to the original supplier. The conjugate comes in solution for distribution into 10 aliquots for storage at -20°C. We found that the solvent used to reconstitute the enzyme was prone to sublimation in frozen storage. Additionally, the assay seemed excessively prone to well-to-well variation when used with the Ultra

TMB substrate. These phenomena raised questions as to the quality of the HRP provided and its compatibility with the more sensitive substrate.

An alternative avidin-HRP conjugate (GE Life Sciences RPN1231) was evaluated at five different concentrations for comparison against the Peprotech provided HRP (at Peprotech's recommended concentration) (Fig. 9). Over a 60 pg range of detection, the GE conjugate provides a greater dynamic range (greater linear slope) than the Peprotech HRP when used at 1:2000 concentrations or higher (Fig. 9A). Additionally, the baseline value (background signal) is lower for GE conjugate across all evaluated concentrations (Fig. 9B). The well-to-well variation often seen with the Peprotech conjugate (depicted by the wide error bars for Peprotech replicates in Fig. 9A and Fig. 9B) is minimized using 1:1000 concentrations of GE conjugate or greater. Following these observations, a 1:1000 dilution of the GE avidin-HRP was chosen for use in future assays.



Determine the duration of TMB incubation

To further optimize the NGF

ELISA, the ideal length of TMB

incubation was evaluated. Following

addition of TMB to the ELISA plate, HRP

oxidizes the substrate into a colored

product until the reaction is stopped with

the addition of a strong acid (2M sulfuric

acid). Sensitivity is enhanced by

increasing the duration of TMB incubation

with HRP (Fig. 10). An increased reaction

time provides greater signal difference

between lower concentrations without

having an excessive negative effect on well-to-well variation between replicates. The

updated protocol, incorporating a 14 minute TMB incubation, establishes an assay

capable of reproducibly quantifying as little as 1 pg of sample in 100 μ L of solvent with a

linear range extending to 30 pg / 100 μ L solvent.

Other miscellaneous contributors to poor assay performance

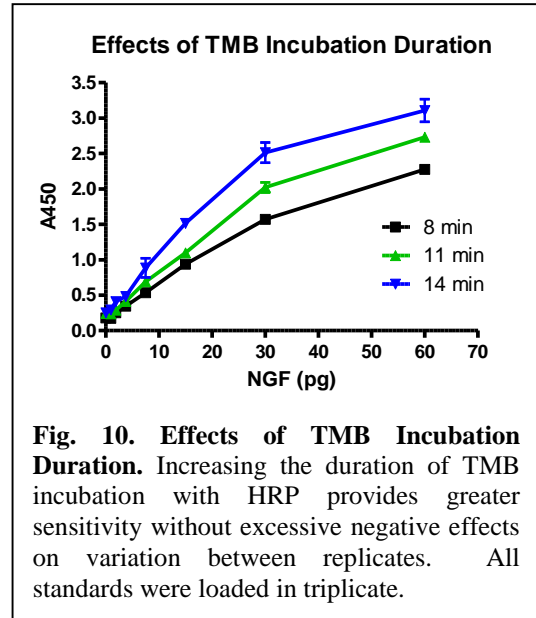
Throughout the course of this research, several other contributors to poor assay

performance or complete assay failure have been identified. As mentioned above, the pH

of PBS contributes greatly to overall performance, but it should also be noted that the

quality and age of the PBS stock solution also has an effect. Aged or potentially

contaminated PBS solutions are capable of causing total assay failure, a condition in



which nonlinearity and/or high variability between replicates is observed. The effects of using PBS made from a five month old 10X stock are presented in Figure 11. To prevent these occurrences, master stock solutions (10X PBS) must be autoclaved, stored at room temperature, and used within three months of preparation.

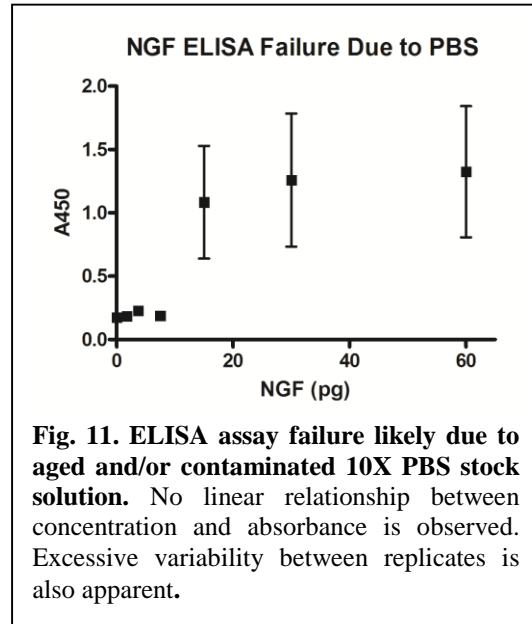


Fig. 11. ELISA assay failure likely due to aged and/or contaminated 10X PBS stock solution. No linear relationship between concentration and absorbance is observed. Excessive variability between replicates is also apparent.

It is also noteworthy that the preparation and subsequent autoclaving of 1X PBS working solutions causes significant changes in pH, leading to poor assay performance (data not shown). Sterile filtration was evaluated as an alternative, but was cost-prohibitive for the amount of assays required by the study. We found that preparation and pH adjustment of fresh 1X PBS (from autoclaved 10X PBS) immediately before beginning the assay was the best method to mitigate assay performance issues from PBS.

Also of note was an increase in background absorbance (absorbance at 0 pg NGF) in the ELISA over time. Basal absorbance at 450 nm for the assay is usually approximately 0.3 au. During the course of this research, we observed a significant rise in this baseline absorbance value. While the most obvious culprit of this phenomenon was the status and quality of bovine serum albumin (BSA) used as a blocking reagent, a new

stock of BSA did not completely resolve the issue (data not shown). We observed that the response was also linked to Tween-20 and TMB. As illustrated in Figure 12, new stocks of Tween-20 and TMB were required to return the background to the expected value and restore resolution at lower concentrations. While no concrete shelf-life can be confirmed for these reagents (the phenomenon did not occur again during the project), both

components should be considered when deterioration in assay performance is observed.

Effects Relating to Cell Culture Media

Effects of media components on the NGF ELISA

Having established the ELISA conditions using purified recombinant hNGF, we next set out to determine if media components would influence the assay. The NGF ELISA was performed using either diluent (standard baseline), Dulbecco's Modified Eagle's Medium + 10% Fetal Bovine Serum (DMEM + 10% FBS; the standard growth medium for the T98G cultured human glial cells), DMEM alone, FBS alone, OptiMEM (a reduced serum media), and OptiMEM + 5% BSA (OptiMEM-B; the addition of a carrier protein such as BSA is expected to facilitate NGF recovery from conditioned

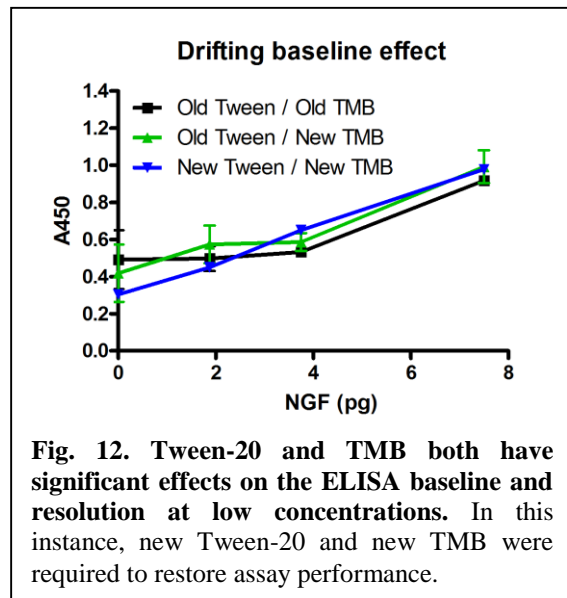
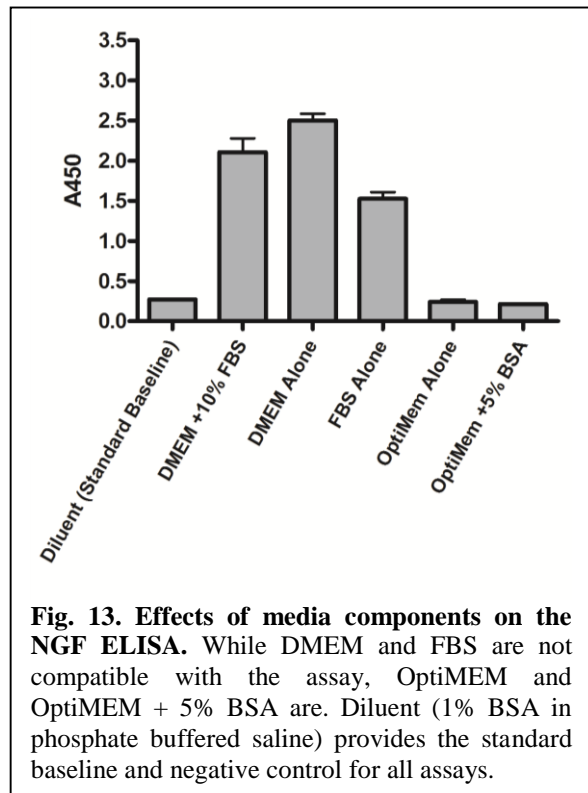


Fig. 12. Tween-20 and TMB both have significant effects on the ELISA baseline and resolution at low concentrations. In this instance, new Tween-20 and new TMB were required to restore assay performance.

media). As illustrated in Figure 13, the results illustrate how the media alone can affect the ELISA results. It is clear that DMEM and FBS each contain a component that causes a significant increase in the ELISA signal. As a result, the ELISA cannot be performed in the presence of either of these solutions. On the other hand, OptiMEM and OptiMEM-B are both compatible with the NGF ELISA.



Stability of extracellular NGF

To reliably quantify the amount of NGF secreted by glial cells into media, it was necessary to confirm that secreted NGF would not be degraded or endocytosed by cells in the media. The stability of extracellular NGF in OptiMEM media was assessed by amending the media with 200 pg/mL of recombinant hNGF and incubating the media over confluent T98G cells for 1 hour, 2.5 hours, and 8 hours (Fig. 14). Upon recovery, the NGF titers in the media were determined using the NGF ELISA (assay results are commonly reported in pg NGF/mL media). Even in the absence of BSA, NGF is stable and completely recoverable from OptiMEM media for at least 8

hours. This confirms that the protein is not lost to cell-binding, potential extracellular protease activity, association with media components, or sorption to cell culture plasticware.

Effects of conditioned-media storage on the NGF ELISA

Our SMI study requires time course data evaluating multiple time points within a 24-hour window of small molecule exposure to glial cells. The ability to store and recover conditioned media without loss of protein would facilitate the collection of all samples prior to the simultaneous assessment of all

samples using the ELISA. In order to determine the effects of freezing conditioned media on downstream ELISA performance, both 8-hour conditioned media supplemented with 200 pg/mL recombinant hNGF and unamended 8-hour conditioned media were subjected to one freeze thaw cycle and NGF titers were assayed using the ELISA. The results show significant loss of NGF protein titers after one freeze thaw cycle (Fig. 15). Repeated cycles cause further loss of NGF protein (data not shown).

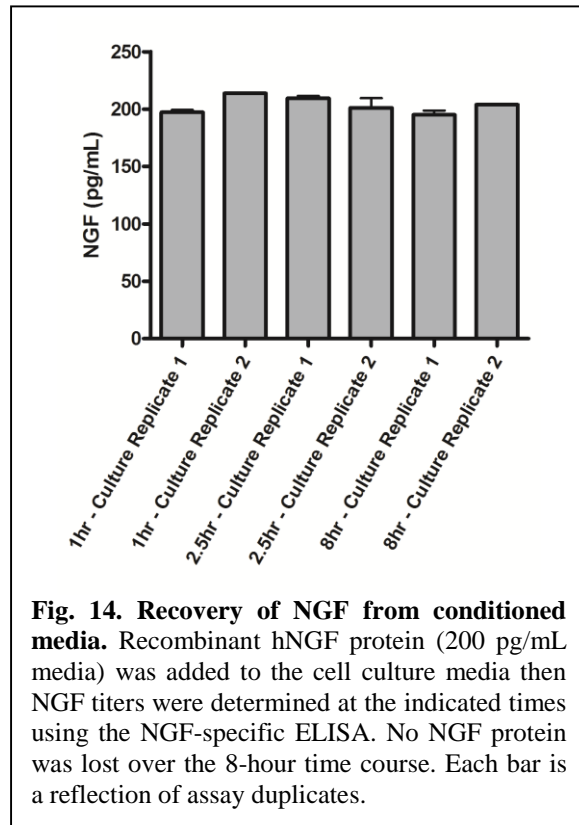
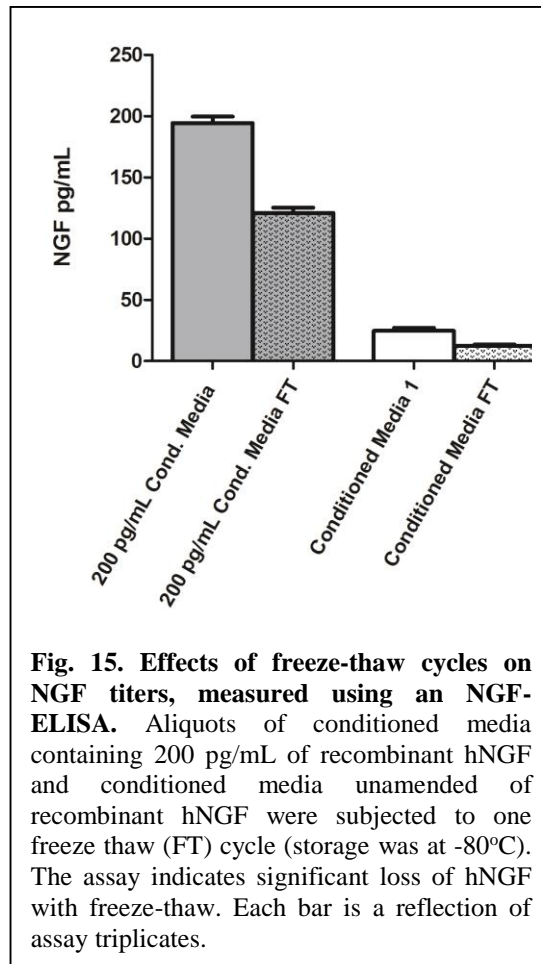
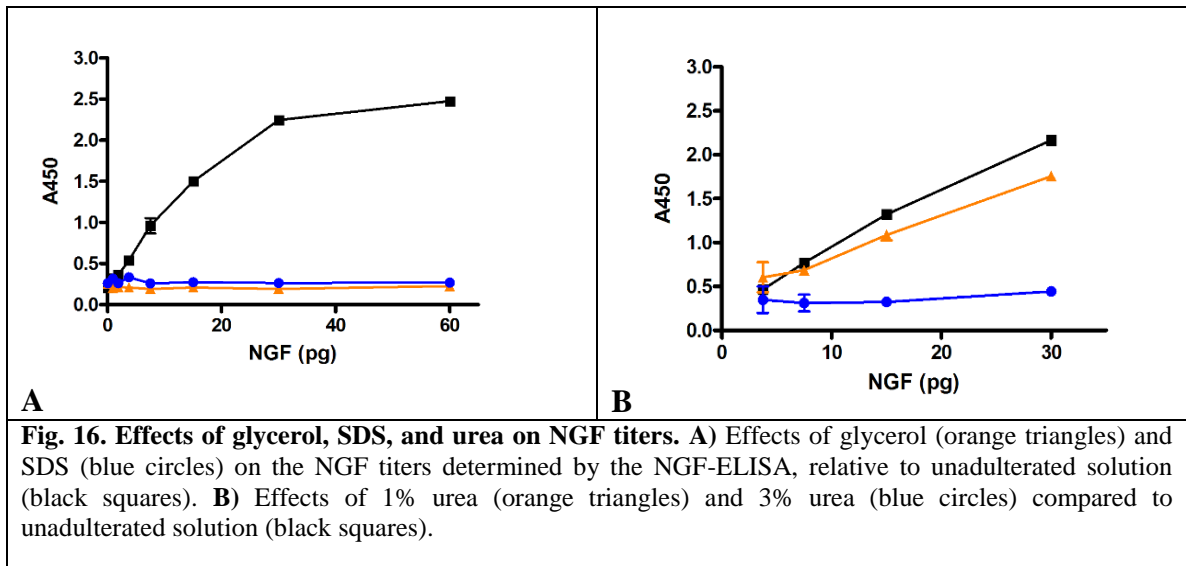


Fig. 14. Recovery of NGF from conditioned media. Recombinant hNGF protein (200 pg/mL media) was added to the cell culture media then NGF titers were determined at the indicated times using the NGF-specific ELISA. No NGF protein was lost over the 8-hour time course. Each bar is a reflection of assay duplicates.

Urea, glycerol, and SDS were each considered as agents to stabilize NGF and enhance its recovery after freeze-thaw cycles. To determine if these additives were compatible with the NGF-ELISA, recombinant hNGF was prepared with each additive and standard curves were evaluated in comparison to an unadulterated standard. (Fig. 16). The results reveal that glycerol and SDS cause complete assay failure (Fig. 16A). Urea at 1% causes a suppression of NGF detection, whereas 3% urea also leads to complete assay failure (Fig. 16B). Hence, it is clear that the NGF-ELISA performs best without the addition of these compounds. Consequently, rather than seek alternative stabilizing additives, we elected to simply avoid freeze-thaw cycles in all subsequent assays. The resulting experimental design requires that all time course evaluations be performed in a manner in which all samples complete their incubations simultaneously (i.e. the initial exposure to SMI is staggered).





Using the optimized ELISA to determine the SMI dose-response

Overview

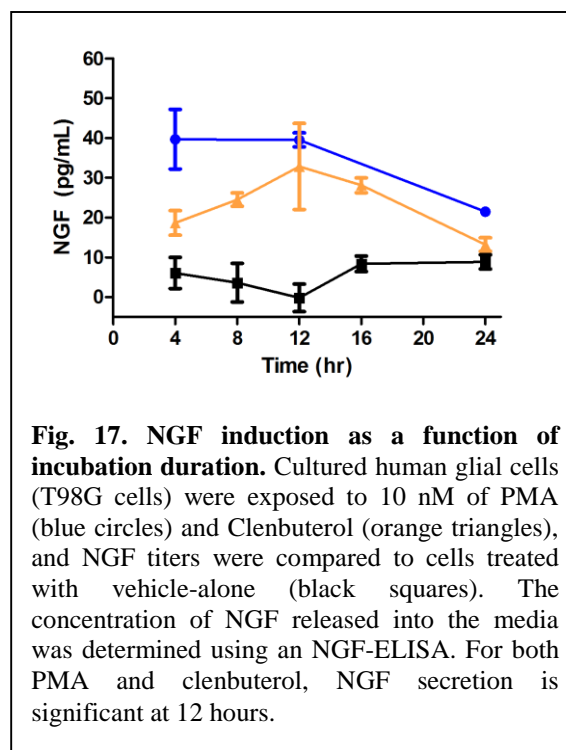
In order to minimize off-targeting (binding of the SMI to lower affinity protein targets in the cell due to excessive concentration of SMI) while still maintaining substantial NGF induction, the half maximal effective concentration (EC_{50}) for each SMI is desirable in pathway analysis. However, high concentrations of SMI achieved when determining the dose-response can cause significant off-targeting and apoptosis that prevent the sigmoidal dose-response plot necessary for clear EC_{50} determination. Additionally, while the dose-response is typically determined at a fixed time point, the effectiveness of an SMI can vary with incubation duration. For example, a given concentration of SMI may be effective at generating NGF secretion after a 4-hour exposure time, but may generate no detectable NGF induction after one hour, and vice versa. These phenomena were considered in multiple ways throughout this analysis.

As detailed below, NGF secretion at incubation durations spanning from 4 hours to 24 hours was first measured for PMA (a Protein Kinase C effector) and Clenbuterol (a Protein Kinase A effector) at 10 nM to identify an ideal incubation duration for EC₅₀ determination. Then, after establishing a 12-hr incubation duration was suitable, NGF secretion was assayed with glial cell exposure to varying concentrations of PMA, Clenbuterol, or Forskolin.

The T98G glial cell line was chosen for all experiments involved in this study. This glioblastoma cell line becomes arrested in G1 phase in response to stationary phase conditions and confluence¹⁰⁸ (which is experimentally achieved by transferring the cells from DMEM + 10% FBS media to OptiMEM-B media once they reach confluence), making T98G cells better suited as a brain cell model in comparison to other continually dividing glial cell lines. Additionally, the T98G cell line is well documented for its ability to express the NGF gene and secrete NGF protein¹⁰⁹.

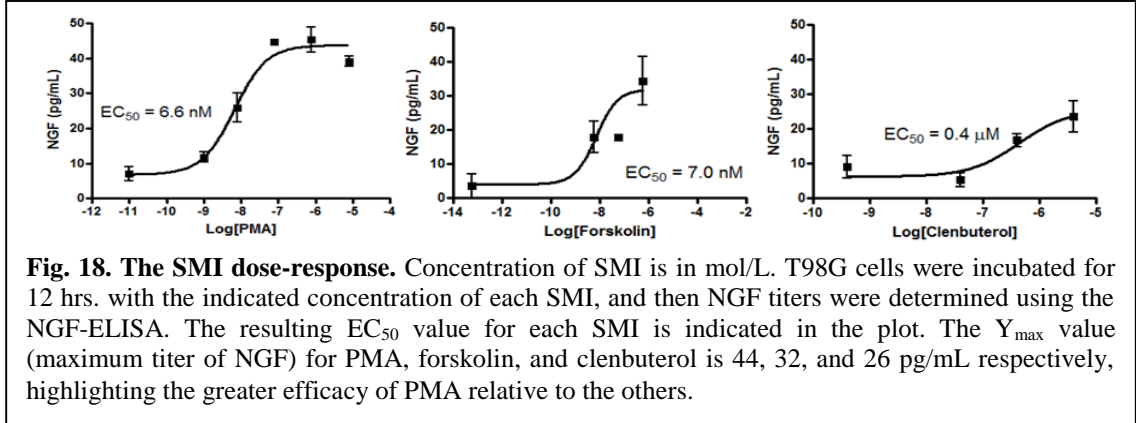
24-hour time course survey of PMA and Clenbuterol

PMA and clenbuterol are both known inducers of NGF secretion^{110,111}. To define an optimal duration of SMI exposure for EC₅₀ determination (i.e. the incubation duration netting the peak amount of NGF released from glial cells), cultured human glial cells were incubated with 10 nM of each SMI for various durations and NGF titers in the isolated culture media were determined using the optimized ELISA. The results (Fig. 17) suggest that a 12-hour incubation duration is suitable for EC₅₀ determination of compounds targeting the PKA pathway (i.e. Clenbuterol) as well as the PKC pathway (i.e. PMA).



Dose response for PMA, forskolin, and clenbuterol with a 12-hour incubation duration
 In light of the above results, the dose-response correlation between SMI

concentration and NGF secretion was then evaluated with a 12-hour incubation (Fig. 18). All three compounds illustrate a sigmoidal dose response. PMA, an agonist of PKC, is the most potent SMI with an EC₅₀ value of 6.6 nM. Forskolin, a PKA pathway agonist, was similar (EC₅₀ of 7.0 nM), but maximal NGF secretion was lower when compared to



PMA. Clenbuterol, also a PKA pathway agonist, achieved half-maximal NGF secretion at 0.4 μM.

Specific Aim 1 Conclusions

Specific Aim 1 has been completed as planned. A sensitive and reproducible assay protocol for the NGF ELISA was optimized to accommodate our specific cell culture/SMI system, using TMB rather than ABTS. The effects of media composition and the approach to storing conditioned media containing induced NGF protein were explored and highlighted OptiMEM and OptiMEM-B as ideal media, while underscoring the importance of not freeze thawing the conditioned media samples before analysis. A time course of NGF induction revealed an optimal duration of SMI exposure (12 hrs.), resulting in maximal NGF secretion from the cultured human glial cells. Subsequent assays with PMA, forskolin, and clenbuterol produced sigmoidal dose-response curves,

indicative of a specific SMI/target interaction, and revealing their EC₅₀ concentrations (6.6 nM, 7.0 nM, and 400 nM, respectively).

Specific Aim 2 – Quantitative PCR to Assess Small Molecule Induction of NGF Gene Expression

Specific Aim 2: Quantitative PCR to Assess Small Molecule Induction of NGF Gene Expression. In addition to causing NGF secretion, small molecules that also upregulate NGF gene expression are preferred for use in NGF-based AD therapies. In order to assess changes in NGF gene expression in response to each SMI, a real-time PCR-based assay will be developed and used to quantify NGF transcript levels.

Small molecules that upregulate NGF gene expression are best suited for use in NGF-based therapies as they have the ability to induce *de novo* synthesis of NGF protein^{112,113}, rather than just causing the secretion of NGF already stored within vesicles of the cell cytosol^{114,115}. Protein synthesis would enable a continuous supply of NGF to be secreted for the purpose of neuroprotection. In order to assess changes in NGF gene expression as a response to SMI, a real-time PCR assay was developed to quantify NGF transcript levels in treated versus untreated cells. Development of such an assay required the identification of stable reference genes (to normalize transcript abundance in cell lysates) and determination and validation of gene-specific primers. Steps involving RNA extraction from whole cell lysates, reverse transcription of mRNA into cDNA, quantitative PCR, and comparative C_T analysis were developed and optimized to provide

a reliable and reproducible assay to discern if small molecule induction of NGF was accompanied by an upregulation of NGF gene expression.

As detailed in the sections that follow, in order to perform the quantitative PCR, primers specific to gene expression products for NGF and the control genes, beta-actin (Actb) and TATA-box binding protein (Tbp), were designed to ensure explicit binding to target sequences. To validate the designed NGF exon-specific PCR primers, a bacterial plasmid containing a NGF cDNA insert was also prepared. PCR was performed using the gene specific primers against plasmid DNA as well as cDNA obtained from T98G cell lysates following RNA extraction and reverse transcription. Agarose gel electrophoresis was used to evaluate PCR products for the presence of only one amplicon of the expected size. Melt-curve analysis in qPCR was performed to obtain a melt point for each amplicon for the purpose of quality control in downstream qPCR assays. The constitutively expressed control genes, beta-actin and TATA-box binding protein, were chosen as reference genes due to their stable expression in related neuronal cells¹¹⁶, and qPCR assays performed here confirmed unchanging expression of these genes in T98G cells treated with various SMIs of NGF (or vehicle alone). Primer efficiency was evaluated and confirmed that the primers are robust and ideal for use in real-time PCR assays.

Gene Specific Primer Sequences

Sequence specific primers for β -NGF, TATA-box binding protein, and β -actin were designed using gene sequence information obtained from the National Center for Biotechnology Information (NCBI). The NGF protein consists of three types of subunits

(alpha, beta, and gamma) which associate to form a 130 kDa complex. This complex contains two identical 118 amino acid β -chains, which are responsible for the nerve growth stimulating activity of NGF. The recombinant hNGF used in ELISA development is composed of the β -NGF sequence, and the β -NGF transcript was selected for monitoring NGF gene expression in the cultured human glial cells. For β -NGF and TATA-box binding protein, the forward and reverse primers were intentionally designed to anneal separate exons flanking an intron, thereby resulting in cDNA amplification products that are shorter than gDNA amplification products (PCR products from gDNA would contain the intron sequence in addition to the exon sequence, thus the primer design facilitates identification of contaminating gDNA by size and altered amplicon melting temperature). Additionally, the gDNA amplicons from Tbp and NGF primed PCR are too lengthy (2405 kb and 7013 kb, respectively) to amplify during the short (15 second) PCR extension cycles in the real-time assay (the processivity of the polymerase is approximately 1 kb/min). The configuration of the exons and introns that define the β -actin gene did not permit an intron-flanking primer design and the resulting gDNA and cDNA amplicons are of the same size. TATA-box binding protein was used as a reference gene for all qPCR assays related to this project, while β -actin was also utilized in various experiments to further confirm reference gene stability. The designed primers are listed in Table 2.

Table 2. Primer sequence information for NGF gene and control genes TATA box binding protein (TBP) and beta-Actin (Actb).

Gene	Primer Sequence	Amplicon gDNA (bp)	Amplicon cDNA (bp)	Melting Temp. (°C)	NCBI Ref. ID	Gene ID
Beta-Actin	F- CAGGTCATCACCATTGGC AATGAG R- ACAGGACTCCATGCCAG GAAG	81	81	F – 71 R – 71	NM_001101	60
Beta-NGF	F- CCAATAACAGTTTTACCA AGGGAGCAGC R- CAAGGGAATGCTGAAGTT TAGTCCAGTG	7014	194	F – 71 R – 71	NM_002506.2	4803
TATA-box binding protein	F- CCACAGTGAATCTTGGTT GTAAACTTGACC R- GTGGTTCGTGGCTCTCTT ATCCTC	2405	121	F – 68 R – 69	NM_001172085.1	6908

Transformation of E. coli with a plasmid containing an NGF cDNA

In order to validate the NGF-specific primers, a human cDNA of the β -NGF gene, cloned in the pCMV6-XL5 vector (Fig. 19A), was purchased from OriGene Technologies and transformed into *E. coli* XL1 blue following standard protocols¹¹⁷. The plasmid contains the full length cDNA sequence for β -NGF, as well as a β -lactamase gene to confer ampicillin resistance to the transformed *E. coli* cells. To confirm plasmid uptake, transformants were plated on Luria-Bertani (LB) agar plates containing 100 μ g/mL ampicillin. Viable colonies were selected and used to inoculate an overnight liquid culture of LB media (37°C, 250 rpm, 120 μ g/mL ampicillin). Following incubation, an aliquot of cells was transferred to a glycerol solution (final concentration 20% glycerol) and placed in a -80°C freezer for long-term storage. The remaining cells were pelleted

(4000 rpm, 4°C) and plasmid DNA was extracted using Plasmid Miniprep Kits (GenElute) according to the manufacturer's protocol. The plasmid sequence was confirmed using a series of restriction enzyme digests (Fig. 19B).

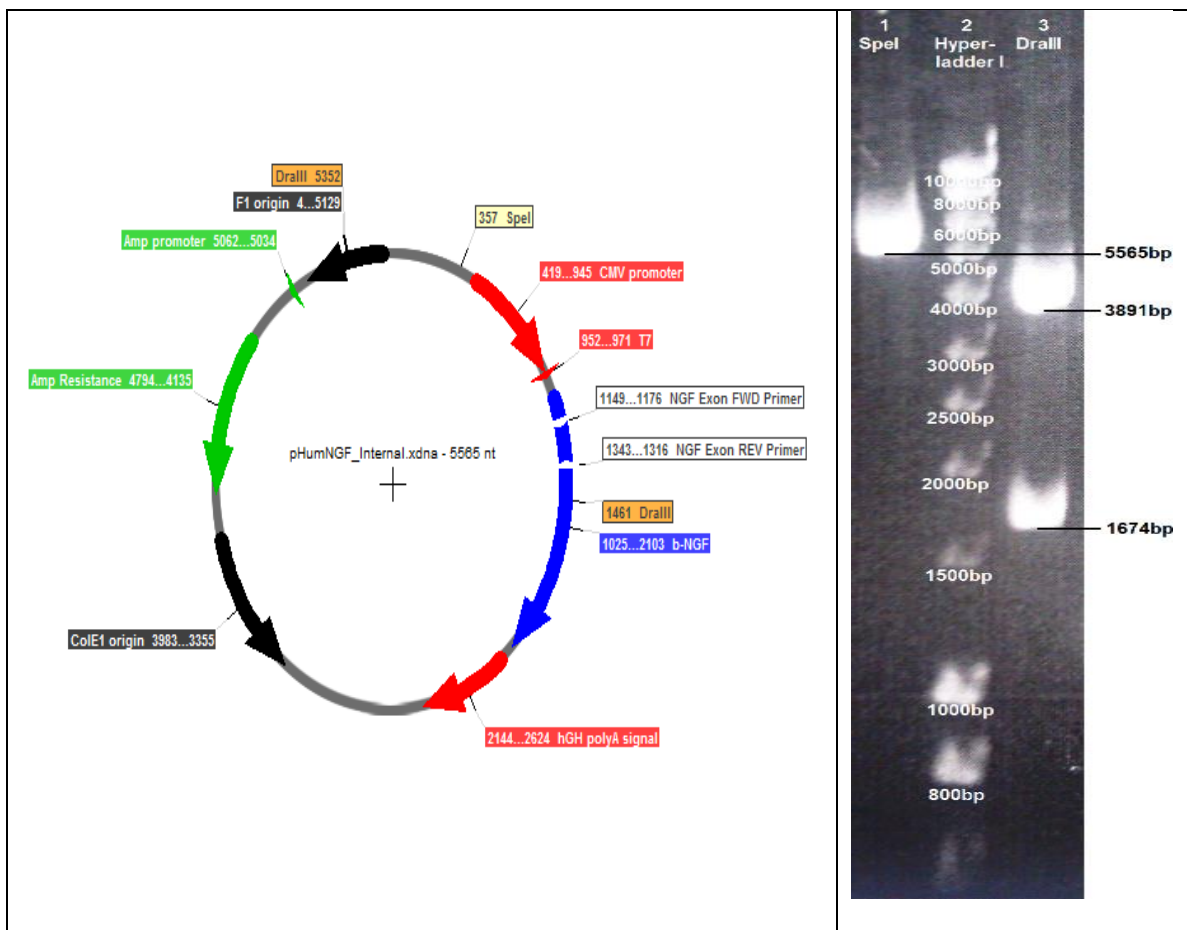


Fig. 19. pHumNGF_Internal plasmid. **A)** Plasmid map of pHumNGF_Internal.xdna, a pCMV6-XL5 plasmid containing human NGF-beta cDNA. The binding sites for the NGF specific primers are shown (FWD and REV primer) which generate a 194 bp amplicon from the cloned NGF cDNA. **B)** Restriction enzyme digest of pHumNGF_Internal.xdna with SpeI and DraIII restriction endonucleases. Single cut using SpeI yields one product of the expected size: 5565 bp. Two restriction sites exist for DraIII, yielding two products of 3891 bp and 1674 bp respectively.

Agarose gel electrophoresis and qPCR melt curve analysis to confirm sequence specific amplification

Following the execution of a real time PCR assay, melt curve analysis is often used to determine the melting temperature of newly synthesized amplicons. The presence of a single peak indicates that the PCR is generating only one product. By performing agarose gel electrophoresis (Fig. 20) following qPCR and melt curve analysis (Fig. 21), a correlation between melting point values and specific amplicon can be established. In melt curve analysis, the temperature in the PCR chamber is raised by 0.1°C increments until the DNA denatures, causing a dramatic change in detected SYBR dye fluorescence. Melting temperatures observed in the melt curve analysis are reproducible, varying by no more than 0.2°C between all assays. Thus, deviation in excess of 0.2°C in the assay is an indicator of contamination and/or non-specific binding leading to untargeted amplification. In agarose gel electrophoresis, the completed PCR product is separated by electrophoresis through a 2% agarose gel, then the DNA is stained with ethidium bromide and examined under UV light. Comparison to a molecular weight marker confirms the presence of a single, size-specific product.

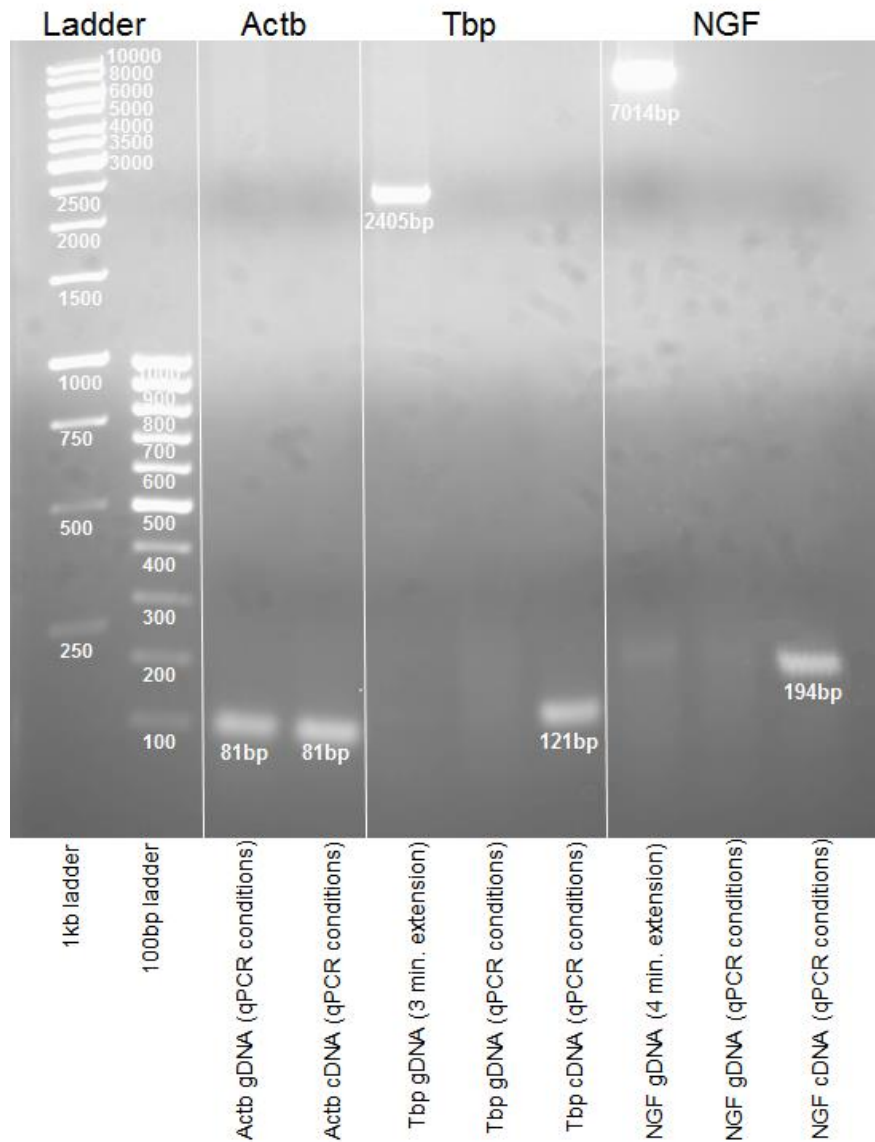
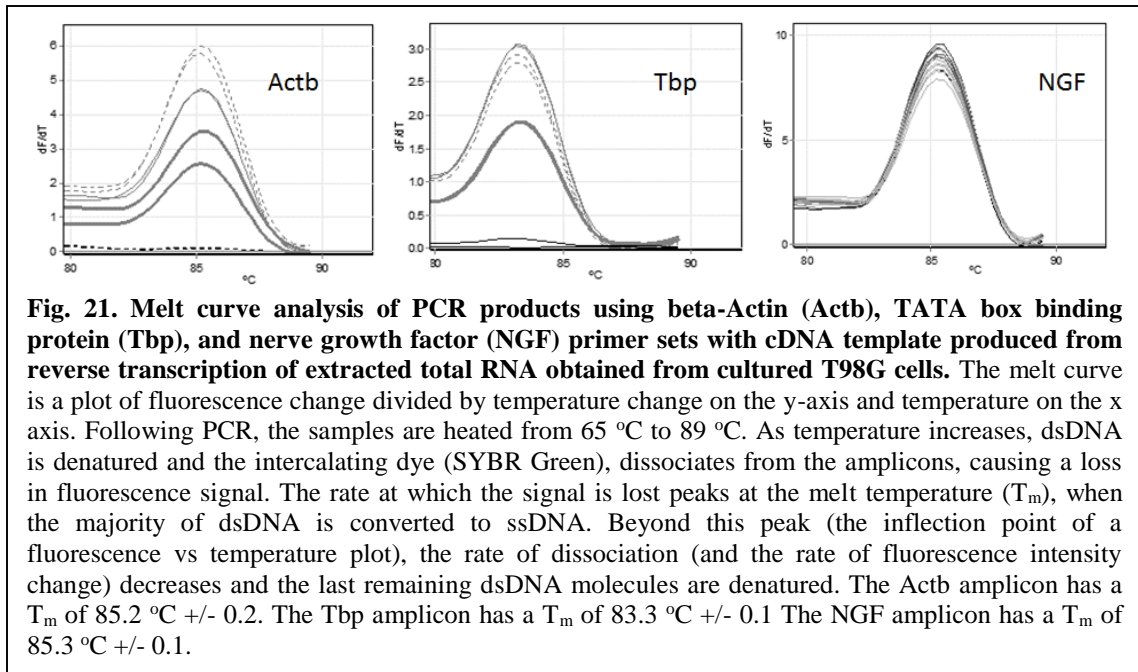


Fig. 20. Agarose gel electrophoresis (2% w/v) confirming the presence of only one, size-specific amplicon for the Actb, Tbp, and NGF primer sets. A high molecular weight marker (1kb ladder) and low molecular weight marker (100 bp ladder) are included in the gel. Actb primers generate 81 bp amplicons from both cDNA template and gDNA template as expected. Tbp primers generate the 2405 bp band expected from gDNA only when provided with a 3-minute PCR extension time, as anticipated. Under standard qPCR conditions (15 second extension), no gDNA amplicon is present. Rather, qPCR conditions produce the anticipated 121 bp amplicon expected from cDNA. While the NGF specific primer pairs generate an expected 7014 bp PCR product predicted with gDNA template (and a 4-minute extension time), with qPCR a single 194 bp band is produced with cDNA as template. Overall, these results clearly demonstrate the specificity of the Actb, Tbp, and NGF PCR primer sets, and illustrate that genomic DNA contamination of cDNA will not be of concern for the qPCR-based analysis.



Confirming primer efficiency

Before the Actb, Tbp, and NGF primer sets can be used in quantitative PCR assays, primer efficiency for each primer set must be determined. Primer efficiency indicates the ability of a primer set to give linear results (amplification vs. template concentration) in a quantitative PCR assay with maximum reproducibility, sensitivity, and dynamic range. Primer efficiency is quantified by performing a dilution series on a confirmed template (e.g. the pHumNGF_Internal.xdna plasmid or cDNA prepared from extracted glial RNA) and evaluating C_T versus template abundance (C_T : Cycle Threshold, which is based on the increase of normalized fluorescence between two successive cycles). The C_T values of 10-fold dilutions will be 3.3 cycles apart (2-fold

change per cycle. $2^n=10$, $n = 3.3$). Thus, a C_T vs. template concentration graph should show a slope of -3.3 if there is 100% primer efficiency. Primer efficiencies greater than 90% are considered excellent for use in quantitative PCR¹¹⁸.

The primer efficiency was determined for the NGF primer set using five 10-fold serial dilutions of pHumNGF_Internal.xdna plasmid as template in the quantitative PCR (the qPCR was performed using a Qiagen Rotor-Gene Q real time PCR machine). Raw fluorescence data (Fig. 22A) was used by the Qiagen software to generate a C_T vs concentration plot (Fig. 22B). The C_T vs. concentration plot for the NGF primer set has a slope of -3.461, indicating a primer efficiency of 94.5%.

$$\text{NGF Primer Efficiency} = 10^{(-1/3.461)} - 1 = 1.945 - 1 = 94.5\% \text{ primer efficiency}$$

Hence, the NGF-specific primers are well suited for use in quantitative PCR.

Likewise, primer efficiency evaluations were repeated for Actb (Fig. 23) and Tbp (Fig. 24), but with cDNA template prepared from extracted glial cell RNA. As found with the NGF primer set, the Actb and Tbp primer sets are both within desirable efficiency values (101% and 95%, respectively).

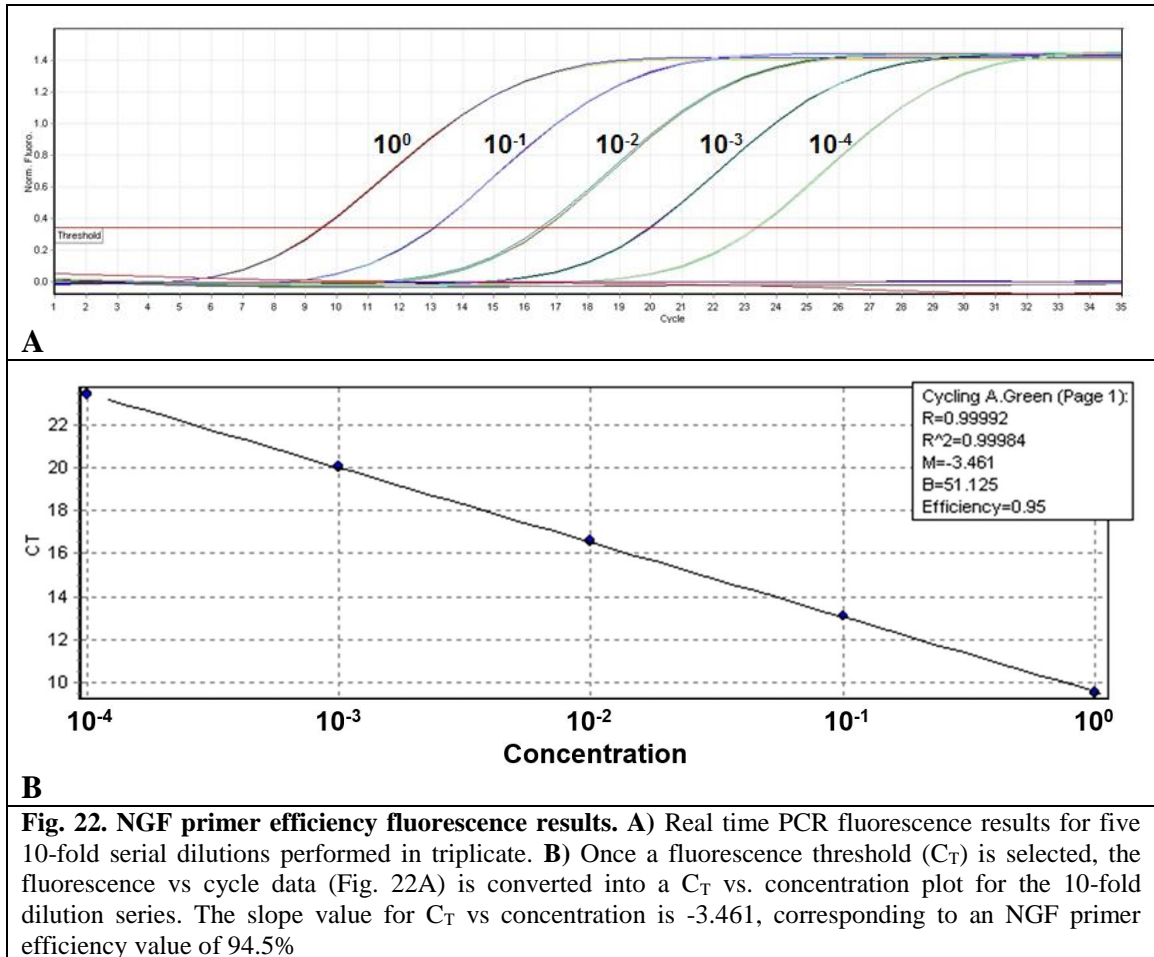
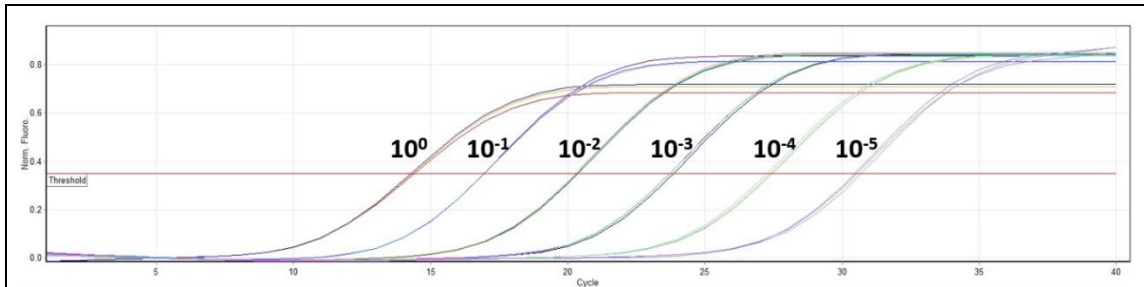
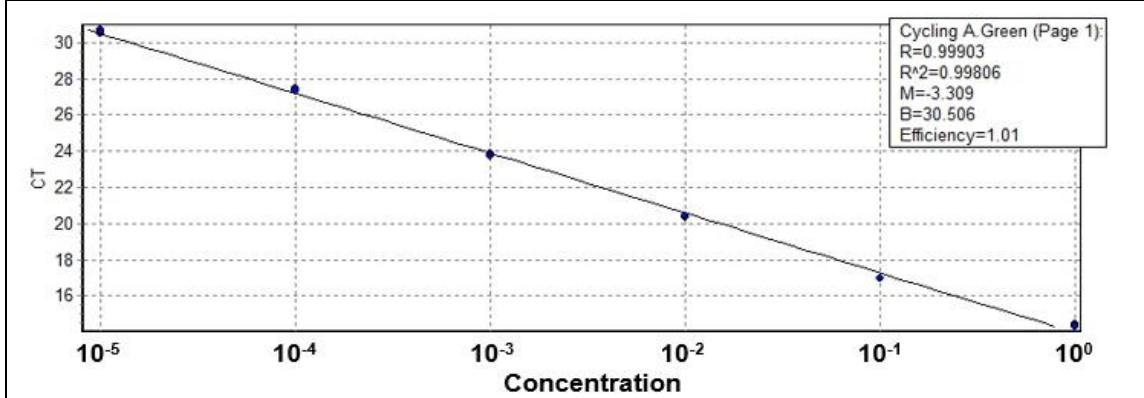


Fig. 22. NGF primer efficiency fluorescence results. **A)** Real time PCR fluorescence results for five 10-fold serial dilutions performed in triplicate. **B)** Once a fluorescence threshold (C_T) is selected, the fluorescence vs cycle data (Fig. 22A) is converted into a C_T vs. concentration plot for the 10-fold dilution series. The slope value for C_T vs concentration is -3.461, corresponding to an NGF primer efficiency value of 94.5%

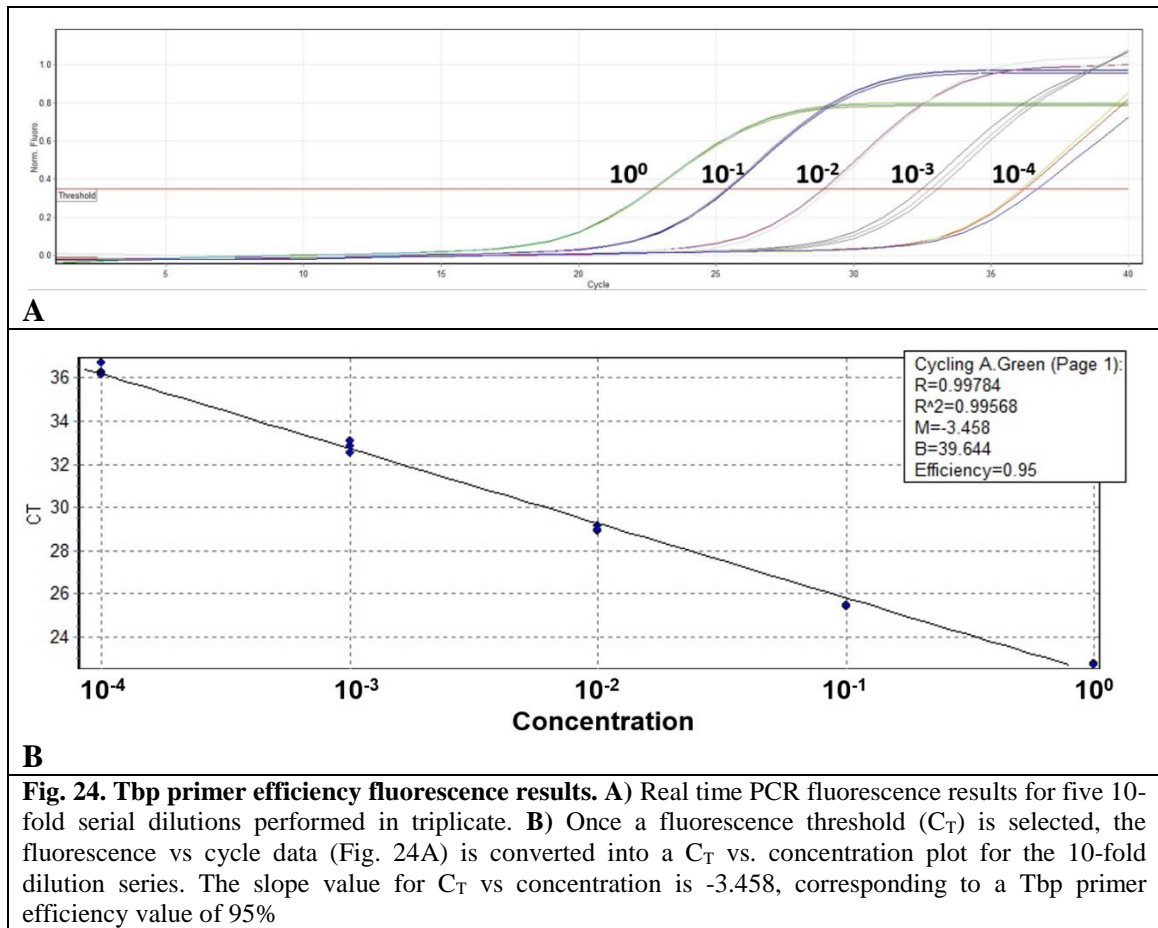


A



B

Fig. 23. Actb primer efficiency fluorescence results. A) Real time PCR fluorescence results for five 10-fold serial dilutions performed in triplicate. **B)** Once a fluorescence threshold (C_T) is selected, the fluorescence vs cycle data (Fig. 23A) is converted into a C_T vs. concentration plot for the 10-fold dilution series. The slope value for C_T vs concentration is -3.309, corresponding to an Actb primer efficiency value of 101%



Real time PCR amplification of NGF mRNA in SMI treated samples – The Goal of Specific Aim 2

Having validated the qPCR assay, attention turned to quantifying transcript abundance in SMI stimulated cultured glial cells. Total RNA was isolated from cells using a commercially available RNA extraction kit (Qiagen RNEasy). Immediately following RNA extraction, the quantity and purity of the RNA was evaluated using UV-Vis spectroscopy. For each sample, the absorbance at 260 nm (A_{260}) and 280 nm (A_{280}) was determined before proceeding with reverse transcription and real time PCR. A_{260} is

used to quantify the nucleic acid content in the sample, as one absorbance unit signifies 40 $\mu\text{g/mL}$ of RNA¹¹⁹. This measure is then used to guide the preparation of 1 μg of RNA per reverse transcription reaction, normalizing the amount of nucleic acid in each extraction before proceeding with the downstream PCR. Additionally, the ratio of A_{260} to A_{280} provides insight as to the extent of protein contamination in the extracted RNA. A ratio of 1.8 or greater indicates high RNA purity and low protein contamination (samples with ratios <1.8 are either discarded or undergo phenol:chloroform extraction to remove the contaminating protein). The UV-Vis spectroscopy results for the extractions are presented in Table 3.

Table 3. UV-Vis spectroscopy evaluation of RNA

Sample	A_{260}	A_{280}	A_{260}/A_{280}	Dilution Factor	RNA ($\mu\text{g/mL}$)	RNA for RT (μL)
PMA-10 μM	1.4995	0.73619	2.037	4.333	259.9	3.85
PMA-10 nM	0.95715	0.46956	2.038	4.333	165.9	6.03
DMSO	0.61637	0.30071	2.050	4.333	106.8	9.36

UV-Vis spectroscopy evaluation of RNA. Extraction purity and quantification of RNA was determined for samples obtained from cultured T98G glial cells treated with either 10 μM PMA, 10 nM PMA, or vehicle alone (DMSO). A_{260}/A_{280} values are all in excess of 1.8, indicating high purity RNA with low protein contamination. The table also indicates the volume of RNA used to add 1 μg of template to the reverse transcription (RT) reactions. Note that this was also performed with the SMIs clenbuterol, forskolin, and carnosol (data not shown).

To generate cDNA from the isolated total RNA, reverse transcription is then performed using M-MuLV reverse transcriptase (Promega), random hexamers (Promega) as primers, and 1 μg of the RNA template, as detailed in *Materials and Methods*. The

subsequent real time PCR is performed using 100 ng of newly synthesized cDNA. Biological triplicates, technical duplicates, no-template controls, and RNA-template controls (i.e. no reverse transcription step to produce cDNA) are used in the real time PCR assay. During each cycle of PCR, the abundance of the specific amplicon (determined by the primer set used) increases, causing an increase in fluorescence by the DNA intercalating agent SYBR green. The change in fluorescence between cycles directly correlates to the amount of transcript present in the original sample. Once the fluorescence reaches a threshold value (set by the user), the cycle at which the threshold is reached is recorded as the C_T value, a measure of transcript abundance. The threshold for any given qPCR experiment is set at least 10 standard deviations above the mean of the experimental background fluorescence, but below the inflection point of fluorescence versus cycle for all samples¹²⁰. Fewer cycles are required to reach the threshold if more transcript is present in the original sample. Thus, for the control genes (reference genes), no change in transcript abundance is anticipated with SMI treatment of the cultured glial cells, and thus all C_T values will be equal (in untreated vs SMI treated cells). These principles are illustrated in Figure 25A and Figure 25B. However, for the NGF gene, higher amounts of NGF transcript should exist for treated samples versus untreated samples, and thus the C_T values will be lower (Fig. 25C).

Comparative C_T analysis is then performed to determine the fold change in gene expression between treated and untreated samples. In comparative C_T analysis, the difference in transcript abundance between the gene of interest (in this case NGF) and a reference gene (Actb or Tbp) is recorded as ΔC_T and used to normalize the results against

biases unrelated to treatment by SMI (cell state, extraction efficiency, reverse transcription efficiency, etc.). Finally, ΔC_T values are compared between treated and untreated samples, using $2^{-\Delta\Delta C_T}$ to quantify fold change. An example of this process is presented in Table 4, with PMA as the tested SMI.

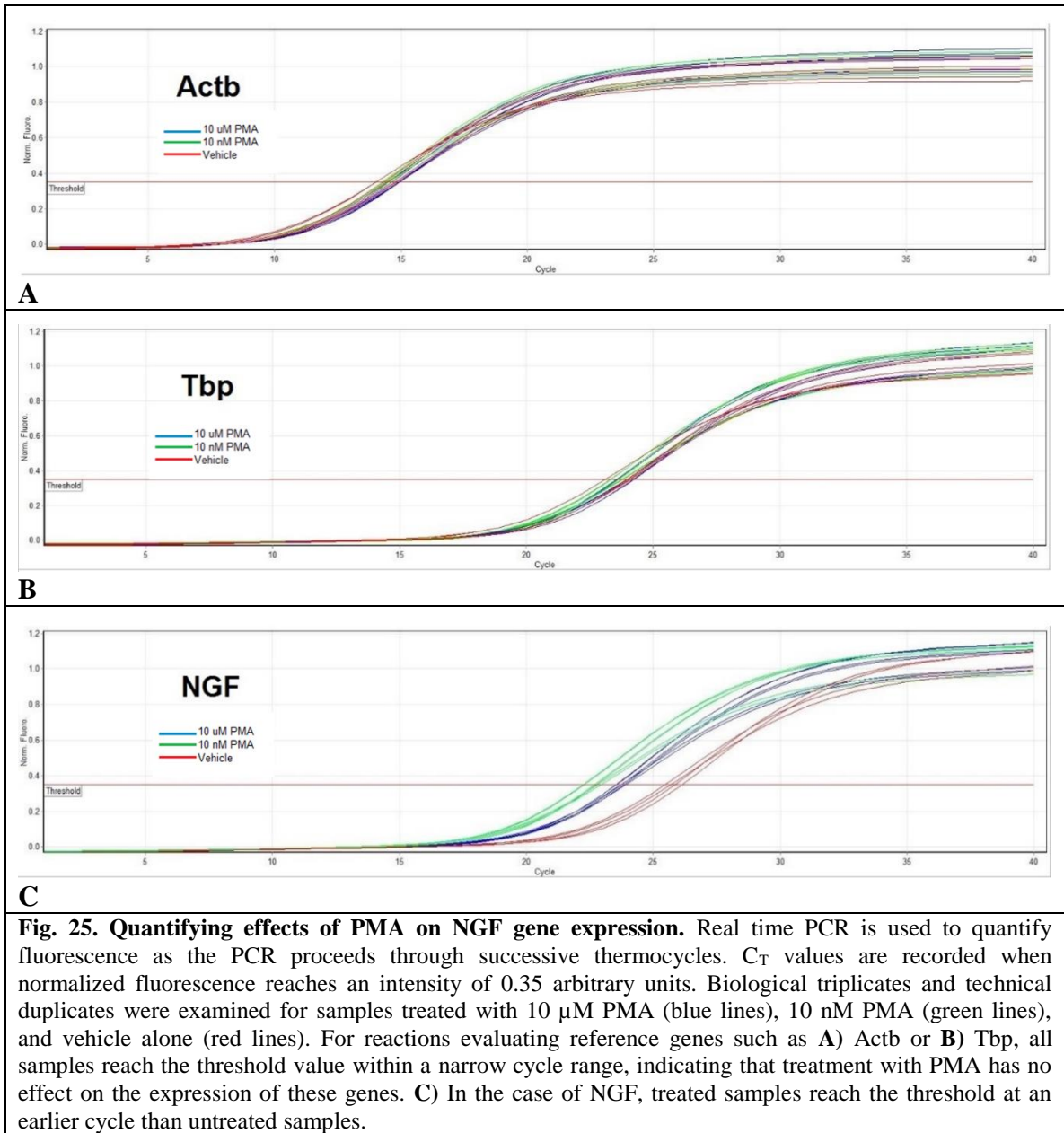


Table 4. Fold change in gene expression in PMA treated glial cells.

Sample	Mean C _T	$\Delta C_{T \text{ Actb}}$	$\Delta C_{T \text{ Tbp}}$	$\Delta\Delta C_{T \text{ Actb}}$	$\Delta\Delta C_{T \text{ Tbp}}$
NGF 10 μM	23.73	8.93	-0.202	4.40	3.80
NGF 10 nM	22.63	8.44	-0.945	6.17	6.33
NGF Vehicle	25.45	11.07	0.202		
Actb 10 μM	14.80				
Actb 10 nM	14.19				
Actb Vehicle	14.38				
Tbp 10 μM	23.93				
Tbp 10 nM	25.58				
Tbp Vehicle	23.74				
Real time PCR assays were performed with cDNA derived from cultured glial cells exposed to either 10 μm , 10 nM, or vehicle alone (DMSO). Biological and technical replicates were each performed in triplicate. The average (mean) C _T values from the replicates are recorded in the table. ΔC_{T} values are calculated from the difference in CT of NGF amplicons versus each reference gene (Actb: C _T NGF - C _T Actb; Tbp: C _T NGF - C _T Tbp). $\Delta\Delta C_{T}$ is the fold change, calculated as $2(\Delta C_{T} \text{ Induced} - \Delta C_{T} \text{ Vehicle})$. Relative to either Actb or Tbp, 10 μM PMA induces a ~4-fold increase in NGF transcript, while 10 nM PMA induces a ~6-fold increase. The difference likely reflects the apoptotic activity associated with higher concentrations of PMA.					

Effects of PMA, clenbuterol, and forskolin on NGF gene expression

Finally, the effects of PMA, forskolin, and clenbuterol on NGF gene expression in human cultured glial cells was evaluated using the optimized qPCR assay and delta C_T method. As anticipated, the results show a significant increase in NGF gene expression after a 4-hour exposure to PMA at 10 μM and 10 nM concentrations (Fig. 26).

Surprisingly, neither clenbuterol nor forskolin had an effect on NGF gene expression under these same conditions. When considering the NGF secretion results from Specific Aim 2, the gene expression data demonstrates that NGF secretion and gene expression are distinguishable events, and an SMI that induces NGF secretion does not necessarily cause upregulation of gene expression.

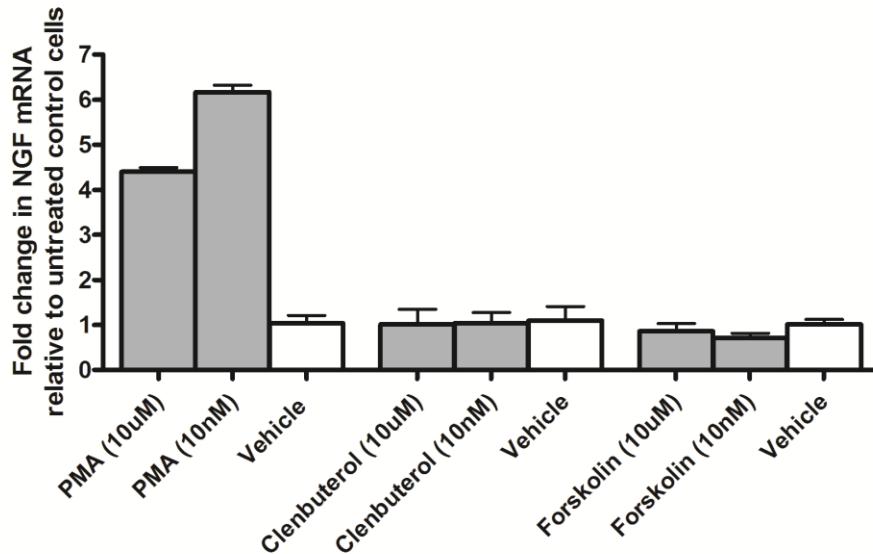


Fig. 26. Fold change analysis of NGF gene expression after 4-hour treatment with SMI.

Comparative C_T analysis was performed using Tbp as a reference gene. Biological triplicates and technical duplicates were used in the real time PCR assay. No-template controls and RNA-template controls (no reverse transcription) showed no amplification. Further detail on the comparative C_T data analysis is presented in *Materials and Methods*.

Specific Aim 2 Conclusions

As illustrated in Table 4, the development of the quantitative real time PCR assay to evaluate changes in NGF gene expression was successful and now provides a powerful tool for investigating small molecule induction of the NGF gene. Here, reference genes beta-Actin (Actb) and TATA-box binding protein (Tbp) were selected and primers were designed to selectively amplify cDNA. Primers were tested for efficiency and gene

specific amplicons were confirmed via agarose gel electrophoresis. Reverse transcription and quantitative PCR protocols were established, and the comparative C_T method was used to evaluate the effects of PMA, clenbuterol, and forskolin on NGF gene expression. PMA is a potent inducer of NGF gene expression; however, clenbuterol and forskolin have no effect on expression after four hours. The results of assay development indicate a viable method for performing NGF gene expression for SMIs of NGF and in pathway validation studies (Specific Aim 4).

Specific Aim 3 – Mapping the Signal Transduction Pathway(s) for Select SMIs of NGF

Specific Aim 3: Mapping the Signal Transduction Pathway(s) for Select SMIs of NGF. Reverse phase protein microarrays will be used to map the signal transduction cascade that occurs in response to small molecule induction of cultured human glial cells. Diverse small molecules representing different chemical classes will be evaluated. Signal transduction mapping will be performed using each SMI at its EC₅₀, and the cells will be assessed at various time points to establish temporal maps of signal transduction.

Determining the glial cell pathways responsible for NGF induction

Reverse phase protein microarrays (RPPA) were selected to map the signal transduction cascade that occurs in glial cells in response to small molecule induction of NGF. To take advantage of the ability of RPPA to analyze hundreds of cell lysates on a single array, five additional small molecules were also selected for inclusion in the analysis (carnosol, calcipitriol, cryptotanshinone, oleanolic acid, and CDDO; Fig. 27). These compounds were selected as they were either readily available terpenoid molecules (carnosol, cryptotanshinone, oleanolic acid, and CDDO; the diterpenes cyathin A¹⁰⁴, scabronine A¹⁰⁵, and PMA each induce NGF so we hypothesized these other terpenes may do so as well) or had been shown to induce NGF elsewhere (calcipitriol¹²¹). In total then, eight small molecules were assayed for their ability to upregulate NGF in T98G cells.

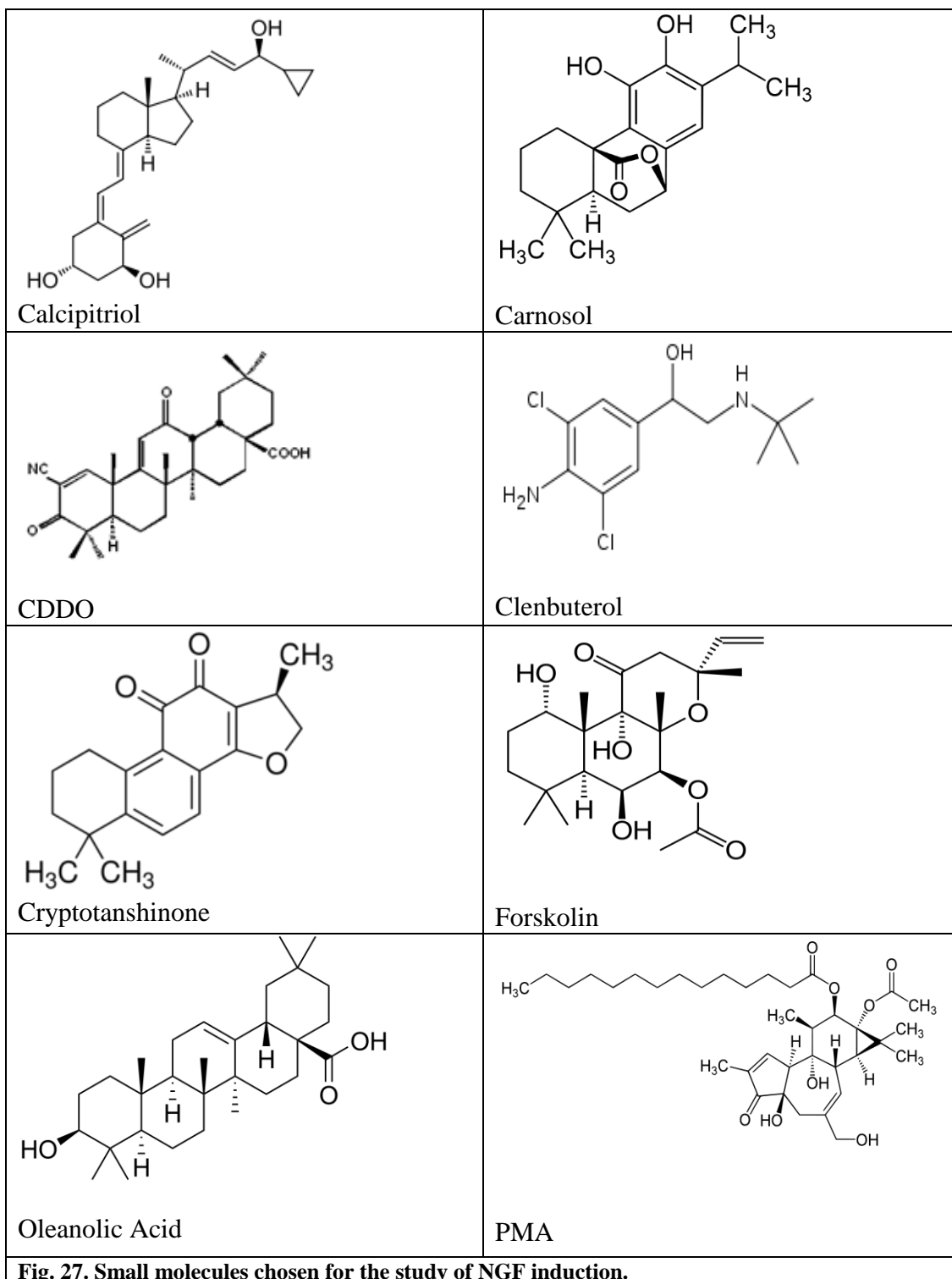


Fig. 27. Small molecules chosen for the study of NGF induction.

As detailed in *Materials and Methods*, cultured T98G cells were exposed to one of the eight small molecules for durations of 2, 15, 60, and 240 minutes. The dose response plots of PMA, clenbuterol, and forskolin (Fig. 18) were considered to determine the ideal concentration to test small molecules with no known history of NGF secretion. PMA and forskolin have EC₅₀ values near 10 nM with a plateau of 10 μM. Clenbuterol was characterized with an EC₅₀ of 400 nM with a plateau of 10 μM. Thus, two concentrations were chosen for study. First, a 10 nM dose was used for all eight compounds. This value may be sufficient to achieve EC₅₀ for some of the compounds, specifically the terpenoids (as they share structural similarity with PMA). A 10 μM concentration was also evaluated for all eight compounds. This value was sufficient to achieve maximal NGF secretion for clenbuterol, forskolin, and PMA (although we are cognizant that the high dose of small molecule may result in some off-targeting effects due to non-specific interactions with intracellular proteins). In choosing time points for the study, the temporal activation of both PKA and PKC were considered, since we implicated these proteins in our hypothesized mechanism (as presented in the *Introduction*). Activation of PKA signaling is evident between 15-30 minutes of β₂-adrenergic receptor activation¹²². Additionally, PMA-induced PKC substrate phosphorylation has been observed to occur within 60 minutes¹²³. Overall signal transduction profiles will vary by SMI, but the time points selected should generally reflect what happens immediately following SMI activation of the target protein and after the signal has propagated to downstream proteins.

At each time point, conditioned media was aspirated from the cells and immediately assayed using the NGF ELISA (as detailed in Specific Aim 1, freezing of the conditioned media causes a measurable loss in NGF titer, therefore immediate sample assaying is required). Concomitantly, the cell culture plates were placed on dry ice and the cells were lysed using a buffered aqueous solution containing an array of phosphatase inhibitors (to preserve the phosphorylation state of the signal transduction proteins). Cell lysates were centrifuged to pellet insoluble cell debris, and the supernatant was collected, snap frozen in liquid nitrogen, then stored at -80°C until RPPA was performed. Cell lysates were also used for real time quantitative PCR experiments evaluating NGF transcript level.

Confirming small molecule induction of NGF protein and transcript

To confirm the ability of the five additional small molecules to induce secretion of NGF protein, cells were exposed to each SMI at 10 μ M and 10 nM concentrations and NGF titers were determined using the optimized NGF-specific ELISA. In each case, vehicle-only controls were used to determine baseline NGF secretion and these values were subtracted from small molecule results. Figure 28 illustrates the increase in NGF secretion as a result of small molecule exposure.

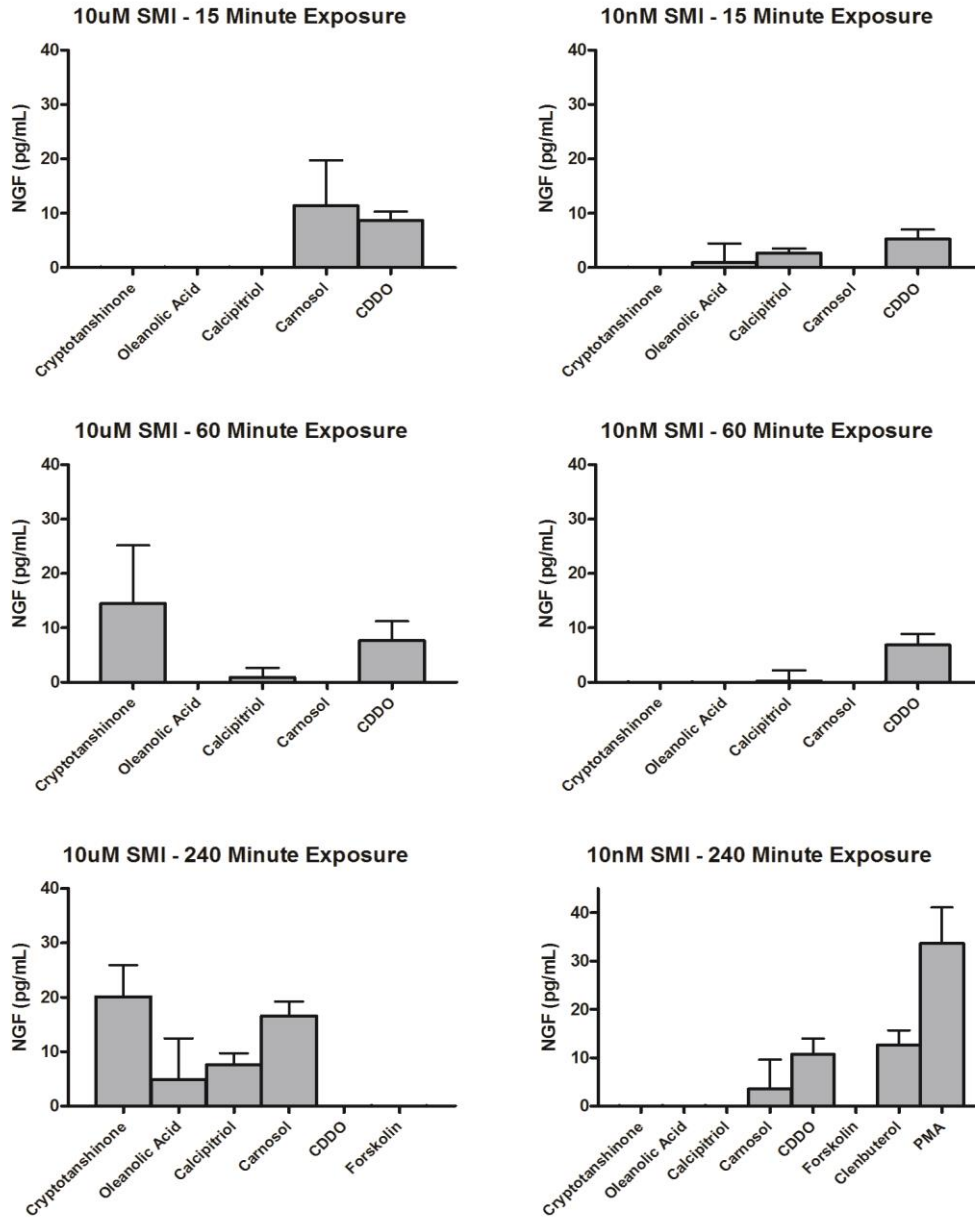


Fig. 28. NGF titers (vehicle-subtracted) as a result of exposure to small molecule. Experiments were performed using 10 μ M and 10 nM concentrations of SMI and incubation durations of 15 minutes, 60 minutes, and 240 minutes. Carnosol, cryptotanshinone, and CDDO all induce increases in detectable NGF secretion compared to vehicle alone, but PMA is clearly the strongest inducer of NGF secretion (see 240 min, 10 nM data). Although forskolin induces NGF at 12 hours, no response is apparent after 4-hour exposure.

Reverse phase protein microarray (RPPA) analysis

Reverse phase protein microarray methodology

RPPA enables an automated, non-subjective, quantitative analysis of hundreds of signal transduction proteins from a limited amount of sample. The RPPA approach readily differentiates active signal transduction pathways from those that are not active. In essence, an automated arrayer prints whole-cell protein (e.g. the proteome obtained from cultured glial cells exposed to a SMI of NGF) in an array on nitrocellulose slides (Fig. 29). Once printed, non-antigenic sites are blocked, and the slides are stained (via an autostainer)

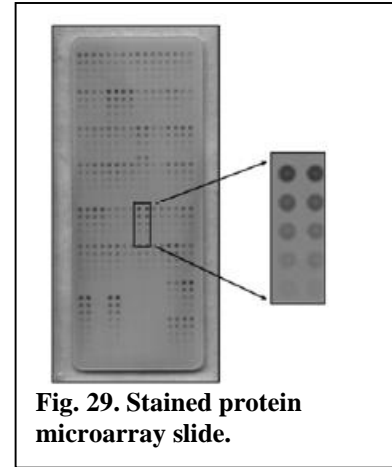


Fig. 29. Stained protein microarray slide.

with a protein specific primary antibody. A fluorescently labeled secondary antibody (specific for the primary antibody) is then added and detected via a fluorometric imaging system that measures the sample's fluorescence intensity, subtracts the background, normalizes the result to the total protein concentration, and extrapolates to a calibration curve to generate a final intensity value.

Reverse phase protein microarray results

Over 130 protein endpoints are evaluated using reverse phase protein microarray technology (see Appendix 1). The RPPA gives an indication of the abundance of phosphorylated and/or unphosphorylated protein, and hence an indication of the activation state of key signal transduction proteins. To process the results, the raw protein abundance data is converted to fold change by dividing values for treated samples

by their corresponding untreated controls. Heat maps are generated for each SMI (see Appendix 2). Two-tailed unpaired heteroscedastic t-tests were performed for PMA (10 nM), forskolin (10 nM), and clenbuterol (10 nM and 10 μ M due to its EC₅₀ concentration and overall efficacy) (see Appendix 3). Changes in the proteome are analyzed to identify specific signal transduction pathways that may be responsible for increases in NGF secretion. Interpretation of the RPPA results is as follows.

PMA

The RPPA results obtained here directly link PMA to the upregulation of cAMP Response Element Binding protein (CREB), a cellular transcription factor shown previously to be essential for NGF gene expression (Fig. 30)⁸⁷. PMA and other related phorbol esters are well documented activators of the Protein Kinase C (PKC) family of enzymes due to their structural similarity to the native activator, diacylglycerol (DAG)¹²⁴. The RPPA data illustrates the mitogen-activated protein kinase

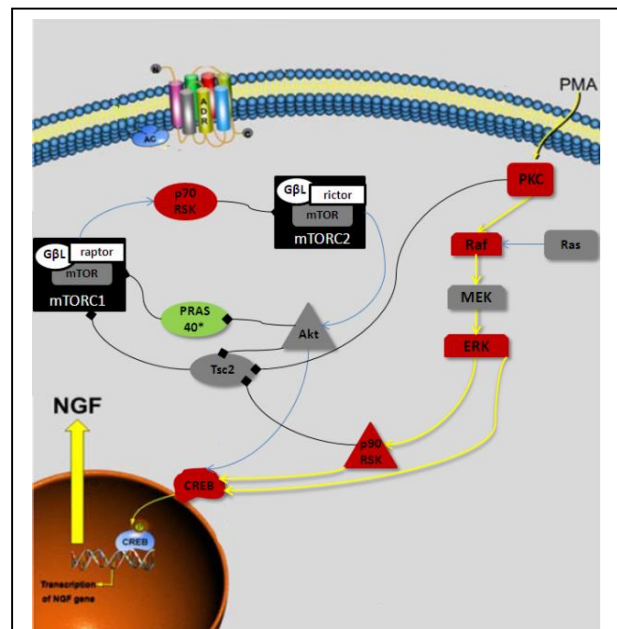


Fig. 30. The glial cell signal transduction pathway activated by PMA. Shades of red indicate the degree of upregulation (dark = high, light = low), shades of green indicate the degree of downregulation (dark = high, light = low), grey = no significant upregulation or downregulation, white = not assayed. Note that the signal transduction cascade depicted here differs significantly from our hypothesized pathway shown in Fig. 2.

(MAPK) pathway as the integral player in PKC based CREB activation.

The data corroborates previous research on the stimulation of the MAPK pathway via the interaction of PKC and Raf¹²⁵. Generally, the MAPK pathway, consisting of Raf, MEK, and ERK is activated by the protein Ras. In this case however, we see higher levels of activated Raf despite basal Ras activity. Our results parallel other observations of PKC activation of Raf independent of Ras¹²⁵. Raf activation leads to a stepwise phosphorylation cascade as a phosphate group is transferred from Raf to MEK and finally to ERK. This triad of kinases collectively makes up the MAPK pathway. Although the heat maps do not clearly indicate higher than basal levels of phosphorylated MEK, we do see higher levels of phosphorylated ERK and Raf, implicating the MAPK pathway as part of the PMA signal transduction pathway. It should be noted that the collective data set shows consistent levels of phosphorylated MEK across all conditions. One cause of this result may be that the paratope of the antibody used, although validated, interacts with an epitope of phospho-MEK different than the one generated by Raf kinase activity. Alternatively, MEK may transfer its newly added phosphate group to ERK immediately upon receipt, such that its overall phosphorylation state appears unaffected. The t-test does reveal a statistically significant ($p < 0.05$) change in the abundance of phosphorylated MEK after 15 minutes and 60 minutes of exposure to 10 nM PMA.

ERK is capable of directly activating CREB via phosphorylation at Serine 133¹²⁶ and elevated levels of phospho-CREB are present as early as 60 minutes after PMA exposure. Additionally, ERK can activate p90RSK¹²⁷. Phosphorylated p90RSK and its isoform, RSK3, are present in higher levels in PMA-treated cells and have also been

linked to phosphorylation of CREB at Serine 133¹²⁷. P90RSK may also be responsible for the lack of mTOR upregulation in PMA treated cells. P90RSK can play a role in the mTOR pathway by preventing inhibition of mTOR Complex 1 (mTORC1) by the TSC1-TSC2 complex¹²⁸. As a result, mTORC1 is able to inhibit mTOR Complex 2 (mTORC2) activity via stimulation of the mTORC2 inhibitor, p70RSK (also known as p70S6K)¹²⁹. P70RSK can interact with rictor, a member of the mTORC2 complex, inhibiting the complex from proceeding with activation of Akt¹²⁹. The results show elevated levels of phosphorylated p70RSK, supporting the conclusion that the mTOR pathway is inactive.

The results of this RPPA-based assay have led to the proposal of a signal transduction map for PMA-induced upregulation of NGF gene expression (Fig. 30). In this pathway, PMA activates PKC, leading to the activation of the MAPK pathway independent of Ras. ERK, the final protein of the MAPK trio, directly upregulates CREB and p90RSK, a second activator of CREB leading to RNA transcription. The treatment of glial cells with either 10 nM or 10 μ M PMA both lead to higher levels of phosphorylated CREB as early as 60 minutes post-induction. This upregulation of CREB occurs independently of Akt and the mTOR pathway. A pictorial representation of the time-dependent change in the proteome is presented in Figure 31.

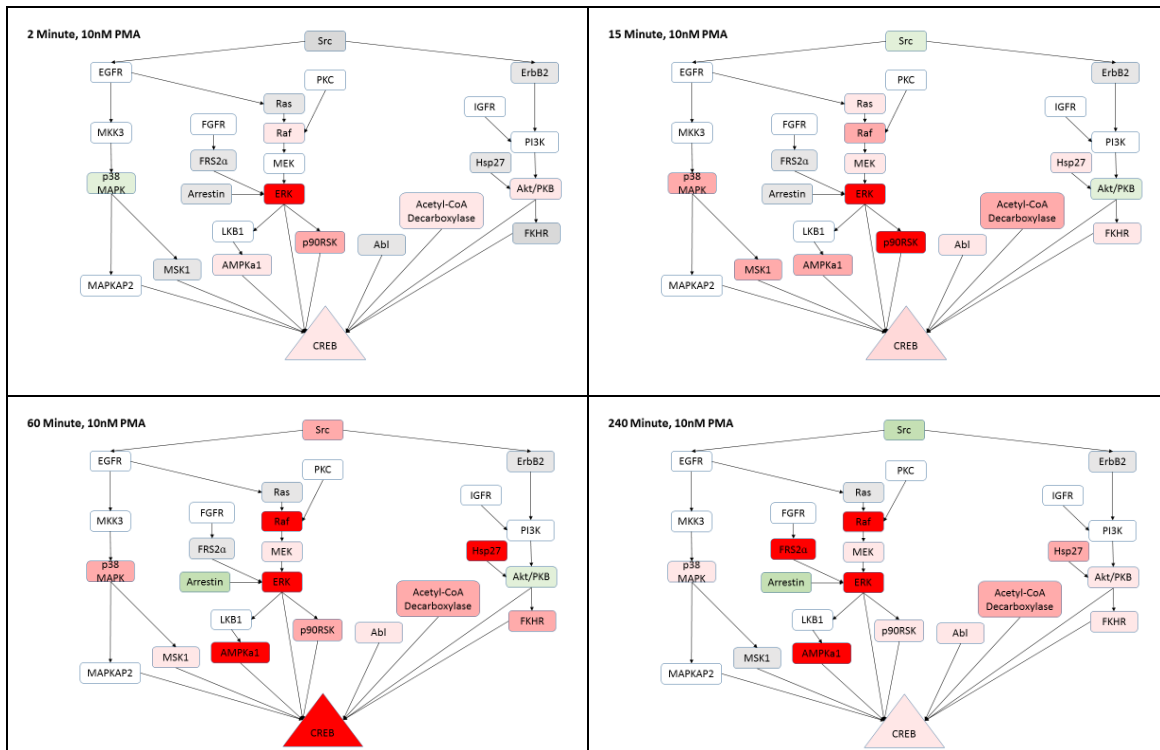


Fig. 31. The PMA induced signal transduction as a function of time. MAPK proteins become increasingly active as time progresses, culminating in peak activation of CREB at 60 minutes. Multiple regulators of CREB outside of the MAPK pathway are affected upon cellular exposure to PMA. These proteins, including MSK1 (Ribosomal protein S6 kinase alpha-5), FKHR (forkhead homolog in rhabdomyosarcoma), and Akt/PKB, may play a role in PMA induction of NGF expression and/or secretion.

Clenbuterol

Clenbuterol treated samples also feature an increase in phosphorylated CREB levels, but not to the same extent as PMA treated cells, and only after four hours of exposure (Fig. 32). As seen in Figure 26, no upregulation of NGF gene expression was observed after 4-hour exposure to clenbuterol. Additional qPCR analysis revealed that no detectable change in NGF gene expression is evident after 6 hours or 8 hours of exposure to 10 nM Clenbuterol (data not shown). These results suggest that the milder upregulation

of phosphorylated CREB observed in the clenbuterol data is not sufficient to drive a noticeable change in NGF gene expression.

Expectedly, clenbuterol induction follows a different signal transduction pathway than PMA. Clenbuterol is known to bind the beta-2 adrenergic receptor, stimulating G-protein coupled receptor activation of cAMP¹³⁰. cAMP activates PKA by binding to its regulatory domains, releasing the catalytic active site¹³⁰.

Previous studies^{131,132} have shown that maximal PKA activity requires a separate phosphorylation event at Thr¹⁹⁷. This event results in a conformational change that increases the interactions between PKA and its substrates¹³². In this RPPA investigation, elevated levels of phosphorylated PKA were not identified, suggesting that treatment with clenbuterol alone will only lead to basal levels of PKA catalysis. This basal catalysis results in a weaker, delayed upregulation of CREB activity when compared to the PMA-PKC response. Clenbuterol stimulation still resulted in a positive correlation between phospho-CREB levels and phospho-ERK/p90RSK.

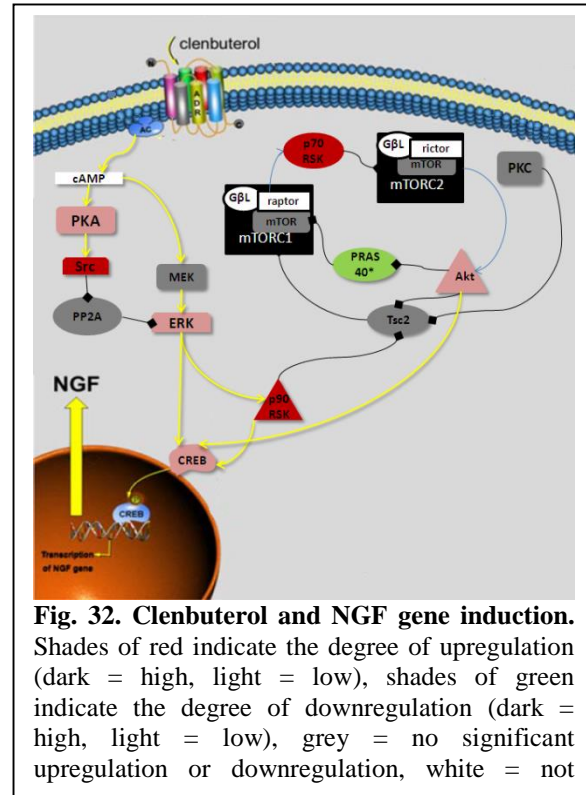


Fig. 32. Clenbuterol and NGF gene induction. Shades of red indicate the degree of upregulation (dark = high, light = low), shades of green indicate the degree of downregulation (dark = high, light = low), grey = no significant upregulation or downregulation, white = not

PKA is capable of stimulating ERK activity by phosphorylating Src¹³³. Our results show a greater than two-fold increase in phosphorylated Src levels for clenbuterol-treated cells relative to controls. Src may then downregulate PP2A, an inhibitor of ERK¹²⁶. Alternatively, the upregulation of ERK may be a result of an interaction between cAMP and MEK¹³⁴. Increased levels of phosphorylated p90RSK are evident in clenbuterol treated cells, a result of ERK activation. The mTOR pathway is not active in the case of clenbuterol treatment, corroborating the previous correlation between p90RSK activity and mTORC2 inhibition.

The upregulation of CREB in clenbuterol-treated cells is slower and weaker than in cells treated by PMA. Upon clenbuterol binding to the beta-2 adrenergic receptor, Protein Kinase A activates Src, leading to the downstream upregulation of ERK. As described previously, ERK can directly activate CREB or act on p90RSK, a second positive effector of CREB.

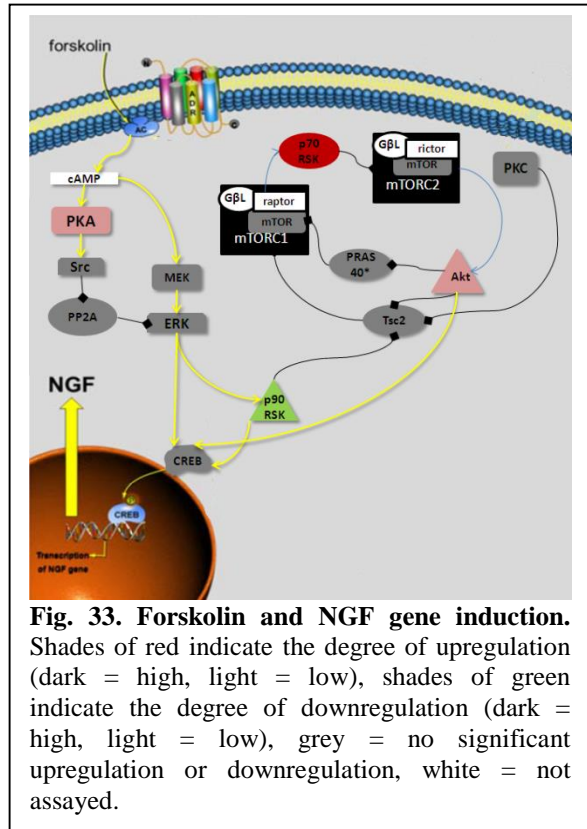
Forskolin

Not surprisingly, given the lack of gene upregulation observed with forskolin in Figure 26, RPPA indicates no significant increase in phospho-CREB levels in cells treated with 10 μ M or 10 nM forskolin (Fig. 33). Although clenbuterol and forskolin are both known activators of the PKA pathway, their mechanism of action as PKA effectors differs. Whereas clenbuterol acts indirectly on adenylyl cyclase through the G α subunit of its target G-protein, forskolin binds adenylyl cyclase directly at an alternative binding site^{135,136}. Additionally, forskolin can bind and inhibit cAMP phosphodiesterase, preventing deactivation of PKA¹³⁷. While both the binding site for G α and forskolin

promote conformational changes that promote catalysis, it is likely that the clenbuterol interaction through G α has a stronger effect. In this study, the stimulated PKA activity is minimized both by diminished response to cAMP and lack of Thr197 phosphorylation. There is little detectable change in the proteome between forskolin-treated cells and untreated cells in terms of proteins evaluated in this study, suggesting alternative proteins are involved in forskolin induced secretion of NGF. The lack of CREB upregulation by four hours at non-toxic, physiologically relevant concentrations makes this SMI a poor model for NGF upregulation.

Note on other small molecules evaluated

RPPA technology affords the ability to test a multitude of lysates over a desired number of inputs. To take advantage of the throughput, RPPA data was also collected for carnosol, calcipitriol, cryptotanshinone, oleanolic acid, and CDDO. NGF ELISA analysis reveals that both carnosol and cryptotanshinone induced a significant increase in NGF



secretion over the four-hour time course. However, the response is significantly weaker than PMA and none of these small molecules had any significant effect on pCREB, the key transcription factor for NGF gene expression. Thus PMA was selected as the optimal SMI for further analysis and pathway validation. Heat maps for the additional SMIs are provided in Appendix 2. This data can be used for future work investigating the mechanisms of these compounds.

Refined model of SMI Induction of NGF

The potent activity of PMA as an SMI of NGF and the clear, temporal activation of signaling proteins in the PKC-MAPK pathway leading to CREB has led to the generation of a new model for NGF induction (Fig. 34A). Our original model, illustrated in the introduction,

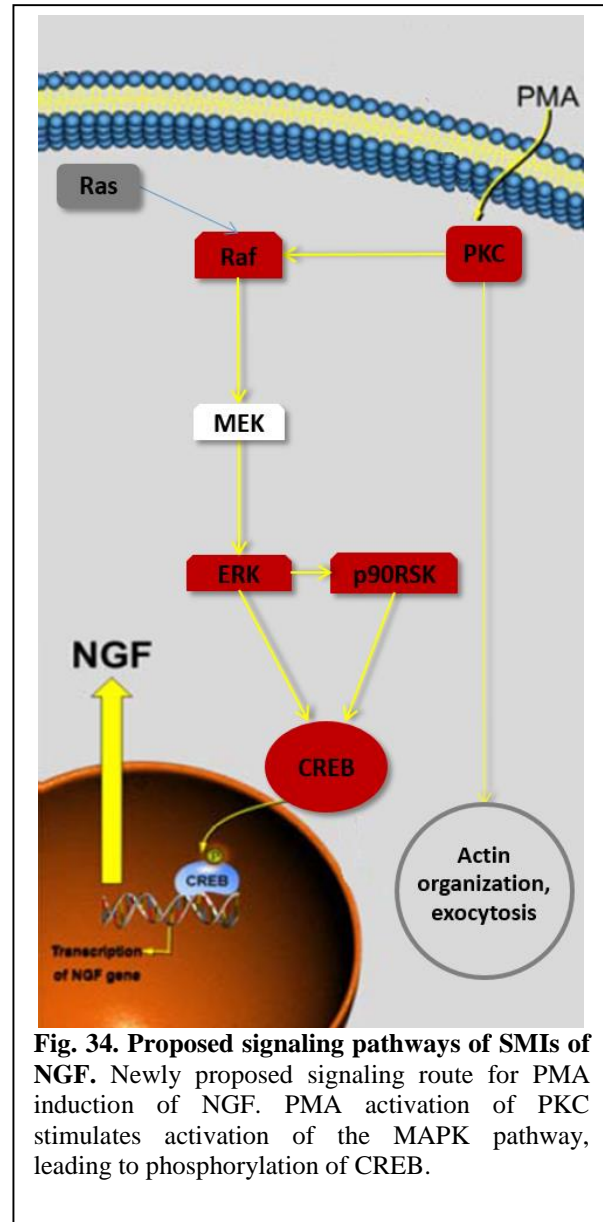


Fig. 34. Proposed signaling pathways of SMIs of NGF. Newly proposed signaling route for PMA induction of NGF. PMA activation of PKC stimulates activation of the MAPK pathway, leading to phosphorylation of CREB.

proposed a PKC pathway dependent on mTOR and Akt signaling for CREB activation. In the new model, PKC-induced activation of CREB follows the activation of the MAPK pathway and the proteins ERK and p90RSK. These proteins represent potential targets for the development of NGF inducing therapeutics and we aim to validate these proteins as critical to the PMA induction of NGF gene expression and secretion in *Specific Aim 4*.

Specific Aim 4 – Validation of the PKC Pathway in NGF Induction

Specific Aim 4: Validation of the Signal Transduction Pathway(s) for NGF

Induction. To validate the involvement of the signal transduction pathway(s) identified in Specific Aim 3, the activity of select pathway proteins will be specifically modulated using commercially available agonists and antagonists. After ensuring pathway agonists/antagonists are nontoxic to cultured human glial cells, established NGF assay protocols (ELISA and quantitative PCR) will be employed to assess the targeted signal transduction pathway.

The process of drug development typically proceeds through five distinguishable phases, including target identification, target validation, lead molecule identification, lead molecule optimization, and preclinical and clinical trials. Through signal transduction mapping, preliminary data identified the PKC pathway as a promising target for the development of neuroprotective therapeutics.

Agonist and Antagonist Assays

All assays were performed using T98G cells, the same human glial cell line used for signal transduction mapping. Cells were seeded in 6-well plates containing DMEM + 10% FBS media at an inoculum size intended to achieve confluence in four days (7.5×10^4 cells/mL). Once near confluence was attained, the media was changed to reduced serum media (OptiMEM) to transition the cells into a state of senescence. After 24 hours

in OptiMEM, the media was exchanged with fresh reduced serum media containing a PKC pathway agonist alone or with a downstream antagonist. When an antagonist was being evaluated, the cells were treated with 10 nM PMA, but only after a 20-minute period of pre-incubation with the antagonist. Antagonists were evaluated over a concentration range of 10 nM to 10 μ M. Cells exposed to PMA or vehicle (DMSO) alone served as reference controls. After four hours, conditioned media was aspirated from culture wells and NGF titers were determined using the NGF ELISA. Treated cells were also collected, snap frozen in liquid nitrogen, and stored at -80°C for quantitative PCR analysis. All assays were performed in triplicate.

For agonist assays, a dose-dependent response confirms the role of the targeted protein in NGF induction. Conversely, unresponsive NGF upregulation suggests an alternate pathway. For antagonist assays, the cells are pre-treated with antagonist before exposure to PMA. If NGF titers and gene expression levels are then suppressed (relative to uninhibited controls), the targeted protein is considered validated. If NGF titers and gene expression remain unaffected, then an alternate route is likely responsible for the SMI response.

The Agonists and Antagonists

Six different commercially available agonist/antagonists of the PKC pathway were used in this study. A description of each is as follows (see also Fig. 35):

i) Bryostatin-1. Bryostatin-1, a macrolide lactone natural product, is a well characterized agonist of PKC. Interestingly, bryostatin-1 has been linked to reduction of amyloid plaque formation and prevention of synapse degradation in the brain, and is currently being evaluated in clinical trials for the treatment of AD¹³⁸. To determine if bryostatin-1 induces dose-dependent NGF protein secretion and transcript upregulation, we exposed numerous wells of cultured glial cells to various concentrations of the agonist. A dose-dependent response would confirm the role of PKC in NGF induction. Conversely, unresponsive NGF regulation raises

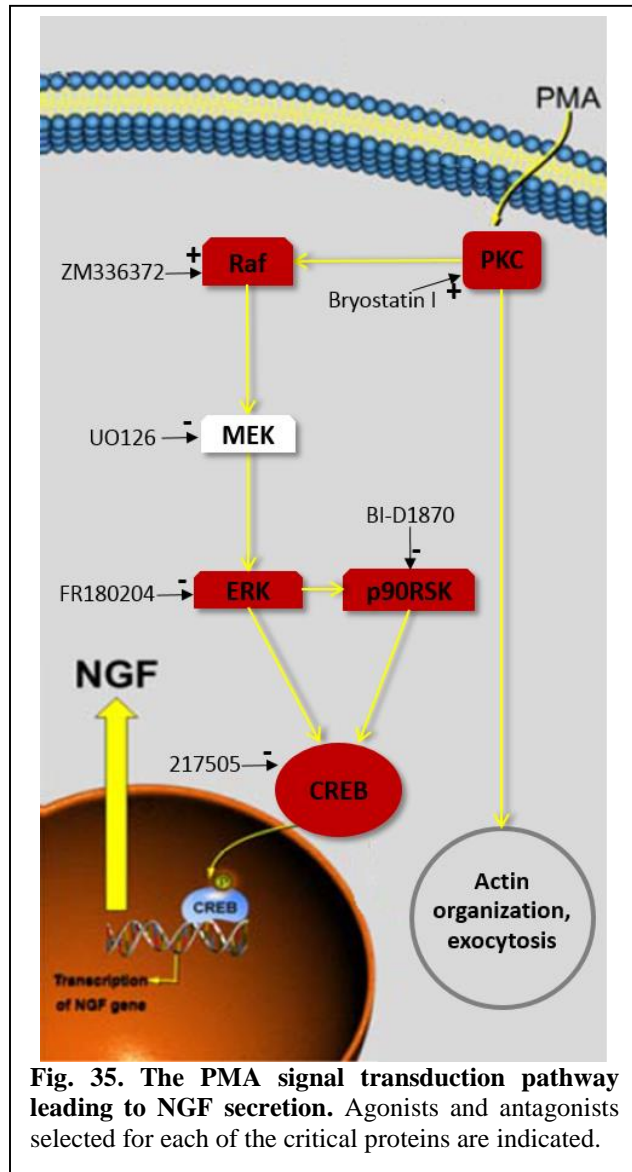


Fig. 35. The PMA signal transduction pathway leading to NGF secretion. Agonists and antagonists selected for each of the critical proteins are indicated.

suspicion on the role of the PKC pathway in NGF induction by PMA, prompting us to perform signal transduction mapping of glial cells treated with bryostatin-1 for differential comparison to cells treated with PMA.

ii) ZM336372 (3-(Dimethylamino)-N-[3-[(4-hydroxybenzoyl)amino]-4-methylphenyl]-benzamide). Cryptically named, ZM336372 has been shown to agonize Raf-1 *in vivo*¹³⁹. ZM336372 was assayed in the manner described for bryostatin-1. Dose-dependent NGF protein and transcript titers would validate the role of Raf-1 in the transduction cascade, in support of the mechanism deduced via transduction mapping (Fig. 35). However, failure of activated Raf-1 to upregulate the expression and secretion of NGF would suggest that other downstream targets of PKC cause NGF secretion by PMA

iii) U0126 (1,4-diamino-2,3-dicyano-1,4-bis[2-aminophenylthio]butadiene). U0126 is a highly selective, noncompetitive inhibitor of MEK¹⁴⁰. The addition of PMA (10 nM) follows a pre-incubation of the glial cells with U0126, as described in *Agonist and Antagonist Assays*, above. If NGF transcript abundance and protein titers were suppressed with U0126 pre-treatment (relative to cells treated with PMA alone), then MEK would be considered a validated member of the PMA-induced PKC induction pathway. Alternatively, if NGF titers remain unaffected, then an alternative route for PMA is likely involved.

iv) FR180204 (5-(2-Phenyl-pyrazolo[1,5-a]pyridin-3-yl)-1H-pyrazolo[3,4-c]pyridazin-3-ylamine). FR180204 is a selective, competitive inhibitor of ERK¹⁴¹. FR180204 was evaluated in the same manner as U0126, using identical concentrations

of inhibitor¹². PMA (10 nM) follows the pre-incubation with FR180204. If NGF titers and expression levels were suppressed, then ERK will be considered validated.

Conversely, if NGF titers and expression remain unaffected, then an alternative route for PMA is involved.

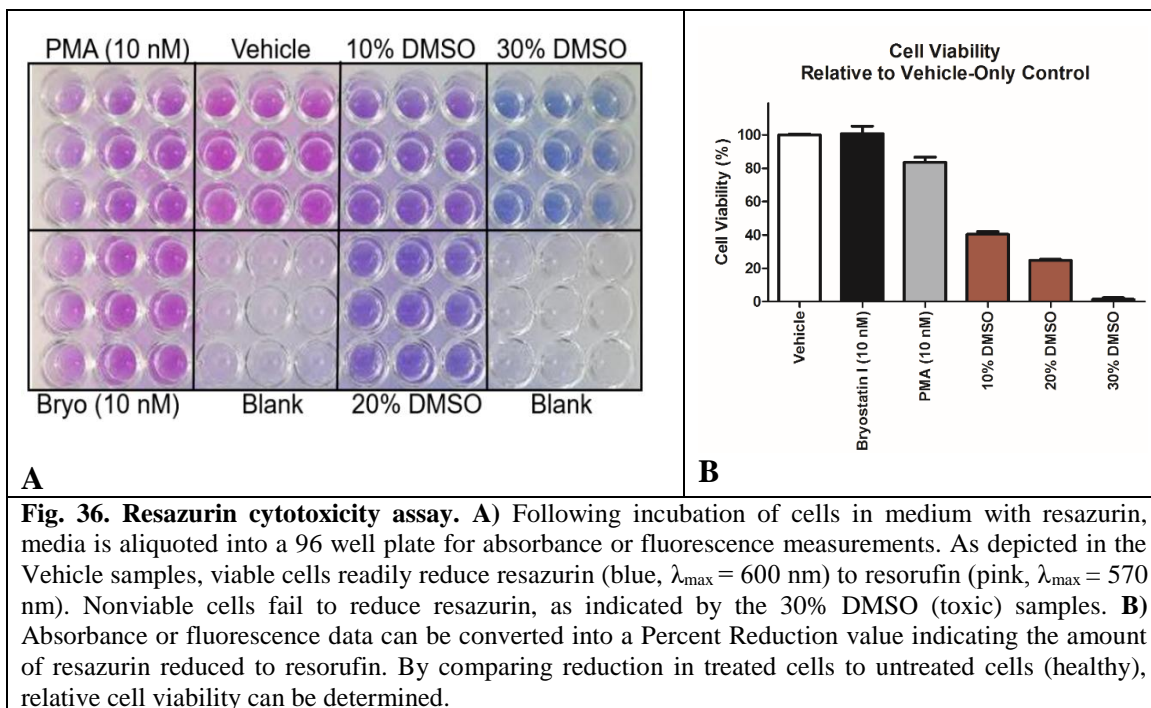
v) **BI-D1870 (2-[(3,5-Difluoro-4-hydroxyphenyl)amino]-7,8-dihydro-5,7-dimethyl-8-(3-methylbutyl)-6(5H)-pteridone)**. BI-D1870 is a selective, competitive inhibitor of p90RSK¹⁴². BI-D1870 was assayed as described for the other two pathway antagonists, using a similar concentration range¹⁴². If NGF transcript abundance and protein titers were suppressed by BI-D1870 (relative to PMA treatment alone), then p90RSK is be considered a validated member of the PKC induction pathway.

Alternatively, if NGF titers remain unaffected, then the role of p90RSK is questioned (as mentioned previously, activated ERK may be sufficient to activate CREB independent of p90RSK).

vi) **217505 (N-(4-Chlorophenyl)-3-hydroxy-2-naphthamide)**. 217505 is a selective, competitive inhibitor of CREB. 217505 binds to the kinase-inducible domain interacting domain (KIX) to inhibit CBP binding to the kinase-inducible domain (KID) of CREB, thus blocking the interaction of CREB and its transcription coactivator¹⁴³. 217505 was assayed to confirm the role of CREB in PMA induction of NGF gene expression; however, no effect on NGF secretion is expected. If NGF transcript abundance is suppressed by 217505, then CREB is considered a validated member of the PKC induction pathway. Alternatively, if NGF titers remain unaffected, then the role of CREB is be questioned and other transcription factors are investigated.

Evaluating cytotoxicity of the agonists and antagonists

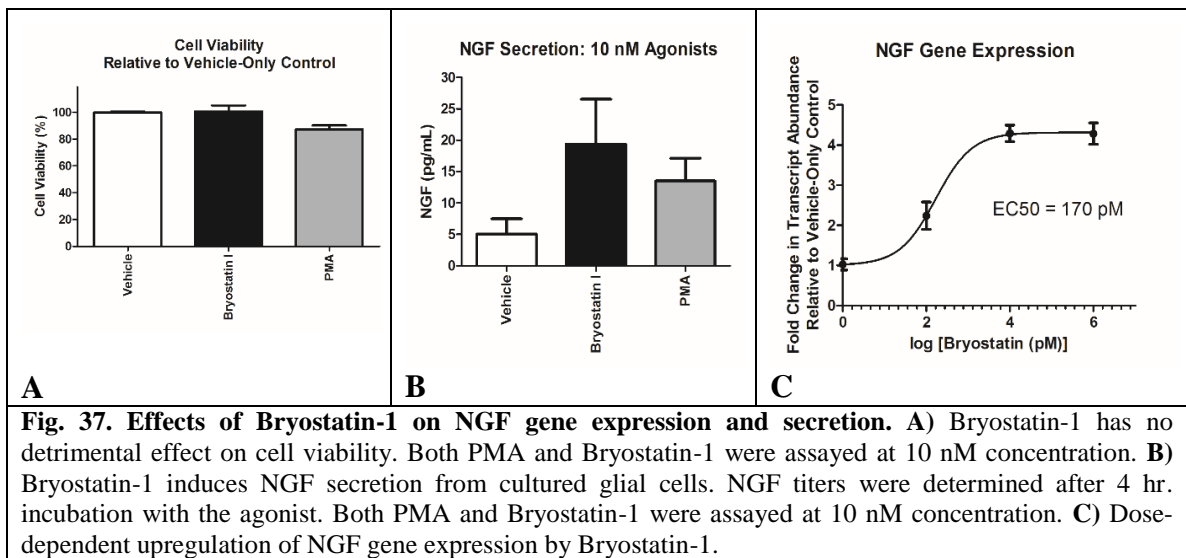
To ensure that observed changes in NGF gene expression and secretion were due to effects on the targeted proteins and not a side-effect of agonist/antagonist induced cytotoxicity, we evaluated the effects of each agonist/antagonist on cell viability. Cells were exposed to the agonists/antagonists for 4 hours (the same duration used in the pathway validation assays). After 4 hours, a non-toxic resazurin indicator dye was added to culture medium for one hour. Resazurin (blue) is reduced in the mitochondria of healthy cells to resorufin (pink), a chemical change that is measurable by fluorescence or absorbance measurements (Fig. 36A). Cell viability was determined by comparing resazurin reduction in untreated cells to resazurin reduction in cells treated with agonists/antagonists (Fig. 36B).



Validation study results

PKC Agonist: Bryostatin-1

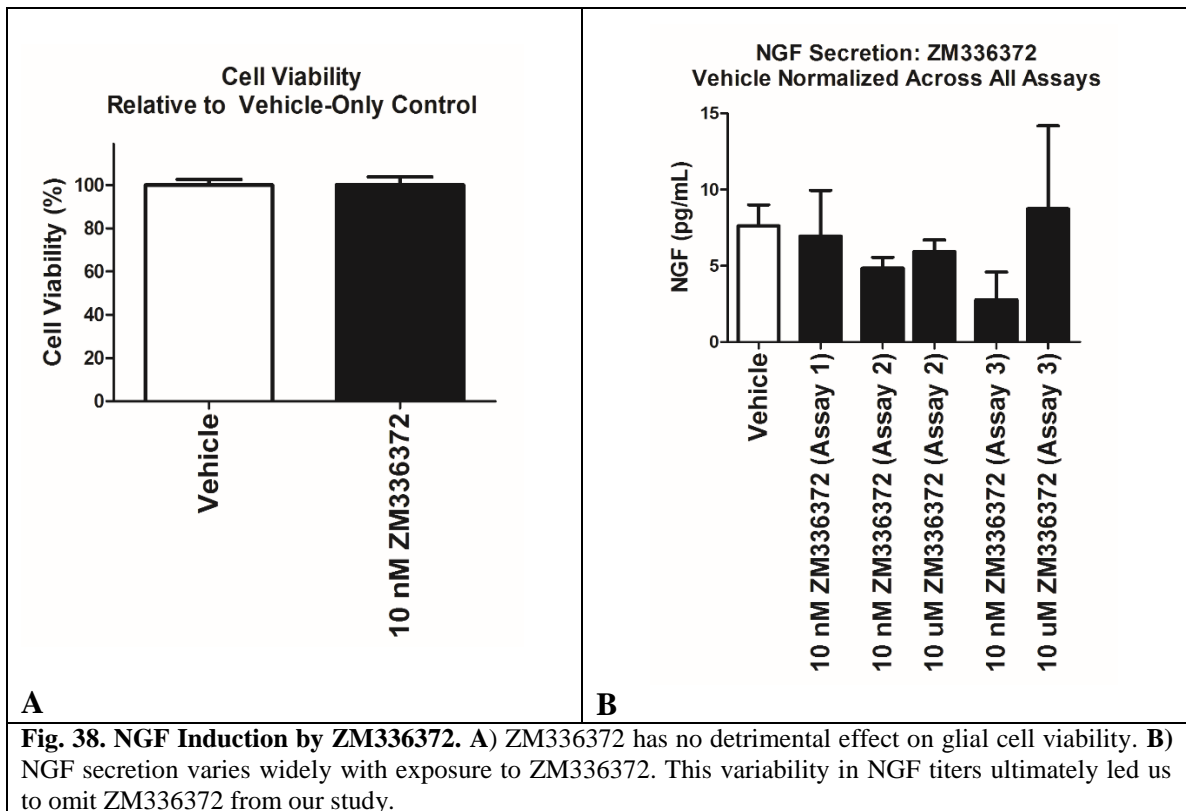
A macrocyclic lactone, the selective PKC agonist known as Bryostatin-1 has no detrimental effects on cell viability (Fig. 37A) and is a more potent inducer of NGF secretion than PMA (Fig. 37B). Bryostatin-1 also generates a four-fold increase in NGF gene expression compared to cells treated with vehicle alone (Fig. 37C). Collectively, these results validate the role of PKC in SMI upregulation of NGF, and also identifies bryostatin-1 as a promising new SMI of NGF.



Raf Agonist: ZM336372

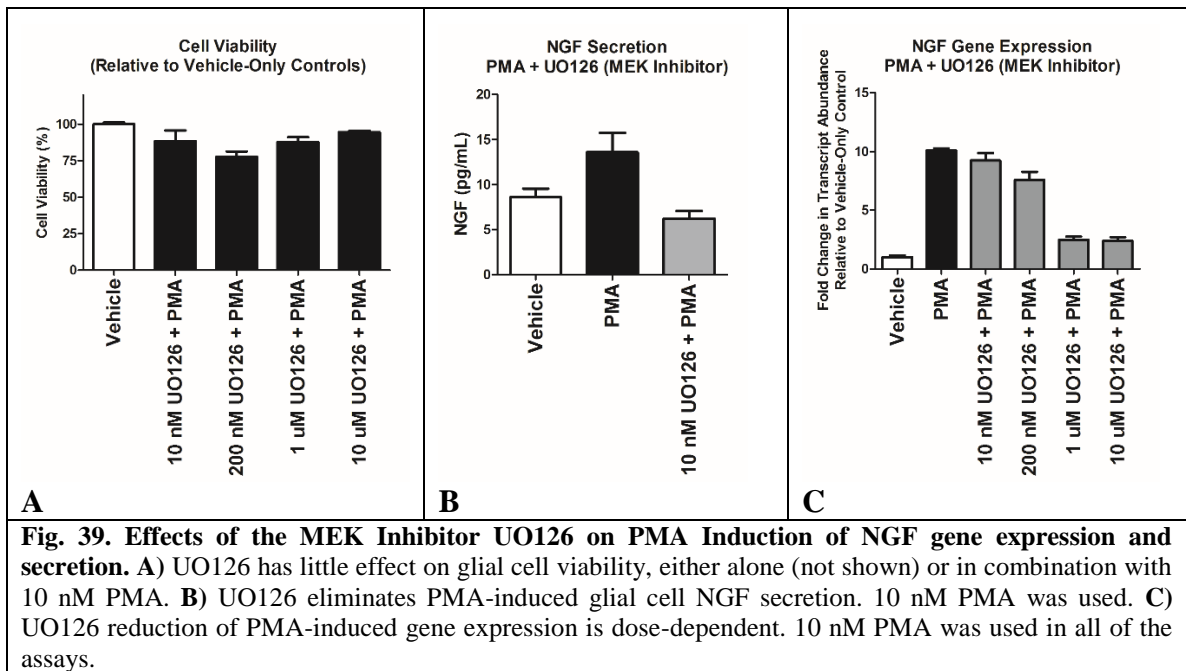
Marketed as a Raf-1 activator, ZM336372 is actually an inhibitor of Raf *in vitro*.

However, *in vivo* the inhibition of Raf by ZM336372 is typically followed by a compensatory rebound response leading to hyperactivation of Raf activity (thus, ZM336372 is considered an activator). Although ZM336372 was not toxic to the cultured glial cells (Fig. 38A), this ‘yo-yo’ type of inhibition-activation activity caused deviations from typical dose response and issues with reproducibility (Fig. 38B). As such, we ultimately elected to eliminate ZM336372 from our study. Currently available alternative antagonists of Raf are not applicable to this research, as they are designed to selectively target specific mutated forms of the Raf protein only.



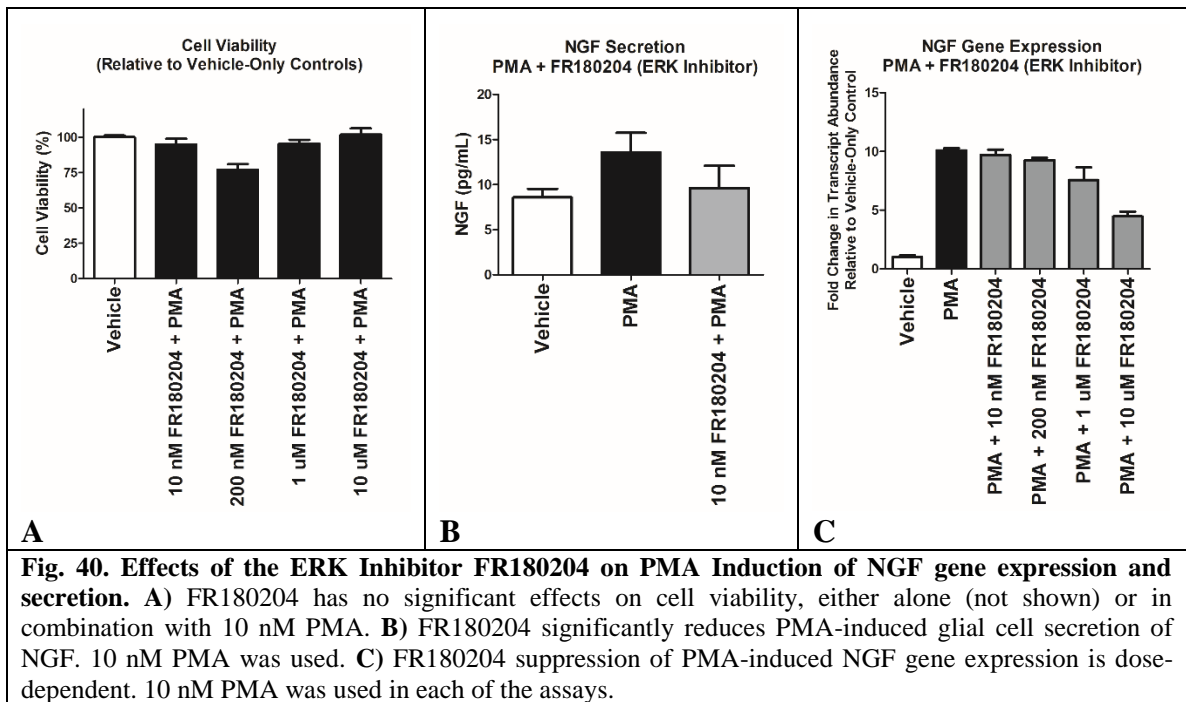
MEK Antagonist: UO126

UO126, a MEK specific inhibitor, demonstrated no significant detrimental effects on cell viability when cultured glial cells were treated with either UO126 alone (not shown) or with PMA and UO126 in combination (Fig. 39A). PMA induction of glial cell NGF release was completely inhibited with 10 nM UO126 (Fig. 39B). Further, pre-treatment of glial cells with the MEK inhibitor successfully suppressed PMA induction of NGF gene expression in a dose dependent manner (Fig. 39C). The results clearly validate MEK as an integral part of the PMA response.



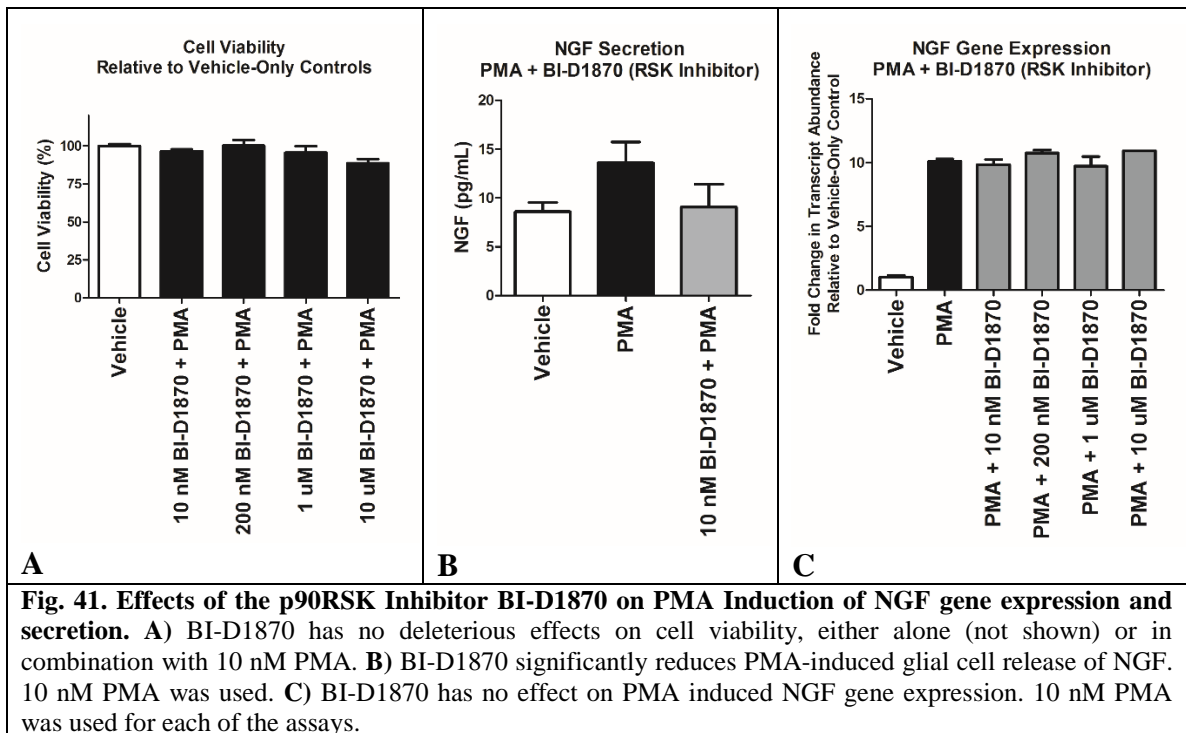
ERK Antagonist: FR180204

FR180204, a specific inhibitor of ERK, demonstrated no detrimental effects on cell viability when cells were treated with either FR180204 alone (not shown) or with PMA and FR180204 in combination (Fig. 40A). It has not escaped our attention though that the combination of 200 nM FR180204 with 10 nM PMA reduces cell viability by ~20%, much like 200 nM UO126 with 10 nM PMA (Fig. 39A). The significance of this (if any) remains unclear. PMA induction of glial cell NGF secretion was greatly suppressed with 10 nM ERK antagonist (Fig 40B). Pre-treatment of cells with FR180204 reduced PMA induction of NGF gene expression in a dose-dependent manner (Fig. 40C). These findings validate ERK as a critical component of the PMA response.



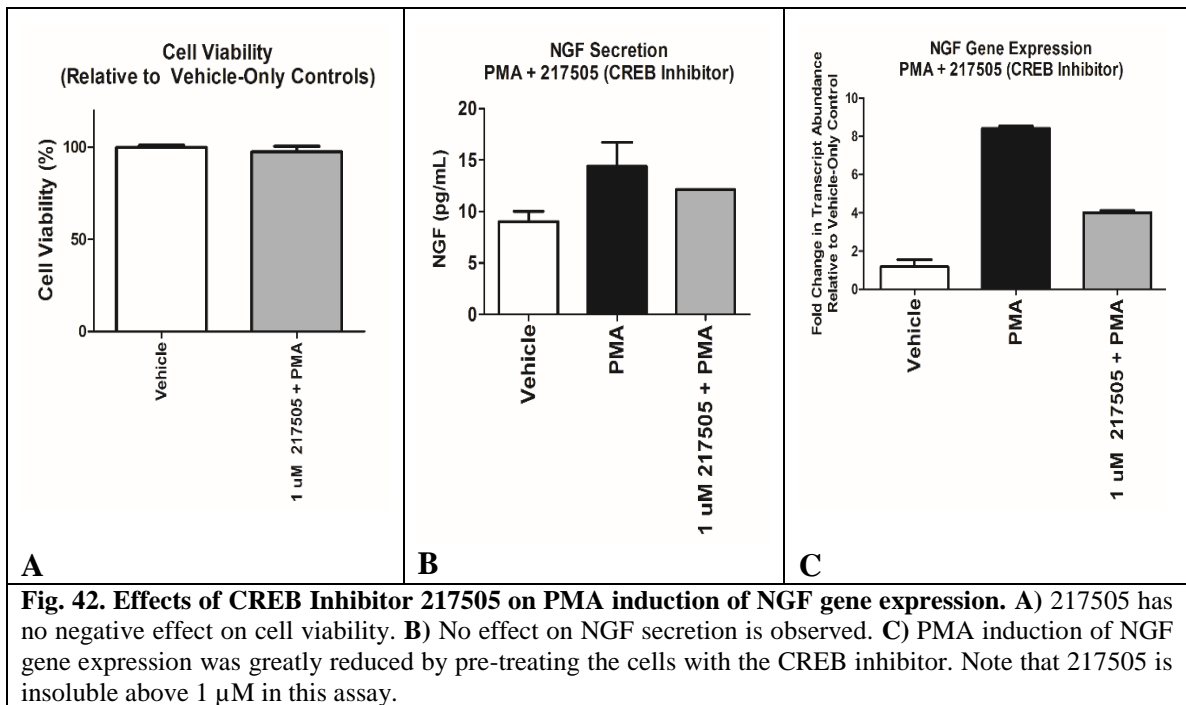
P90RSK Inhibitor: BI-D1870

Our reverse phase protein microarray results suggested the involvement of p90RSK in the PMA signal transduction cascade. Following activation by ERK, both ERK and p90RSK might then phosphorylate CREB, thereby initiating transcription of the NGF gene (see Fig. 2). BI-D1870 is a specific inhibitor of p90RSK. BI-D1870 has no deleterious effect on cultured glial cell viability, either alone (not shown) or in combination with PMA (Fig. 41A). The p90RSK inhibitor significantly reduced PMA induction of NGF release (Fig. 41B). However, no effect on NGF gene expression was observed (Fig. 41C). Thus, we conclude that p90RSK participates in the PMA signal transduction cascade, regulating NGF release (exocytosis) but not transcription of the NGF gene.



CREB Antagonist: 217505

217505, a specific inhibitor of the transcription factor CREB, was evaluated to confirm the role of CREB in PMA induced NGF gene expression. At 1 μM 217505 concentration, there is no deleterious effect on cell viability (Fig 42A). Pre-treatment of cultured glial cells with 1 μM 217505 greatly reduced the ability of PMA to induce NGF gene expression (Fig. 42B), thereby validating the role of CREB in the SMI response. No effect on NGF secretion was expected or observed (Fig. 42C). Note that higher concentrations of 217505 could not be explored due to insolubility in culture media.



Revised signal transduction cascade

As a consequence of the investigation, we can now refine the PMA signal transduction pathway presented in Figure 34 to that shown in Figure 43. We have directly validated the roles of PKC, MEK, ERK, p90RSK, and CREB in PMA induced upregulation of NGF secretion and secretion. While we were unable to confirm the involvement of Raf directly, it is a known substrate of PKC and modulator of MEK activity, implicating its involvement as depicted in the figure. As illustrated in the figure, the PMA signal transduction pathway branches at ERK, with the p90RSK path regulating exocytosis of NGF, to the exclusion of influencing transcription. P90RSK does not play a role in influencing transcription of the NGF gene.

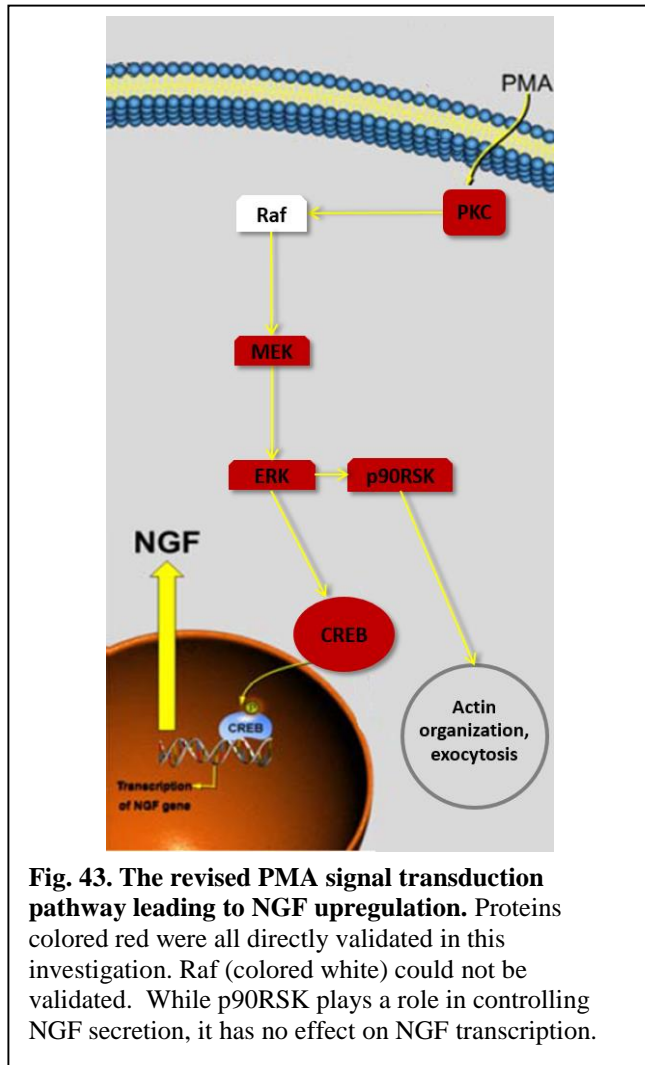


Fig. 43. The revised PMA signal transduction pathway leading to NGF upregulation. Proteins colored red were all directly validated in this investigation. Raf (colored white) could not be validated. While p90RSK plays a role in controlling NGF secretion, it has no effect on NGF transcription.

We have proven that the NGF response is not due to side effects associated with PMA's phorbol ester structure, but is a direct result of PKC agonism. The key downstream component following PMA activation of PKC is the classical MAPK signaling cascade of Raf/MEK/ERK, and CREB is the major transcription factor for the induction of NGF gene expression. These signaling proteins are ideal targets for the design of therapeutics capable of stimulating persistent generation of NGF in glial cells. These proteins, as well as p90RSK, also appear to play a role in the release of stored NGF from the cell. This phenomenon strengthens the argument for targeting the PKC/MAPK pathway for NGF induction.

Pitfalls and Alternative Approaches.

While the PKC pathway described herein is the predominant signal transduction route we identified for PMA-induced upregulation of NGF, our signal transduction mapping also identified significant upregulation of two other proteins known to interact directly with CREB: Ribosomal protein S6 kinase alpha-5 (MSK1) and AMP-activated protein kinase α (AMPK α). Hence, these proteins may also be involved components of PKC signaling to CREB. Additionally, the RPPA data reveals that several other non MAPK-related proteins/pathways known to modulate CREB are affected by PMA stimulation. These proteins, depicted in Figure 31, include FKHR (forkhead homolog in rhabdomyosarcoma), Akt/PKB (Protein Kinase B), and p38 MAP Kinase (p38MAPK). Finally, PMA induction of NGF may also utilize an alternative transcription factor, in addition to CREB. A list of transcription factors with binding sites on the NGF gene is provided in Appendix 4.

Although the T98G glioblastoma serve as powerful tool for the completion of this study, the use of a transformed cell line has associated pitfalls. In comparison to a primary cell line, the transformed glioblastoma feature altered gene copy numbers, metabolisms, and growth rates. As such, observed changes in gene expression, protein phosphorylation states, and protein secretion may differ from what would be observed in a primary cell line or an animal model. Reproducing these results in model systems that more closely mimic the human brain is a necessary evolution of this research.

Methods and Materials

NGF ELISA and Related Experiments

NGF ELISA protocol

NGF ELISA Protocol. The Peprotech NGF ELISA includes capture antibody, detection antibody, human β -NGF for use as a standard, and an avidin-HRP conjugate. Antibodies are delivered as lyophilized powder and are reconstituted to a concentration of 100 $\mu\text{g}/\text{mL}$ for each antibody and 1 $\mu\text{g}/\text{mL}$ for the NGF protein using sterile filtered phosphate buffered saline (PBS). Each reagent is stored as 10 individual aliquots. Before beginning each ELISA, 1x PBS is pH adjusted to 7.20 in sterile water. Capture antibody is diluted to 0.50 $\mu\text{g}/\text{mL}$ by delivering 50 μL of 100 $\mu\text{g}/\text{mL}$ to a 15 mL tube containing 950 μL PBS. Capture antibody is loaded (100 $\mu\text{L}/\text{well}$) to individual wells of a 96 well plate (Nunc MaxiSorp) and incubated at room temperature overnight on a plate shaker (slow) with the plate sealed in parafilm. The following morning, block buffer is prepared by dissolving bovine serum albumin (BSA) (Millipore Probumin 82-100-6) to PBS to a concentration of 300 mg/mL and sterile filtering the solution. Wash buffer is prepared by adding Tween-20 to PBS to a concentration of 0.05%. Diluent is prepared by preparing a PBS solution that is 0.05% Tween-20 and 0.1% sterile-filtered BSA. Capture antibody is aspirated from the wells and a multi-channel pipet is used to perform 4 300 μL washes of each well of the multi-well plate using wash buffer. Block solution is added (300 μL per well) and incubated at room temperature on a plate shaker (slow) for 1 hour. Standards

are prepared by performing serial dilutions of the 1 µg/mL NGF protein aliquot. A 1 ng / 100µL dilution is prepared by mixing 10 µL of 1 µg/mL NGF and 990 µL diluent. A 60 pg / 100 µL is prepared by mixing 60 µL of 1 ng / 100 µL dilution into 940 µL diluent. The 30 pg / 100 µL is prepared by mixing 500 µL of 60 pg / 100 µL NGF into 500 µL diluent. Serial dilutions are performed in this manner until 15 pg / 100 µL, 7.5 pg / 100 µL, 3.75 pg / 100 µL, 1.875 pg / 100 µL, and 0.9375 pg / 100 µL standards are obtained. After removal of the block solution and four washes of the plate, standards are loaded into the ELISA plate in duplicate (100 µL per well). Samples are also loaded into the plate at this time (100 µL per well). Standards and samples are allowed to incubate on a shaker (slow) for 3 hours. Following incubation of samples and standards, solutions are aspirated and the plate is washed four times. Detection antibody is diluted to 1 µg/mL by adding 100 µL of 100 µg/mL antibody to 900 µL diluent. The antibody is loaded into individual wells of the multi-well plate (100 µL per well) and allowed to incubate on a shaker (slow) for 2 hours. A working solution of avidin-HRP conjugate is prepared by loading 5.5 µL of the provided solution into 11 mL of diluent. Following aspiration of detection antibody and four successive washes of the plate, the HRP conjugate working solution is loaded into individual wells of the ELISA plate (100 µL per well) and incubated on the plate shaker (slow) for 30 minutes. After removing the avidin-HRP conjugate and washing the plate four times, TMB is diluted 1:2 by adding 6 mL of TMB to 6 mL of diluent in a 15 mL tube. A multichannel pipet is used to deliver 100 µL TMB to 8 wells of the plate. Subsequent sets of 8 wells are loaded 15 seconds apart. Once all lanes have been prepared, the plate is placed on the shaker and covered with aluminum

foil. After 13 minutes and 30 seconds, the TMB-HRP reaction is stopped using 2 M sulfuric acid by adding the acid solution to 8 wells at a time, in the original order, 15 seconds apart. The plate is recovered and allowed to shake (slow) for 2 minutes before being placed in the plate reader for absorption readings at 450 nm (A450). Samples are evaluated for their NGF titers by fitting A450 to linear regression provided by the standard curve. $\text{NGF abundance} = \text{A450 of sample} / \text{slope of linear regression} + \text{y intercept (background signal)}$.

Effects of media components on NGF ELISA

To determine the effect of media components on the NGF ELISA, the ELISA was performed using various media types as samples. OptiMEM + 5% BSA (OptiMEM-B) was prepared by dissolving 5.0 mg of BSA (Millipore Probumin) in 1 mL OptiMEM and inverting until well dissolved and then sterile filtering the solution. Aliquots of standard growth media (DMEM + 10% FBS), DMEM without FBS, OptiMEM reduced serum media, and OptiMEM-B were loaded in duplicate (100 μL per well) as standards. Their resulting A450 values were compared to the standard baseline of diluent alone.

Stability of NGF in cell environment

Cells were seeded in 6 wells of a 6 well plate at a density of 75000 cells/mL and grown for three days in DMEM + 10% FBS (2.5 mL per well). On the fourth day following seeding, media was aspirated and changed to OptiMEM containing no FBS (2.5 mL per well). On day 5, OptiMEM reduced serum media was prepared to contain 20 pg recombinant NGF-beta protein per 100 μL of media. To do this, 6.5 μL of 100 ng / 100 μL recombinant NGF was loaded into 32.5 mL OptiMEM (6500 pg NGF in 32500

$\mu\text{L} = 20 \text{ pg} / 100 \mu\text{L NGF}$). Media from n day 4 was aspirated and cells were washed twice with 1 mL OptiMEM. The new media, containing the recombinant NGF was then added (2.5 mL per well). Two wells were incubated for 1 hour, 2.5 hours, and 8 hours respectively. After incubation, media was snap frozen in liquid nitrogen and stored at -80°C . The subsequent ELISA was run four days later after thawing the samples and loading 100 μL of each sample in the ELISA plate in duplicate. The remaining samples were divided into four 0.5 mL aliquots, snap frozen, and stored at -80°C .

Effects of conditioned-media storage/freeze-thaw cycles on NGF ELISA

Stored aliquots were thawed, snap frozen, and stored at -80°C overnight. The following day, two aliquots from each sample underwent the same treatment. On the third day, the process was repeated for one aliquot that had already been subjected to three freeze-thaw cycles. After the fourth freeze-thaw cycle, the freeze-thawed aliquots were analyzed via the ELISA.

Effects of glycerol and SDS denaturing solution

A 50% glycerol solution was prepared by mixing glycerol in an equal volume of water. A 6X denaturing buffer solution was prepared from 15 mL glycerol, 7.5 mL 1 M Tris-Cl pH 6.8, and 3.00 g sodium dodecyl sulfate (SDS). 1X denaturing buffer was prepared by mixing 1 mL of the solution in 5 mL of sterile filtered water. The ELISA protocol was performed using three different standard curves. The first standard curve was prepared using diluent (standard protocol). A second standard curve was prepared using 50% glycerol solution instead of diluent. A third standard curve was prepared using 1X SDS denaturing solution instead of diluent. Standards of 60 $\text{pg} / 100 \mu\text{L}$, 30 $\text{pg} / 100$

μL , 15 pg / 100 μL , 7.5 pg / 100 μL , and 3.75 pg / 100 μL , 1.875 pg / 100 μL , and 0 pg / 100 μL were loaded into the plate and the effects of glycerol and SDS on the ELISA were evaluated.

Effects of urea.

Solutions of 1% urea (100 mg/mL) and 3% urea (300 mg/mL) were prepared in water. The ELISA protocol was performed using three different standard curves. The first standard curve was prepared using diluent (standard protocol). A second standard curve was prepared using 1% urea solution instead of diluent. A third standard curve was prepared using 3% urea solution instead of diluent. Standards of 30 pg / 100 μL , 15 pg / 100 μL , 7.5 pg / 100 μL , and 3.75 pg / 100 μL were loaded into the plate and the effects of urea on the ELISA were evaluated.

Cell culture and related experiments

Cell culture

Cells are originally seeded from frozen stock by thawing a beaker containing Mili-Q water that has acclimated to temperature in a 37°C water bath. Once cells have been thawed, they are added to DMEM containing 10% FBS (DMEM-F) such that the final volume is 10 mL. Cells are pelleted at 125 x g for 5 minutes. Pellets are resuspended in 2 mL DMEM-F and added to a pre-equilibrated flask containing 15.5 mL DMEM-F. Cells are passaged by 1:4 split or 1:5 split every 2-3 days. To do this, media is removed from the flask and the cells are rinsed using a small volume (1 mL in 75 cm² flask, 0.3 mL in 25 cm² flask) PBS or 0.25% w/v Trypsin. This wash is removed and 0.25% w/v volume is added to the flask (3 mL in 75 cm² flask, 1 mL in 25 cm² flask). Cells are observed under the microscope. Upon detachment, cells are washed with a 4x volume of

DMEM-F, transferred into a centrifuge tube, and pelleted at $125 \times g$ for 5 minutes. The pellet is resuspended in a small volume of DMEM-F and transferred to a flask containing an appropriate volume of pre-equilibrated DMEM-F.

24-hour time course survey of PMA and Clenbuterol

Working solutions of Clenbuterol and PMA were prepared such that they would be at 10 nM concentrations in cell media. In both cases, 2 mg/mL solutions were prepared in dimethyl sulfoxide (DMSO). For clenbuterol, the 2 mg/mL solution was diluted to 2.5×10^{-3} mg/mL in DMSO (8 μ M). For PMA, the 2 mg/mL solution was diluted to 4.93×10^{-3} mg/mL in DMSO (8 μ M). Cells were seeded in 25 cm² flasks to achieve near confluence in 3 days. On the fourth day, cell growth media (DMEM + 10% FBS) was changed to OptiMEM media containing no serum. On the fifth day, media was prepared by adding 10 μ L of 8 μ M SMI or 10 μ L DMSO per 8 mL OptiMEM media. Media in the T25 flasks was removed, cells were rinsed twice with 2 mL OptiMEM, and media containing SMI or vehicle only was added to the culture vessel. Cells were incubated for 4, 8, 12, 16, and 24 hours for clenbuterol and 4, 12, and 24 hours for PMA. After incubation, conditioned media was aspirated, snap frozen in liquid nitrogen, and stored at -80°C for ELISA. ELISA was performed on all samples using technical duplicates.

Dose response for PMA, forskolin, and clenbuterol at 12 hours

Cells were seeded in culture flasks to achieve confluence in 3 days. On day 4, growth medium (DMEM + 10% FBS) was changed to OptiMEM. On day 5, cells were rinsed twice with OptiMEM and media was switched to OptiMEM containing SMI. SMIs

were prepared at different concentrations in DMSO by performing serial dilutions of 5 mg/mL PMA (8.1 mM), 20 mg/mL forskolin (48 mM), 100 mg/mL clenbuterol (318 mM). Cells were treated with media containing the SMI or an equal volume of vehicle-alone and incubated for 12 hours. Immediately after 12 hours, conditioned media was analyzed via the NGF ELISA to determine the correlation between NGF secretion and SMI dose. NGF titers from cells treated with vehicle alone were subtracted from NGF titers from SMI affected cells in order to determine SMI effect.

Evaluating small molecule induction of NGF secretion into conditioned media

For all SMI experiments, cells are seeded in 6 well plates at a density of 75000 cells/mL (2.5 mL final volume in DMEM + 10% FBS growth medium). After 3 full days, DMEM + 10% FBS is removed, cells are rinsed twice with 1 mL OptiMEM, and OptiMEM-B (OptiMEM + 5% sterile filtered BSA) is added to the wells (2.5 mL per well). On the fifth day, OptiMEM-B is removed from the wells and OptiMEM-B containing SMI or vehicle alone is added. Cells were incubated for 2 minutes, 15 minutes, 60 minutes, and 240 minutes. After incubation, cell culture media was aspirated for ELISA. Cells were then immediately rinsed with ice cold PBS and lysed on ice for 20 minutes using a lysis buffer composed of TPER Reagent (Pierce, Rockford, IL), 300 mM sodium chloride, 1 mM sodium orthovanadate, 200 mM PEFABLOC (AEBSF) (Roche, Basel, Switzerland), 1 µg/mL Apropitin (Sigma, St. Louis, MO), 5 mg/mL Pepstatin A (Sigma), 1 mg/mL Leupeptin (Sigma). Cell lysates were cleared via centrifugation and supernatants and pellets were snap frozen in liquid nitrogen and stored at -80°C for reverse phase protein microarray analysis and real time PCR analysis.

Preparation of SMI

PMA. Media for PMA testing was prepared by loading 19.75 μL of 8.1 mM PMA in DMSO into 16 mL OptiMEM-B (final concentration of 10 μM in media). The 8.1 mM PMA was diluted to 8.1 μM PMA in DMSO and 19.75 μL of 8.1 μM PMA was added to 16 mL media (final concentration of 10 nM in media). Vehicle-only media was prepared by adding 19.75 μL DMSO to 16 mL OptiMEM-B. **Clenbuterol.** Media for clenbuterol testing was prepared by loading 19.3 μL of 8.75 mM clenbuterol in water into 16 mL OptiMEM-B (final concentration of 10 μM in media). The 8.75 mM clenbuterol was diluted to 8.75 μM clenbuterol in water and 19.3 μL of 8.75 μM clenbuterol was added to 16 mL media (final concentration of 10 nM in media). Vehicle-only media was prepared by adding 19.3 μL water to 16 mL OptiMEM-B. **Forskolin.** Media for forskolin testing was prepared by loading 19.7 μL of 8.1 mM forskolin in DMSO into 16 mL OptiMEM-B (final concentration of 10 μM in media). The 8.1 mM forskolin was diluted to 8.75 μM forskolin in DMSO and 19.3 μL of 8.75 μM forskolin was added to 16 mL media (final concentration of 10 nM in media). Vehicle-only media was prepared by adding 19.5 μL DMSO to 16 mL OptiMEM-B. **Oleanolic Acid.** Media for oleanolic acid testing was prepared by loading 14.6 μL of 10.9 mM oleanolic acid in DMSO into 16 mL OptiMEM-B (final concentration of 10 μM in media). The 10.9 mM oleanolic acid was diluted to 10.9 μM oleanolic acid in DMSO and 14.6 μL of 10.9 μM oleanolic acid was added to 16 mL media (final concentration of 10 nM in media). Vehicle-only media was prepared by adding 14.6 μL DMSO to 16 mL OptiMEM-B. **Cryptotanshinone.** Media for cryptotanshinone testing was prepared by loading 9.5 μL of 16.9 mM cryptotanshinone in DMSO into 16 mL OptiMEM-B (final concentration of 10 μM in media). The 16.9 mM

cryptotanshinone was diluted to 16.9 μM cryptotanshinone in DMSO and 9.5 μL of 16.9 μM cryptotanshinone was added to 16 mL media (final concentration of 10 nM in media). Vehicle-only media was prepared by adding 9.5 μL DMSO to 16 mL OptiMEM-B.

Calcipitriol. Media for calcipitriol testing was prepared by loading 13.2 μL of 12.1 mM calcipitriol in DMSO into 16 mL OptiMEM-B (final concentration of 10 μM in media). The 12.1 mM calcipitriol was diluted to 12.1 μM calcipitriol in DMSO and 13.2 μL of 12.1 μM calcipitriol was added to 16 mL media (final concentration of 10 nM in media). Vehicle-only media was prepared by adding 13.2 μL DMSO to 16 mL OptiMEM-B.

Carnosol. Media for carnosol testing was prepared by loading 10.6 μL of 15.3 mM carnosol in DMSO into 16 mL OptiMEM-B (final concentration of 10 μM in media). The 15.3 mM carnosol was diluted to 15.3 μM carnosol in DMSO and 10.6 μL of 15.3 μM carnosol was added to 16 mL media (final concentration of 10 nM in media). Vehicle-only media was prepared by adding 10.6 μL DMSO to 16 mL OptiMEM-B.

CDDO. Media for CDDO testing was prepared by loading 9.6 μL of 16.6 mM CDDO in DMSO into 16 mL OptiMEM-B (final concentration of 10 μM in media). The 16.6 mM CDDO was diluted to 16.6 μM CDDO in DMSO and 9.6 μL of 16.6 μM CDDO was added to 16 mL media (final concentration of 10 nM in media). The 16.6 mM CDDO was also diluted to 1.66 mM CDDO and 9.6 μL of 1.66 mM CDDO was added to 16 mL media (final concentration of 1 μM in media). Vehicle-only media was prepared by adding 9.6 μL DMSO to 16 mL OptiMEM-B.

Reverse phase protein microarrays and data analysis

Reverse phase protein microarrays

Using the 2470 Aushon Arrayer (Aushon BioSystems, Billerica, MA, USA), approximately 9 nl of each cell lysate was printed in triplicate onto nitrocellulose-coated slides (Grace BioLabs, Bend, OR, USA). Samples were printed along with a series of standard curves of positive and negative control lysates for quality assurance. For estimation of total protein amounts, selected arrays were stained with Sypro Ruby Protein Blot Stain (Invitrogen, Carlsbad, CA) according to the manufacturer's instructions and visualized on a Powerscanner fluorescent scanner (Tecan US, Inc., Research Triangle Park, NC). Printed slides were prepared for staining by treating with 1x Reblot (Chemicon, Temecula, CA) for 15 min, followed by 2 x 5 min washes with PBS. Slides were treated for at least 1 hour with blocking solution (1g I-block (Applied Biosystems, Bedford, MA), 0.5% Tween-20 in 500 mL PBS) with constant rocking. Blocked arrays were stained with antibodies on an automated slide stainer (DakoCytomation, Carpinteria, CA) using the Catalyzed Signal Amplification System kit according to the manufacturer's recommendation (CSA; Dako). Briefly, endogenous biotin was blocked for 10 minutes with the biotin blocking kit (Dako), followed by application of protein block for 5 minutes; primary antibodies were diluted in antibody diluent and incubated on slides for 30 minutes and biotinylated secondary antibodies were incubated for 15 minutes. Signal amplification involved incubation with a streptavidin-biotin-peroxidase complex provided in the CSA kit for 15 minutes, and amplification reagent (biotinyl-tyramide/hydrogen peroxide, streptavidin-peroxidase) for 15 minutes each. A signal was generated using streptavidin-conjugated IRDye680 (LI-COR, Lincoln, NE). Slides were

allowed to air dry following development. All antibodies used were subjected to extensive validation for single band, appropriate MW specificity by Western blot as well as phosphorylation specificity through the use of cell lysate controls (e.g. HeLa +/- pervandate, Jurkat +/- Calyculin).

Reverse phase protein microarray data analysis

Heat maps were generated using *R*. Protein abundance values for treated samples were divided by the average protein abundance for the corresponding untreated protein controls. Fold change determined by taking \log_2 of the resulting values and plotting in *R* using the *heatmap* script. The raw data output uses a 256-degree color palette to indicate fold change, with more intense reds indicating greater upregulation and more intense greens indicating greater downregulation. Because some analytes achieve a \log_2 fold change in excess of +25 or -25, small changes in fold change (<2) are difficult to distinguish visually. To mitigate this, the data was processed such that values more positive than +10 or more negative than -10 were set to +10 or -10 respectively (thus imposing a +10/-10 cap). This data iteration was still not sufficient to clearly emphasize the changes in abundance of several key proteins of interest (i.e. pCREB). Successive analyses were performed employing this capping strategy to emphasize lesser degrees of fold change. For illustrative purposes in the appendix, values more positive than +2 or more negative than -2 were capped at +2 and -2 respectively to clearly indicate any proteins showing a 50% change in protein phosphorylation state. It is critical to emphasize the importance of not relying on this data iteration exclusively, as it underemphasizes the high fold-change values for some analytes.

Six-replicate data from treated and untreated cells were compared using a two-tailed unpaired heteroscedastic t-test. Comparisons generating p-values < 0.05 were considered statistically significant. For statistically significant analytes, Log2 fold change was determined using the median values for the treated and untreated data sets.

Quantitative reverse transcription PCR and related experiments

Transformation of XL1-Blue E. coli with pHumNGF_Internal plasmid.xdna

Luria broth (LB) agar for cell growth was prepared by adding 4.0 g LB Agar to a final volume of 100 mL sterile water. Ampicillin was added to the center of culture plates at a concentration of 100 µg/mL (26 µL of 50 mg/mL ampicillin per 13 mL media). LB agar was autoclaved, added to the plate (13 mL per plate), mixed with the ampicillin, and allowed to cool. XL1 blue *E. coli* cells were thawed on ice and the pCMV6-XL1 plasmid containing the NGF insert (OriGene Rockville, MD) was resuspended in 100 µL sterile filtered water. A 50 µL aliquot of XL1 blue cells was loaded into a centrifuge tube and 2 µL of the vector solution was added. Cells and vector are co-incubated on ice for 30 minutes. Cells were then placed at 42°C for 30 seconds. Cells were immediately removed and placed back on ice. LB broth (250 µL) was transferred to the cells and cells were placed in the incubator/shaker for 1 hour at 37°C and 250 rpm. LB agar plates were seeded with 20 µL, 50 µL, or 100 µL of the transformation mixture. A successful colony was cultured in 10 mL of LB media containing 120 µg/mL ampicillin (24 µL of 50 mg/mL). The culture was incubated overnight on an incubator/shaker at 37°C and 250 rpm. Cells were harvested by centrifugation at 3200 \times g and 40°C. DNA was extracted

according to manufacturer's protocol for the *GenElute Plasmid Miniprep kit* (Sigma) and stored at -20°C.

Agarose gel electrophoresis and qPCR melt curve analysis

RNA extraction. Cells were grown in a 25 cm² flask to confluence and removed from the culture flask using trypsin. Cells were pelleted at 200 *x g* and pellets were washed twice with PBS. RNA extraction was performed according to the manufacturer's protocol for *RNEasy RNA extraction* (Qiagen). RNA abundance and purity was evaluated using absorbance at 260 nm and 280 nm (2.1.4). **Reverse transcription.** Immediately after UV-Vis analysis, reverse transcription was performed in 20 µL reactions containing random hexamer (500ng, Promega), dNTP (1.25 mM in each, Life Technologies), 4x reverse transcriptase buffer (Promega), 200 units of M-MLV reverse transcriptase (Promega), and 1 µg of RNA. **Real time PCR.** Real time PCR was performed on the newly synthesized cDNA in 25 µL reactions containing 12.5 µL Rotor Gene Q master mix (Qiagen), 12.5 µmol forward primer, 12.5 µmol reverse primer, and 100 ng of cDNA from reverse transcription (for NGF testing, 1µL plasmid). Manufacturer's suggested thermal cycling conditions of 5 second denaturing and 10 second annealing and extension for 40 cycles were used. Following PCR, reactions were loaded into a 2% agarose gel containing 25 µg ethidium bromide. After electrophoresis, the gel was analyzed on a UV transilluminator (Kodak).

Confirming primer efficiency

Primer efficiency analysis was performed by making 10 consecutive 10-fold serial dilutions (in water) of the NGF plasmid. Real time PCR was performed using NGF

specific primers according to the qPCR protocol using 2 μ L of each plasmid dilution as template. Each reaction was performed in duplicate.

UV-Vis spectroscopy to quantify RNA extraction and identify protein contamination

A UV-Vis spectrophotometer was zeroed against Tris-Cl (10 mM, pH 7.5), and absorbance at 260 nm (A260) and 280 nm (A280) was recorded by taking readings of RNA extractions diluted in Tris-Cl. RNA abundance was determined from the formula $A_{260} * 40 \text{ ng}/\mu\text{L}/\text{a.u.} = \text{RNA ng}/\mu\text{L}$.

Real time PCR and comparative C_T analysis

Real time PCR is performed on thawed four hour lysates and pellets from the SMI survey using the protocols for RNA extraction, reverse transcription, and real time PCR. Biological triplicates and technical duplicates are used in the study. In data analysis, C_T values are obtained by setting the threshold above background fluorescence, but below the inflection point of the normalized fluorescence plot. Next, C_T values for NGF amplicons are directly subtracted from corresponding reference gene amplicon C_T values to generate ΔC_T values. Fold change between treated samples and untreated samples are derived from the formula: $\text{Fold change} = 2^{-(\Delta C_{T\text{treated}} - \Delta C_{T\text{untreated}})}$. In this case, the median ΔC_T value amongst the untreated samples or the average ΔC_T value amongst the untreated samples can be used. For each experiment, non-template controls are run for each primer set, and each sample is run using RNA (no reverse transcription) as negative controls to test DNA contamination.

Agonist and Antagonist Assays and Related Experiments

Cytotoxicity Assay

After exposure to compound or vehicle-alone in OptiMEM media for four hours, Alamar blue dye was added directly to the media at 1 μ L dye / 10 μ L media and allowed to incubate for one hour. Following incubation, A₅₇₀/A₆₀₀ measurements were made to determine reduction of resazurin dye to resorufin using the following calculation: Percent Reduction = $[(E_{ox600} * A_{570}) - (E_{ox570} * A_{600})] / [(E_{red600} * C_{600}) - (E_{red570} * C_{570})]$, where C₆₀₀ and C₅₇₀ are absorbance of negative controls at 600 nm and 570 nm respectively, E_{ox} and E_{red} are the molar extinction coefficient of oxidized and reduced Alamar blue reagent at the corresponding wavelength, and A₅₇₀ and A₆₀₀ are the absorbance values at 570 nm and 600 nm for the samples of interest. Alternatively, fluorescence measurements (excitation: 535 nm, emission: 590 nm) can be taken and percent reduction calculated by: Percent Reduction = (Experimental RFU – Negative Control RFU) / (Positive Control RFU – Negative Control RFU). Positive control requires a fully reduced calibration sample (generated by autoclaving 10% Alamar blue in Opti-MEM for 15 minutes). A ratio of reduction in treated versus untreated cells is calculated in order to determine overall cell viability.

Preparation of agonists and antagonists

ZM336372 (Sigma Aldrich), UO126 (Sigma Aldrich), FR180204 (Merck Millipore), and BI-D1870 (Santa Cruz Biotechnology) were prepared as 2.5 mM solutions in DMSO and stored in 40 μ L aliquots at -20°C until use. Bryostatin (Sigma Aldrich) was prepared as a 25 μ M solution in DMSO and stored in 40 μ L aliquots at -20°C until use. 217505 (Merck Millipore) was prepared as a 250 μ M solution in DMSO

and stored in 40 μ L aliquots at -20°C until use. Immediately before the assay, required aliquots were thawed and working solutions were prepared in DMSO. Aliquots were not reused to avoid degradation by multiple freeze-thaw cycles.

Antagonist assays

To perform the antagonist assays, cells were prepared in 6-well plates as previously described in the ELISA section. To begin the antagonist assay, media was prepared containing the inhibitor of choice at the appropriate concentration and added to culture wells in triplicate. After 20 minutes, media from the triplicate wells were aspirated, loaded into a 15 mL tube, supplemented with 10 nM PMA, mixed by inversion, and reloaded into the culture wells for 4-hour incubation (thus, the total incubation time with inhibitor is 4 hours, 20 minutes).

Appendix 1 – Reverse phase protein microarray protein antibodies

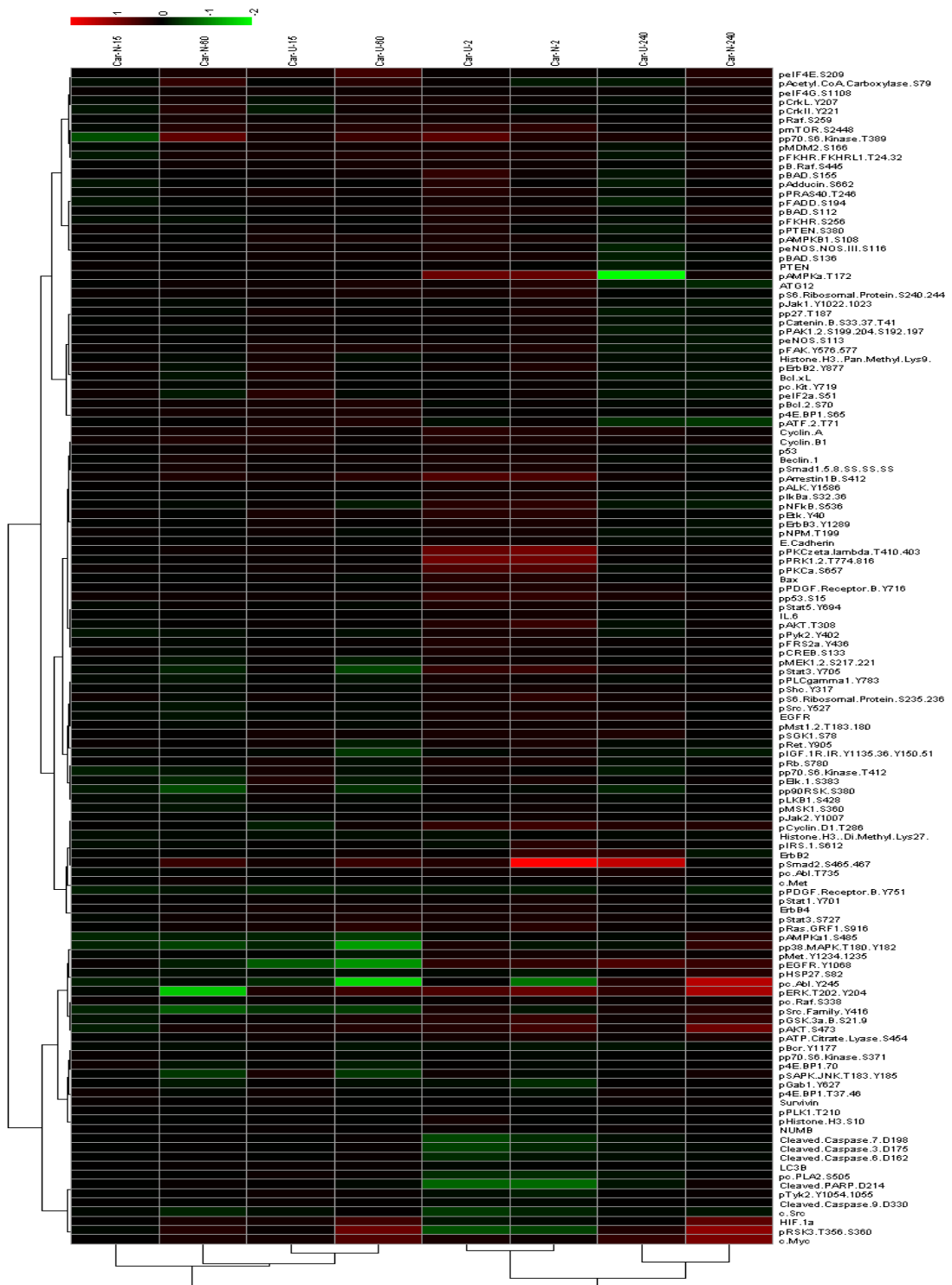
ATG12	pc-Abl T735	pMst1/2 T183/180
Bax	pc-Abl Y245	pmTOR S2448
Bcl-xL	pCatenin B S33/37/T41	pNFkB S536
Beclin 1	pc-Kit Y719	pNPM T199
Cleaved Caspase-3 D175	pc-PLA2 S505	pp27 T187
Cleaved Caspase-6 D162	pc-Raf S338	pp38 MAPK T180/Y182
Cleaved Caspase-7 D198	pCREB S133	pp53 S15
Cleaved Caspase-9 D330	pCrkII Y221	pp70 S6 Kinase S371
Cleaved PARP D214	pCrkL Y207	pp70 S6 Kinase T389
c-Met	pCyclin D1 T286	pp70 S6 Kinase T412
c-Myc	pEGFR Y1068	pp90RSK S380
c-Src	pEGFR Y1148	pPAK1/2 S199/204/S192/197
Cyclin A	pEGFR Y1173	pPDGF Receptor B Y716
Cyclin B1	peIF2a S51	pPDGF Receptor B Y751

E-Cadherin	peIF4E S209	pPKCa S657
EGFR	peIF4G S1108	pPKCzeta/lambda T410/403
ErbB2	pElk-1 S383	pPLCgamma1 Y783
ErbB4	peNOS S113	pPLK1 T210
HIF-1a	peNOS/NOS III S116	pPRAS40 T246
Histone H3, Di-Methyl Lys27	pErbB2 Y1248	pPRK1/2 T774/816
Histone H3, Pan-Methyl Lys9	pErbB2 Y877	pPTEN S380
IL-6	pErbB3 Y1289	pPyk2 Y402
LC3B	pERK T202/Y204	pRaf S259
NUMB	pEtk Y40	pRas-GRF1 S916
p4E-BP1 70	pFADD S194	pRb S780
p4E-BP1 S65	pFAK Y576/577	pRet Y905
p4E-BP1 T37/46	pFKHR S256	pRSK3 T356/S360
p53	pFKHR/FKHRL1 T24/32	pS6 Ribosomal Protein S235/236
pAcetyl-CoA Carboxylase S79	pFRS2a Y436	pS6 Ribosomal Protein S240/244
pAdducin S662	pGab1 Y627	pSAPK/JNK T183/Y185
pAKT S473	pGSK-3a/B S21/9	pSGK1 S78
pAKT T308	pHistone H3 S10	pShc Y317
pALK Y1586	pHSP27 S82	pSmad1/5/8 SS/SS/SS

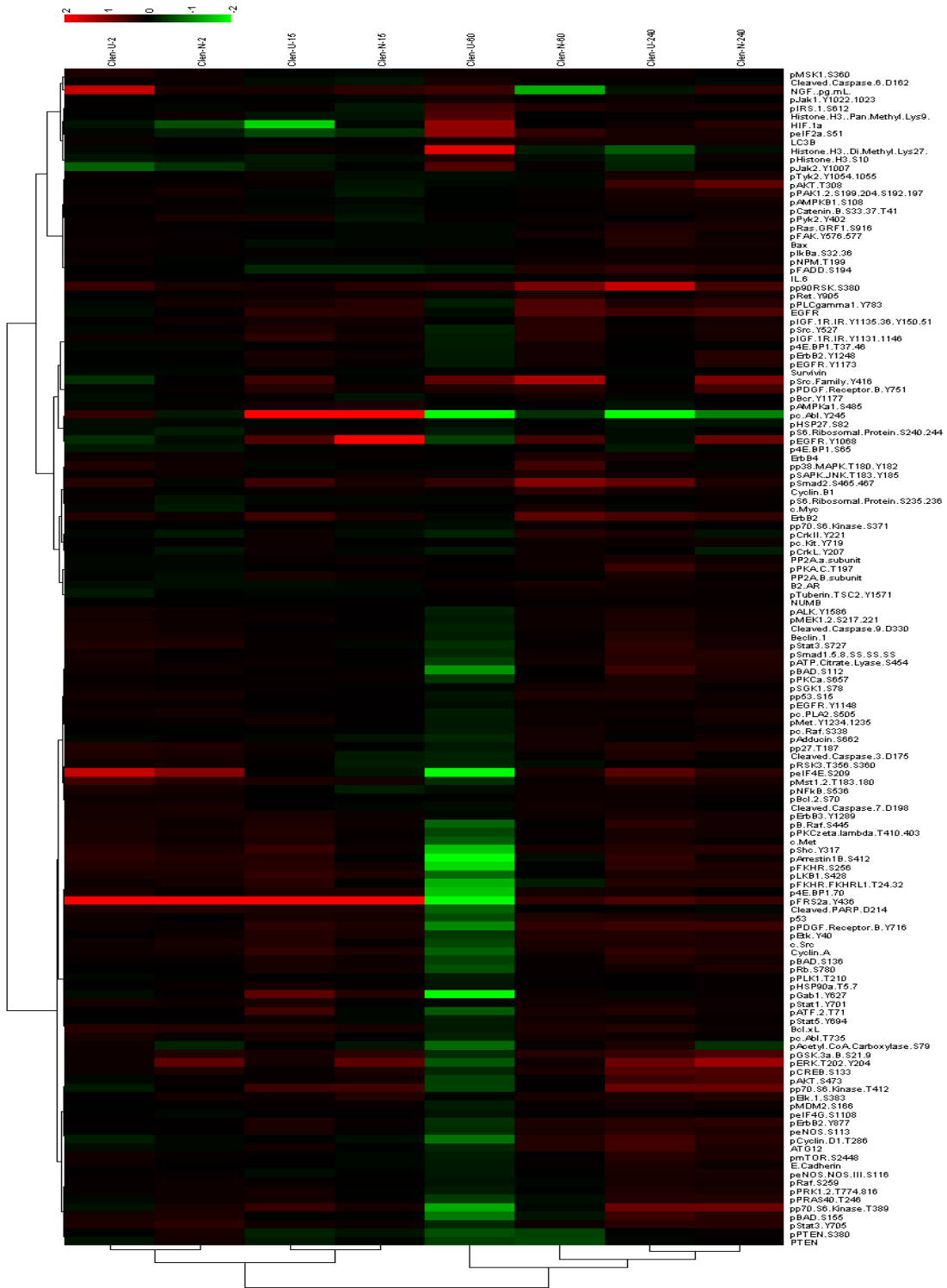
pAMPKa T172	pHSP90a T5/7	pSmad2 S465/467
pAMPKa1 S485	pIGF-1R/IR Y1131/1146	pSrc Family Y416
pAMPKB1 S108	pIGF-1R/IR Y1135/36/Y150/51	pSrc Y527
pArrestin1B S412	pIkBa S32/36	pStat1 Y701
pATF-2 T71	pIRS-1 S612	pStat3 S727
pATP-Citrate Lyase S454	pJak1 Y1022/1023	pStat3 Y705
pBAD S112	pJak2 Y1007	pStat5 Y694
pBAD S136	pLKB1 S428	PTEN
pBAD S155	pMDM2 S166	pTyk2 Y1054/1055
pBcl-2 S70	pMEK1/2 S217/221	Survivin
pBcr Y1177	pMet Y1234/1235	pMst1/2 T183/180
pB-Raf S445	pMSK1 S360	pmTOR S2448

Appendix 2 – Reverse phase protein microarray results for all tested SMI

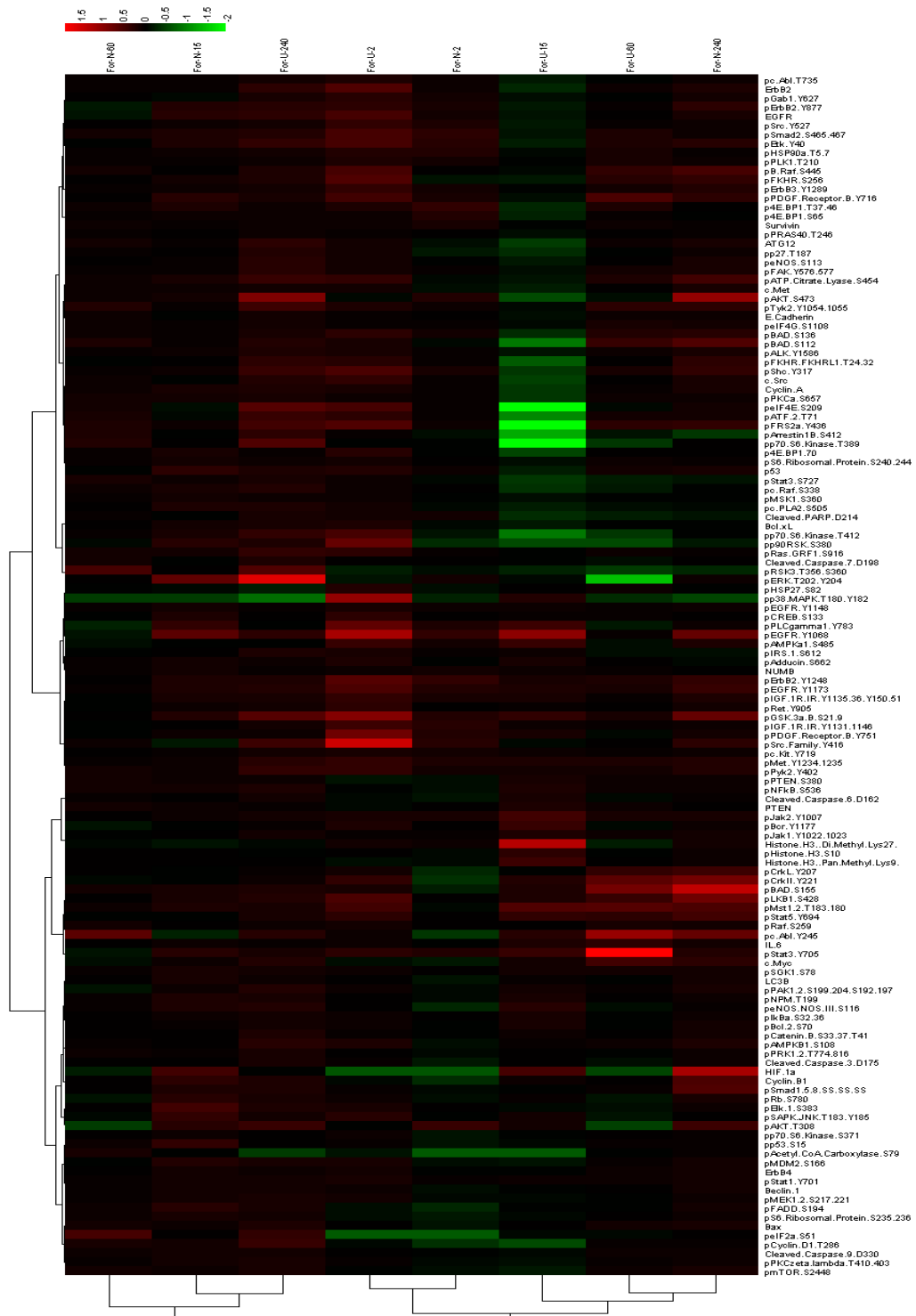
Carnosol



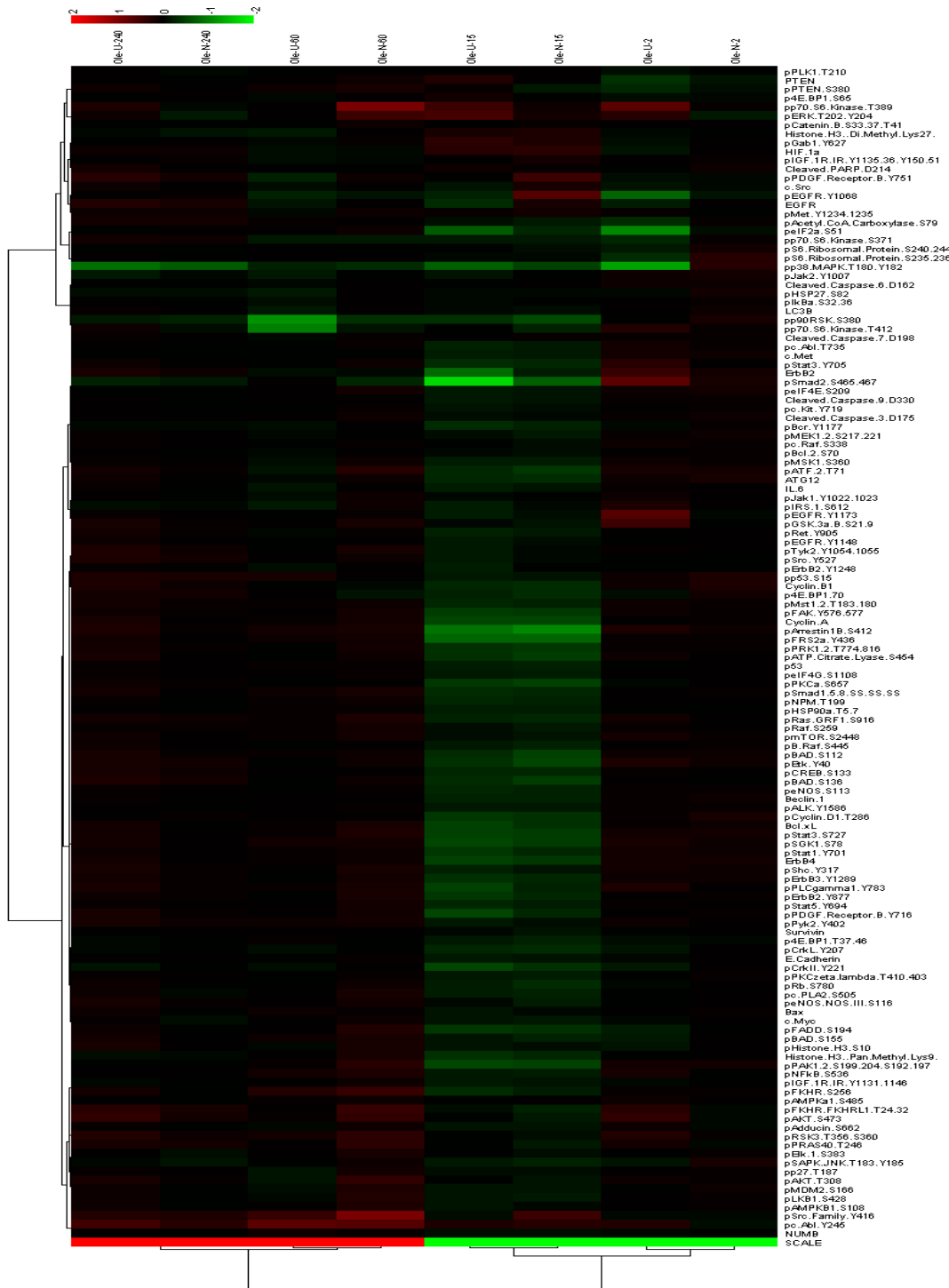
Clenbuterol



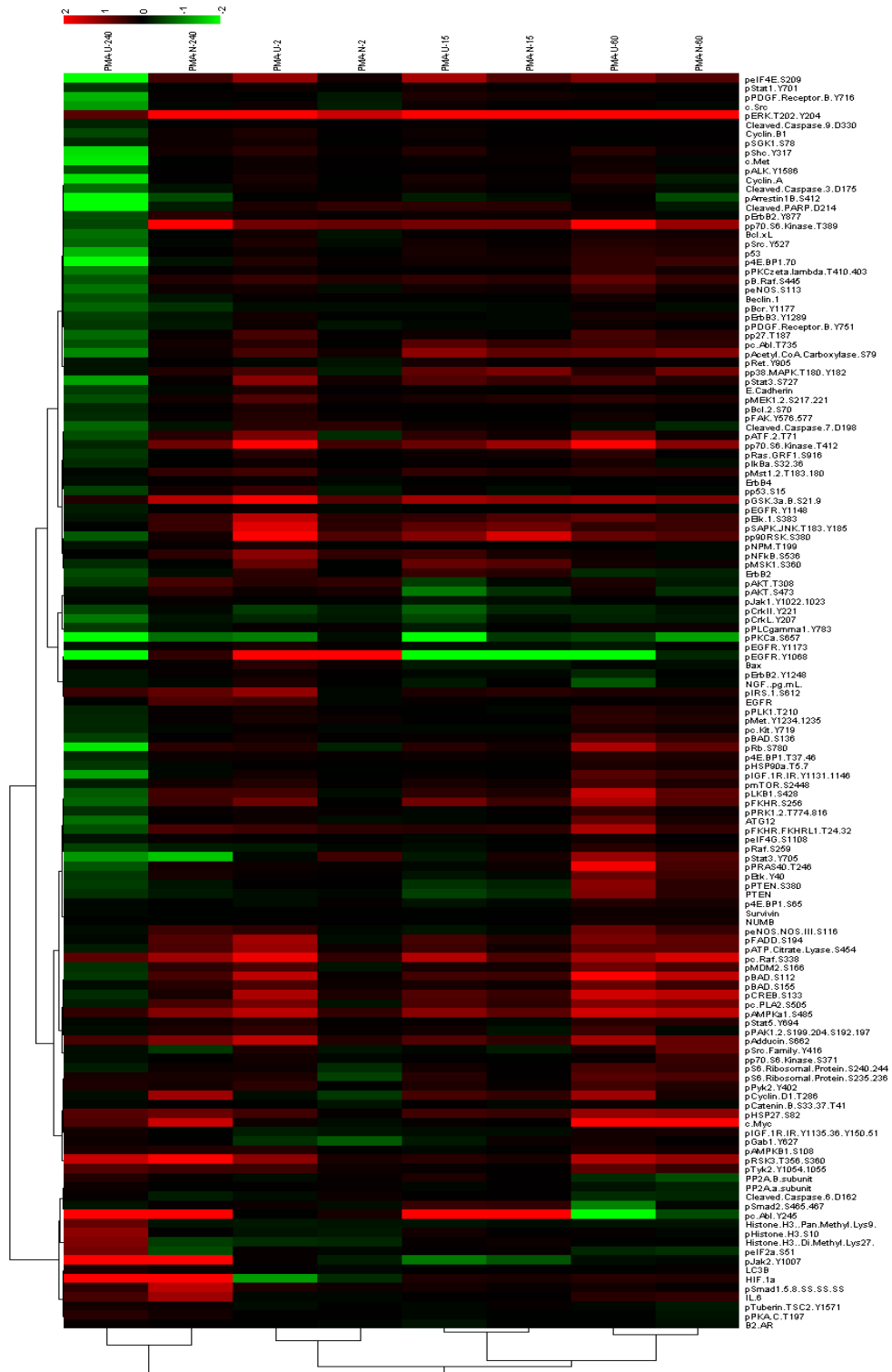
Forskolin



Oleanolic Acid



PMA



Appendix 3 – Two tailed unpaired heteroscedastic t-test data and associated fold change

Clenbuterol (10 nM, 10 μ M)

Variable	Exposure Duration (min)	10 nM		10 μ M	
		<i>p</i> value	Log2 Median Fold Change	<i>p</i> value	Log2 Median Fold Change
c-Src	15			0.04991	-0.56554
	240	0.01875	0.26401		
pAdducin S662	60			0.00740	-0.42127
pAkt S473	60			0.00550	-0.59006
	240	0.00242	0.52803		
pAkt T308	240	0.02046	0.79925	0.00175	0.64633
pc-Abl Y245	60			0.00827	-26.62927
	240			0.08502	-25.29333
pc-Raf S338	60			0.00080	-0.22506
	240	0.02046	0.11542	0.00422	0.10099
pEGFR Y1068	240	0.01662	0.99979		
peIF2a S51	15			0.00142	-0.69105
	60			0.00846	1.05172
pERK T202/Y204	60			0.00997	-0.55400
	240			0.00091	0.98247
pFKHR S256	15			0.04646	0.29142
	60			0.00457	-1.36623
	240			0.00035	0.44291
pGSK3a/B S21/9	2	0.00041	0.29719		
	15	0.04290	0.39530		
	60			0.00483	-0.48475
	240	0.02085	0.73145	0.00465	0.52370
pp38MAPK T180/182	2			0.03518	0.27411
pp70 S6 Kinase T389	15			0.00694	0.44579
	60			0.00232	-1.19744
	240	0.04102	0.79348	0.04488	0.77906

pp70 S6 Kinase T412	15			0.01259	0.56265
	60			0.00589	-0.60737
	240	0.01717	0.65498	0.02067	0.72712
pp90RSK S380	15	0.04725	0.39530		
	60	0.01272	1.04884	0.02213	0.46743
	240	0.00888	0.63479	0.00092	1.31141
pPDGF Receptor B Y716	15			0.01786	0.38231
	60			0.01821	-1.01854
	240	0.00137	0.54101	0.02489	0.44291
pPDGF Receptor B Y751	15	0.04292	0.09954		
	240	0.00582	0.57852		
pPKCa S657	60			0.00025	-0.54678
	240			0.01998	0.25824
pPLCgamma1 Y783	15	0.02439	0.41694		
	60	0.00730	0.68672		
	240			0.01108	0.33470
pPyk2 Y402	15	0.01842	-0.17889		
pRSK3 T356/S360	15	0.02424	-0.30585		
	60			0.01919	-0.33903
pS6 Ribosomal Protein S240/244	15	0.04301	0.17312		
	60			0.03512	-0.24526
pSAPK/JNK T183/Y185	60	0.02927	0.30729		
pSrc Family Y416	2			0.02771	-0.33182
	240	0.01370	0.97093		
pStat3 Y705	2	0.00400	0.43137	0.04813	0.27123
	60			0.03414	-0.45445
	240	0.00314	0.39097		
PTEN	60			0.04259	-0.60593
ATG12	240	0.04213	0.22362	0.04085	0.53380
Cleaved Caspase-9 D330	2	0.00675	0.16158	0.00331	0.29143
	60			0.00288	-0.33380
	240	0.01621	0.14427	0.00886	0.23083
Cleaved PARP D214	60			0.00029	-0.92188
c-MET	15			0.03616	0.29720
	60			0.00024	-0.75886
	240			0.02208	0.24526
E-Cadherin	240			0.01429	0.02969
EGFR	15	0.04460	0.44579		
	60	0.01088	0.64344		
	240	0.01660	0.59872	0.03555	0.52658

ErbB2	240	0.00365	0.49340		
ErbB4	2			0.03865	0.18322
HIF-1a	60			0.02802	1.15704
LC3B	2			0.00020	0.12407
	60			0.00257	0.23083
	240	0.04896	0.17312	0.00834	0.18755
NUMB	60	0.00128	0.10099		
p4E-BP1 S65	240			0.00892	-0.21640
pAcetyl-CoA Carboxylase S79	60			0.02357	-0.84830
pAMPKa1 S485	15	0.01658	0.22939		
pAMPKB1 S108	240			0.02450	0.18466
pATF-2 T71	60			0.01848	-0.75886
pATP-Citrate Lyase S454	60			0.00123	-0.53235
	240			0.00522	0.44868
pBAD S112	60			0.00013	-1.12819
	240	0.00474	0.34625	0.00028	0.57708
pBAD S136	2	0.01568	0.10099		
	15	0.01430	0.01645	0.04073	0.30729
	60	0.02499	0.07791	0.00004	-0.58141
	240	0.00675	0.18899	0.00223	0.31739
pBAD S155	60			0.00071	-1.02864
	240			0.00566	0.54678
pBcl-2 S70	2	0.03597	0.11109		
	240			0.00912	0.15004
pBcrY1177	240	0.00944	-0.07358		
pB-Raf S445	15	0.02296	0.12840	0.01220	0.26401
	60			0.00045	-0.83965
	240			0.00300	0.52947
pc-Abl T735	15			0.01987	0.21208
	60			0.00529	-0.32893
pCatenin B S33/37/T41	240	0.04856	0.11686		
pc-PLA2 S505	60			0.03660	-0.26780
	240	0.02929	0.25536		
pCREB S133	2	0.03681	0.16302		
	60			0.02422	-0.46311
	240	0.01920	0.62036	0.01577	0.62613
pCyclin D1 T286	2			0.02063	-0.25680
	60			0.01076	-0.88870
	240	0.00880	0.35779	0.00137	0.59583
pEGFR Y1148	240	0.01992	0.12984	0.00386	0.08656

pEGFR Y1173	240	0.03008	0.42415		
peIF4G S1108	60			0.00239	-0.21640
	240			0.02166	0.10099
pElk-1 S383	15	0.04908	0.39963		
	240	0.04303	0.45878		
pENOS/NOS III S116	240			0.04862	0.31306
pErbB2 Y1248	240	0.02078	0.45301		
pErbB2 Y887	60	0.04359	0.28854	0.02019	-0.45156
	240	0.02913	0.40828		
pErbB3 Y1289	240			0.02761	0.23227
pEtk Y40	15	0.04983	0.23660		
	60	0.00872	0.32893	0.01108	-0.54101
	240	0.00489	0.34336	0.00481	0.35202
pFADD S194	60			0.02855	-0.21208
	240			0.00718	0.48186
pFKHR/FKHRL1 T24/32	15			0.03027	0.42560
	60			0.00790	-1.29410
	240			0.03617	0.37077
pFRS2a	60			0.00494	-27.00004
	240	0.01161	0.56265	0.00745	0.77761
pGab1 Y627	15			0.00172	0.78627
	60	0.04128	0.14860	0.00046	-1.65044
pHistone H3 S10	60			0.04581	0.35779
pIGF-1R/1R Y1131/1146	15	0.02942	0.21785	0.15070	0.37943
	60			0.03055	-0.28421
pIGF-1R/1R Y1135/36/Y150/51	15	0.04575	0.21208		
	60	0.03098	0.21640		
pIkBa S32/36	60	0.04642	0.10099		
	240	0.00606	0.12984		
pIRS-1	60			0.03456	0.74587
pJAK2 Y1007	60			0.03668	0.65643
pLKB1 S428	15	0.00233	0.29575		
	60			0.00002	-0.91611
	240			0.02990	0.22362
pMDM2 S166	60			0.01486	-0.33182
pMEK1/2 S217/221	2	0.04380	0.14283		
	60			0.00184	-0.25968
	240	0.01570	0.17168	0.00274	0.24382
pMet Y1234/1235	60			0.01731	-0.21929
	240	0.04308	0.15581		

pSMSK1 S360	2			0.04564	0.30729
pMst1/2 T183/180	2	0.01614	0.32605	0.01222	0.48763
	15	0.01569	0.18322	0.01263	0.31739
	60			0.01740	-0.42415
	240			0.04810	0.32172
pmTOR S448	60			0.03098	-0.33182
	240	0.02965	0.34625	0.00134	0.37514
pNFkB S536	15	0.03867	-0.35202		
	240			0.04469	0.17457
pNPM T199				0.01691	0.20775
pp27 T197	240			0.04860	0.29287
pPAK1/2 S199/204/S192/197	15	0.03848	-0.24670		
	240			0.02131	0.26257
pPLK1 T210	60			0.00528	-0.26257
pPRAS40 T246	15			0.03194	0.16591
	60			0.00263	-0.57708
pPRK1/2 T774/816	2	0.00528	0.15004		
	60			0.01190	-0.33182
	240			0.00924	0.30152
pPTEN S380	60			0.02297	-0.73433
pRaf S259	2	0.03366	0.15293		
	15			0.03301	0.10099
	60			0.00890	-0.17312
	240	0.02455	0.12984	0.01792	0.15870
pRas-GRF1 S916	240			0.00792	0.25969
pRb S780	60			0.00031	-0.64344
	240	0.02413	0.25969		
pRet Y905	15	0.00221	0.14138		
	60	0.02189	0.22939		
	240	0.01712	0.25969		
pShc Y317	60			0.01022	-1.28111
	240	0.00272	0.39963	0.02059	0.32894
pSmad1/5/8 SS/SS/SS	2			0.01855	0.19476
	60			0.01800	-0.36356
	240	0.00680	0.35779	0.00358	0.41694
pSrc Y527	60			0.01372	
	240	0.00977	0.21208		
pStat1 Y701	2	0.04950	0.18322		
	15			0.03476	0.23516
	240			0.04510	0.18034

pStat3 S727	60			0.01377	-0.48042
	240			0.01599	0.38087
pTyk2 Y1054/1055	240	0.00969	0.18611		
Bcl-xL	2	0.00391	0.03075	0.00370	0.40684
	15	0.03075	0.29287	0.01182	0.39963
Beclin 1	2	0.01995	0.19188	0.30370	0.23516
	60			0.03489	-0.26978
	240			0.00564	0.37510
Cyclin A	15	0.04135	0.26401		
	60			0.00331	1.64756
	240			0.03695	-0.74443
Histone H3, Di-Methyl Lys27	60			0.00331	1.64756
	240			0.03695	-0.74443
Histone H3, Pan-Methyl Lys9	60			0.00630	0.71414
p4E-BP1 70	60			0.00063	-1.29843
p53	2			0.00309	0.15870
	15	0.01643	0.16447	0.03476	0.14571
	60			0.00002	-0.68528
	240	0.03809	0.20342	0.02336	0.27555
pALK Y1586	2	0.04761	0.15581		
	60	0.04043	0.14427	0.00028	-1.65333
	240	0.04376	0.19476	0.00758	0.36067
pArrestin1B S412	60			0.00028	-1.65333
	240			0.00758	0.36067
pEIF4E S209	2	0.02100	1.15271	0.03654	1.33738
	60	0.04451	0.23372	0.00078	-2.25349
	240	0.00031	0.42415	0.01724	0.67230
peNOS S113	60			0.04127	-0.46888
	240	0.02513	0.26257	0.00420	0.42560
pHSP90a T5/7	15			0.00672	0.16735
	60			0.02998	-0.16591
pPKCzeta/lambda T410/403	2	0.03048	0.15870	0.01214	0.24526
	60			0.00252	-0.64633
	240			0.00633	0.25968

Forskolin (10 nM)

Variable	Exposure Duration (min)	<i>p</i> value	Log2 Median Fold Change
c-Myc	240	0.00800	0.30297
Cyclin B1	2	0.03164	-0.04718
	15	0.00600	0.36789
	60	0.03338	0.60593
pAdducin S662	240	0.04828	-0.16014
pAkt S473	240	0.00000	1.03730
pAkt T308	240	0.00633	0.49484
pc-Abl Y245	60	0.03493	0.56265
	240	0.12161	0.68817
pc-Raf S338	60	0.04984	0.17312
	240	0.01038	-0.14427
pCrkII Y221	240	0.02296	0.89736
peIF2a S51	60	0.03481	0.42127
pERK T202/Y204	15	0.02420	0.62036
pFKHR S256	240	0.04752	0.33182
pGSK3a/B S21/9	240	0.00449	0.78050
pp38MAPK T180/182	240	0.01809	-0.85408
pp70 S6 Kinase T389	2	0.00501	-0.26546
pp90RSK S380	15	0.03205	0.23083
pPDGF Receptor B Y716	15	0.04655	0.36356
pPLCgamma1 Y783	15	0.04834	0.20775
pPyk2 Y402	240	0.00902	0.24381
pRSK3 T356/S360	240	0.02217	-0.44435
pSAPK/JNK T183/Y185	15	0.00907	0.41550
pStat3 Y705	15	0.01826	0.27844
	240	0.00164	0.22795
pStat5 Y694	240	0.03003	0.49484
Bax	240	0.04465	0.08945
Cleaved Caspase-3 D175	2	0.04167	-0.39097
c-MET	240	0.02775	0.08656
EGFR	240	0.03915	0.13417
HIF-1a	2	0.02905	-0.80791
	15	0.04072	0.41405
	240	0.00113	1.11953
IL-6	240	0.02022	0.07358
LC3B	240	0.04555	0.05338

NUMB	2	0.04850	0.08656
p4E-BP1 S65	240	0.01566	-0.01298
p4E-BP1 T37/46	240	0.03746	-0.06492
pAcetyl-CoA Carboxylase S79	2	0.03688	-0.90168
pAMPKa1 S485	15	0.00288	0.16158
pATP-Citrate Lyase S454	240	0.01093	0.54245
pBAD S112	240	0.01696	0.66508
pBAD S136	240	0.00191	0.27123
pBAD S155	240	0.01962	1.24645
pB-Raf S445	240	0.00866	0.57996
pCrkL Y207	2	0.00496	-0.44435
	240	0.00541	0.45012
pCyclin D1 T286	2	0.04943	-0.49196
pElk-1 S383	15	0.02054	0.44724
pENOS/NOS III S116	2	0.02322	-0.39530
pErbB2 Y887	240	0.03534	0.29864
pErbB3 Y1289	240	0.01494	0.19909
pEtk Y40	15	0.04501	0.15870
	240	0.03718	0.25536
pFKHR/FKHRL1 T24/32	240	0.00907	0.35346
pHSP27 S82	15	0.03236	-0.18755
pIGF-1R/1R Y1131/1146	15	0.00541	0.24093
pIGF-1R/1R Y1135/36/Y150/51	15	0.00934	-0.16303
	60	0.04605	0.18178
pIRS-1	240	0.02669	-0.20053
pLKB1 S428	15	0.02041	0.79925
pMet Y1234/1235	240	0.00607	0.17188
pMst1/2 T183/180	240	0.00004	0.54967
pRaf S259	240	0.02166	0.10099
pShc Y317	240	0.01751	0.39963
pSmad1/5/8 SS/SS/SS	240	0.00036	0.58862
pStat1 Y701	240	0.01920	0.08800
pStat3 S727	240	0.01040	-0.29720
pTyk2 Y1054/1055	60	0.01942	0.22218
	240	0.00178	0.33182
p53	15	0.00245	0.33182
	240	0.02912	0.16014
pALK Y1586	240	0.03609	0.10243
pArrestin1B S412	240	0.04042	-0.50061
pEIF4E S209	15	0.04718	-0.17457

pHSP90a T5/7	2	0.04150	0.23660
pSGK1 S78	240	0.00542	0.08223

PMA (10 nM)

Variable	Exposure Duration (min)	<i>p</i> value	Log2 Median Fold Change
c-Myc	60	0.00949	1.93310
pAdducin S662	60	0.03556	1.02287
	240	0.00338	1.03730
pc-Raf S338	15	0.00569	0.69249
	60	0.02553	1.62303
	240	0.01858	1.11087
peIF2a S51	240	0.04710	-0.79925
pERK T202/Y204	15	0.00002	1.93177
	60	0.00059	1.75143
pFKHR S256	15	0.02628	0.61747
	60	0.01349	0.89014
pGSK3a/b S21/9	2	0.00986	0.90168
	15	0.00063	0.93487
	60	0.01711	1.01710
	240	0.00768	1.20177
pp38MAPK T180/Y182	15	0.00802	0.75597
	60	0.00326	0.79493
pp70 S6 Kinase T389	60	0.02690	1.28833
	240	0.00355	1.96784
pp70 S6 Kinase T412	15	0.00020	1.17003
	240	0.04363	0.76318
pp90RSK S380	2	0.01847	0.77328
	15	0.00530	1.28977
	60	0.02397	0.66941
pPKCa S657	15	0.00619	-0.46311
	60	0.03333	-1.08491
	240	0.01591	-0.92040
pRSK3 T356/S360	60	0.00977	1.09356
	240	0.01321	1.90580
pS6 Ribosomal Protein S235/236	2	0.00193	-0.59150
	60	0.00384	0.62324
pS6 Ribosomal Protein S240/244	2	0.00904	-0.49196
	60	0.00177	0.46166
pSAPK/JNK T183/Y185	15	0.00164	0.82234

	60	0.00117	0.52370
pSmad2 S465/467	15	0.04230	0.47609
pStat3 Y705	2	0.00702	0.59151
Bax	15	0.01904	-0.24560
Cleaved Caspase-7 D198	2	0.03378	0.38953
	60	0.02972	-0.44146
Cleaved PARP D214	2	0.04417	0.30297
	15	0.01665	0.31306
IL-6	60	0.00227	0.54390
	240	0.04199	1.09501
NUMB	60	0.00356	0.15870
p4E-BP1	60	0.00174	0.30008
pAcetyl-CoA Carboxylase S79	15	0.03434	0.75020
pAMPK α 1 S485	15	0.00250	0.75597
	60	0.01083	1.33728
	240	0.00230	1.05172
pATP-Citrate Lyase S454	60	0.02009	0.87572
pBAD S112	15	0.00801	0.57852
	60	0.00032	1.29554
pBAD S136	60	0.02653	0.53091
pBAD S155	60	0.03500	0.57708
pBcr Y1177	240	0.01398	0.52514
pB-Raf S445	2	0.00587	0.31739
	15	0.00993	0.33182
	60	0.03395	0.42560
pc-Abl	15	0.00286	0.50062
	60	0.00114	0.41838
pc-PLA2 S505	15	0.03711	0.02770
	60	0.01503	1.02864
pCREB S133	15	0.02058	0.48619
	60	0.00062	1.20609
peIF4G S1108	15	0.01547	-0.04905
pElk-1 S383	15	0.00146	0.65210
	60	0.00701	0.54245
pEtk Y40	60	0.00423	0.58718
pFADD S194	60	0.03601	1.14839
pFKHR/FKHRL1 T24/32	2	0.00331	0.42560
	15	0.04177	0.54390
pFRS2a Y436	240	0.03381	25.77000
pHSP27 S82	15	0.02510	0.39674
	60	0.00126	0.95939

	240	0.00873	0.79925
pIRS-1 S612	15	0.00911	0.38520
pLKB1 S428	60	0.02392	1.02864
pMDM2 S166	60	0.00970	0.74587
pMEK 1/2 S217/221	15	0.03810	0.11830
	60	0.01037	0.39530
pMetY1234/1235	60	0.03248	0.35057
pMSK1 S360	15	0.00035	0.75742
pMst 1/2 T183/180	15	0.01007	0.36067
	60	0.02292	0.39530
pPLK1 T210	60	0.04029	0.23516
pStat3 S727	15	0.02765	0.54678
pTyk2 Y1054/1055	60	0.00916	0.51504
	240	0.04294	0.04617
Survivin	60	0.04331	0.07214
p53	60	0.00397	0.36644
peIF4E S209	15	0.03731	0.68672

Appendix 4 – Transcription factors with multiple binding sites on the NGF gene

Transcription Factor	Number of Sites
STAT5A	13
CREB	8
STAT3	8
deltaCREB	7
FOXO1	5
POU3F2	5
AREB6	4
GR	3
p53	3
AP-1	2
ATF-2	2
C/EBP/beta	2
c-Fos	2
c-Jun	2
CUTL1	2
ER-alpha	2
FNF-1	2
FoxB	2
FOXD3	2
FOXI1	2
FOXJ2	2
Fra-1	2
GATA-1	2
HFH-3	2
HOXA9	2
JunB	2
JunD	2
Meis-1	2
MRF-2	2
Msx-1	2
RSRFC4	2

S8	2
Sox5	2
SRF	2
TBP	2
TFIID	2

References

1. Alzheimer's Association. 2014 Alzheimer's Disease Facts and Figures. *Alzheimers Dement.* **10**, (2014).
2. Karran, E., Mercken, M. & Strooper, B. D. The amyloid cascade hypothesis for Alzheimer's disease: an appraisal for the development of therapeutics. *Nat. Rev. Drug Discov.* **10**, 698–712 (2011).
3. Murphy, M. P. & LeVine, H., 3rd. Alzheimer's disease and the amyloid-beta peptide. *J. Alzheimers Dis. JAD* **19**, 311–323 (2010).
4. Chasseigneaux, S. & Allinquant, B. Functions of A β , sAPP α and sAPP β : similarities and differences: A β and sAPPs functions. *J. Neurochem.* **120**, 99–108 (2012).
5. O'Brien, R. J. & Wong, P. C. Amyloid Precursor Protein Processing and Alzheimer's Disease. *Annu. Rev. Neurosci.* **34**, 185–204 (2011).
6. Thinakaran, G. & Koo, E. H. Amyloid precursor protein trafficking, processing, and function. *J. Biol. Chem.* **283**, 29615–29619 (2008).
7. Roberson, E. D. & Mucke, L. 100 Years and Counting: Prospects for Defeating Alzheimer's Disease. *Science* **314**, 781–784 (2006).
8. Sgourakis, N. G., Yan, Y., McCallum, S. A., Wang, C. & Garcia, A. E. The Alzheimer's Peptides A β 40 and 42 Adopt Distinct Conformations in Water: A Combined MD / NMR Study. *J. Mol. Biol.* **368**, 1448–1457 (2007).
9. Winkler, E. *et al.* Generation of Alzheimer disease-associated amyloid β 42/43 peptide by γ -secretase can be inhibited directly by modulation of membrane thickness. *J. Biol. Chem.* **287**, 21326–21334 (2012).
10. Tyler, S. J., Dawbarn, D., Wilcock, G. K. & Allen, S. J. alpha- and beta-secretase: profound changes in Alzheimer's disease. *Biochem. Biophys. Res. Commun.* **299**, 373–376 (2002).

11. Szczepanik, A. M., Rampe, D. & Ringheim, G. E. Amyloid-beta peptide fragments p3 and p4 induce pro-inflammatory cytokine and chemokine production in vitro and in vivo. *J. Neurochem.* **77**, 304–317 (2001).
12. Higgins, L. S., Murphy, G. M., Forno, L. S., Catalano, R. & Cordell, B. P3 beta-amyloid peptide has a unique and potentially pathogenic immunohistochemical profile in Alzheimer's disease brain. *Am. J. Pathol.* **149**, 585–596 (1996).
13. Ali, F., Thompson, A. J. & Barrow, C. The p3 Peptide, a Naturally Occurring Fragment of the Amyloid- β Peptide ($A\beta$) Found in Alzheimer's Disease, Has a Greater Aggregation Propensity In Vitro Than Full-Length $A\beta$, But Does Not Bind Cu^{2+} . *Aust. J. Chem.* **4**, 321–326 (2000).
14. Han, W., Ji, T., Mei, B. & Su, J. Peptide p3 may play a neuroprotective role in the brain. *Med. Hypotheses* **76**, 543–546 (2011).
15. Dulin, F. *et al.* P3 peptide, a truncated form of A beta devoid of synaptotoxic effect, does not assemble into soluble oligomers. *FEBS Lett.* **582**, 1865–1870 (2008).
16. Zhang, Y., Thompson, R., Zhang, H. & Xu, H. APP processing in Alzheimer's disease. *Mol. Brain* **4**, 3 (2011).
17. FINDER, V. H. & GLOCKSHUBER, R. Amyloid-beta aggregation. *Neurodegener. Dis.* **4**, 13–27 (2007).
18. Cohen, S. I. A. *et al.* Proliferation of amyloid-42 aggregates occurs through a secondary nucleation mechanism. *Proc. Natl. Acad. Sci.* **110**, 9758–9763 (2013).
19. Hersh, L. B. & Rodgers, D. W. Neprilysin and amyloid beta peptide degradation. *Curr. Alzheimer Res.* **5**, 225–231 (2008).
20. Farris, W. *et al.* Insulin-degrading enzyme regulates the levels of insulin, amyloid beta-protein, and the beta-amyloid precursor protein intracellular domain in vivo. *Proc. Natl. Acad. Sci. U. S. A.* **100**, 4162–4167 (2003).
21. Eckman, E. A., Reed, D. K. & Eckman, C. B. Degradation of the Alzheimer's amyloid beta peptide by endothelin-converting enzyme. *J. Biol. Chem.* **276**, 24540–24548 (2001).
22. Buggley, J., Mentz, R. J., DeVore, A. D. & Velazquez, E. J. Angiotensin Receptor Neprilysin Inhibition in Heart Failure: Mechanistic Action and Clinical Impact. *J. Card. Fail.* (2015). doi:10.1016/j.cardfail.2015.07.008

23. Malito, E., Hulse, R. E. & Tang, W.-J. Amyloid β -degrading cryptidases: insulin degrading enzyme, presequence peptidase, and neprilysin. *Cell. Mol. Life Sci.* **65**, 2574–2585 (2008).
24. Eckman, E. A., Watson, M., Marlow, L., Sambamurti, K. & Eckman, C. B. Alzheimer's disease beta-amyloid peptide is increased in mice deficient in endothelin-converting enzyme. *J. Biol. Chem.* **278**, 2081–2084 (2003).
25. Funalot, B. *et al.* Endothelin-converting enzyme-1 is expressed in human cerebral cortex and protects against Alzheimer's disease. *Mol. Psychiatry* **9**, 1059–1059 (2004).
26. Deane, R., Bell, R. D., Sagare, A. & Zlokovic, B. V. Clearance of amyloid-beta peptide across the blood-brain barrier: implication for therapies in Alzheimer's disease. *CNS Neurol. Disord. Drug Targets* **8**, 16–30 (2009).
27. Kierdorf, K. & Fritz, G. RAGE regulation and signaling in inflammation and beyond. *J. Leukoc. Biol.* **94**, 55–68 (2013).
28. Toledo, J. B., Shaw, L. M. & Trojanowski, J. Q. Plasma amyloid beta measurements - a desired but elusive Alzheimer's disease biomarker. *Alzheimers Res. Ther.* **5**, 8 (2013).
29. De Strooper, B. Loss-of-function presenilin mutations in Alzheimer disease. Talking Point on the role of presenilin mutations in Alzheimer disease. *EMBO Rep.* **8**, 141–146 (2007).
30. Leverenz, J. B. *et al.* Lewy body pathology in familial Alzheimer disease: evidence for disease- and mutation-specific pathologic phenotype. *Arch. Neurol.* **63**, 370–376 (2006).
31. Accordi, B. *et al.* Functional Protein Network Activation Mapping Reveals New Potential Molecular Drug Targets for Poor Prognosis Pediatric BCP-ALL. *PLoS ONE* **5**, e13552 (2010).
32. Holmes, C. Genotype and phenotype in Alzheimer's disease. *Br. J. Psychiatry* **180**, 131–134 (2002).
33. Jiang, Q. *et al.* ApoE Promotes the Proteolytic Degradation of A β . *Neuron* **58**, 681–693 (2008).
34. Sagare, A. P. *et al.* A lipoprotein receptor cluster IV mutant preferentially binds amyloid- β and regulates its clearance from the mouse brain. *J. Biol. Chem.* **288**, 15154–15166 (2013).

35. Kim, J., Basak, J. M. & Holtzman, D. M. The role of apolipoprotein E in Alzheimer's disease. *Neuron* **63**, 287–303 (2009).
36. Verghese, P. B. *et al.* ApoE influences amyloid- β (A β) clearance despite minimal apoE/A β association in physiological conditions. *Proc. Natl. Acad. Sci. U. S. A.* **110**, E1807–1816 (2013).
37. Ferretti, M. T., Allard, S., Partridge, V., Ducatzenzeiler, A. & Cuello, A. C. Minocycline corrects early, pre-plaque neuroinflammation and inhibits BACE-1 in a transgenic model of Alzheimer's disease-like amyloid pathology. *J. Neuroinflammation* **9**, 62 (2012).
38. Zou, Y. *et al.* Virtual Screening and Structure-Based Discovery of Indole Acylguanidines as Potent β -secretase (BACE1) Inhibitors. *Molecules* **18**, 5706–5722 (2013).
39. He, P., Cheng, X., Staufenbiel, M., Li, R. & Shen, Y. Long-term treatment of thalidomide ameliorates amyloid-like pathology through inhibition of β -secretase in a mouse model of Alzheimer's disease. *PLoS One* **8**, e55091 (2013).
40. Holthoewer, D. *et al.* Acitretin, an enhancer of alpha-secretase expression, crosses the blood-brain barrier and is not eliminated by P-glycoprotein. *Neurodegener. Dis.* **10**, 224–228 (2012).
41. Semagacestat's fall: where next for AD therapies? *Nat. Med.* **19**, 1214–1215 (2013).
42. Mullard, A. Sting of Alzheimer's failures offset by upcoming prevention trials. *Nat. Rev. Drug Discov.* **11**, 657–660 (2012).
43. Castellani, R. J. & Smith, M. A. Compounding artefacts with uncertainty, and an amyloid cascade hypothesis that is 'too big to fail'. *J. Pathol.* **224**, 147–152 (2011).
44. Teich, A. F. & Arancio, O. Is the amyloid hypothesis of Alzheimer's disease therapeutically relevant? *Biochem. J.* **446**, 165–177 (2012).
45. Ballatore, C., Lee, V. M.-Y. & Trojanowski, J. Q. Tau-mediated neurodegeneration in Alzheimer's disease and related disorders. *Nat. Rev. Neurosci.* **8**, 663–672 (2007).
46. Brunden, K. R., Trojanowski, J. Q. & Lee, V. M.-Y. Advances in tau-focused drug discovery for Alzheimer's disease and related tauopathies. *Nat. Rev. Drug Discov.* **8**, 783–793 (2009).

47. Mohandas, E., Rajmohan, V. & Raghunath, B. Neurobiology of Alzheimer's disease. *Indian J. Psychiatry* **51**, 55 (2009).
48. Bunker, J. M. Modulation of Microtubule Dynamics by Tau in Living Cells: Implications for Development and Neurodegeneration. *Mol. Biol. Cell* **15**, 2720–2728 (2004).
49. Butner, K. A. & Kirschner, M. W. Tau protein binds to microtubules through a flexible array of distributed weak sites. *J. Cell Biol.* **115**, 717–730 (1991).
50. Buée, L., Bussièrre, T., Buée-Scherrer, V., Delacourte, A. & Hof, P. R. Tau protein isoforms, phosphorylation and role in neurodegenerative disorders. *Brain Res. Brain Res. Rev.* **33**, 95–130 (2000).
51. Llorens-Martin, M. *et al.* Tau isoform with three microtubule binding domains is a marker of new axons generated from the subgranular zone in the hippocampal dentate gyrus: implications for Alzheimer's disease. *J. Alzheimers Dis. JAD* **29**, 921–930 (2012).
52. Johnson, G. V. W. & Stoothoff, W. H. Tau phosphorylation in neuronal cell function and dysfunction. *J. Cell Sci.* **117**, 5721–5729 (2004).
53. Alonso, A. d. C., Li, B., Grundke-Iqbal, I. & Iqbal, K. Polymerization of hyperphosphorylated tau into filaments eliminates its inhibitory activity. *Proc. Natl. Acad. Sci.* **103**, 8864–8869 (2006).
54. Wang, J.-Z., Xia, Y.-Y., Grundke-Iqbal, I. & Iqbal, K. Abnormal hyperphosphorylation of tau: sites, regulation, and molecular mechanism of neurofibrillary degeneration. *J. Alzheimers Dis. JAD* **33 Suppl 1**, S123–139 (2013).
55. Trojanowski, J. Q. & Lee, V. M.-Y. Pathological tau: a loss of normal function or a gain in toxicity? *Nat. Neurosci.* **8**, 1136–1137 (2005).
56. Morishima-Kawashima, M. *et al.* Hyperphosphorylation of tau in PHF. *Neurobiol. Aging* **16**, 365–371; discussion 371–380 (1995).
57. Giacobini, E. & Gold, G. Alzheimer disease therapy—moving from amyloid- β to tau. *Nat. Rev. Neurol.* **9**, 677–686 (2013).
58. Meraz-Ríos, M. A., Toral-Rios, D., Franco-Bocanegra, D., Villeda-Hernández, J. & Campos-Peña, V. Inflammatory process in Alzheimer's Disease. *Front. Integr. Neurosci.* **7**, (2013).

59. Tuppo, E. E. & Arias, H. R. The role of inflammation in Alzheimer's disease. *Int. J. Biochem. Cell Biol.* **37**, 289–305 (2005).
60. Rapoport, S. I., Hatanpää, K., Brady, D. R. & Chandrasekaran, K. Brain Energy Metabolism, Cognitive Function and Down-Regulated Oxidative Phosphorylation in Alzheimer Disease. *Neurodegener. J. Neurodegener. Disord. Neuroprotection Neuroregeneration* **5**, 473–476 (1996).
61. Sun, J., Feng, X., Liang, D., Duan, Y. & Lei, H. Down-regulation of energy metabolism in Alzheimer's disease is a protective response of neurons to the microenvironment. *J. Alzheimers Dis. JAD* **28**, 389–402 (2012).
62. Shah, K., DeSilva, S. & Abbruscato, T. The Role of Glucose Transporters in Brain Disease: Diabetes and Alzheimer's Disease. *Int. J. Mol. Sci.* **13**, 12629–12655 (2012).
63. Hoyer, S. The brain insulin signal transduction system and sporadic (type II) Alzheimer disease: an update. *J. Neural Transm. Vienna Austria 1996* **109**, 341–360 (2002).
64. Henderson, S. T. *et al.* Study of the ketogenic agent AC-1202 in mild to moderate Alzheimer's disease: a randomized, double-blind, placebo-controlled, multicenter trial. *Nutr. Metab.* **6**, 31 (2009).
65. Zhao, W. *et al.* Caprylic triglyceride as a novel therapeutic approach to effectively improve the performance and attenuate the symptoms due to the motor neuron loss in ALS disease. *PloS One* **7**, e49191 (2012).
66. Gold, G., Giannakopoulos, P., Herrmann, F. R., Bouras, C. & Kovari, E. Identification of Alzheimer and vascular lesion thresholds for mixed dementia. *Brain* **130**, 2830–2836 (2007).
67. Kalaria, R. N. Vascular basis for brain degeneration: faltering controls and risk factors for dementia: Nutrition Reviews©, Vol. 68, No. s2. *Nutr. Rev.* **68**, S74–S87 (2010).
68. Vikas, D. & Singh, A. K. Are Vascular Factors Linked to the Development of Hippocampal Atrophy in Alzheimer's Disease? *J. Alzheimer's Dis.* 711–718 (2012). doi:10.3233/JAD-2012-120928
69. Guglielmo, M. *et al.* The up-regulation of BACE1 mediated by hypoxia and ischemic injury: role of oxidative stress and HIF1alpha. *J. Neurochem.* **108**, 1045–1056 (2009).

70. Scheff, S. W., DeKosky, S. T. & Price, D. A. Quantitative assessment of cortical synaptic density in Alzheimer's disease. *Neurobiol. Aging* **11**, 29–37 (1990).
71. Scheff, S. W. & Price, D. A. Synapse loss in the temporal lobe in Alzheimer's disease. *Ann. Neurol.* **33**, 190–199 (1993).
72. Henneman, W. J. P. *et al.* Hippocampal atrophy rates in Alzheimer disease: Added value over whole brain volume measures. *Neurology* **72**, 999–1007 (2009).
73. Davies, P. & Maloney, A. J. Selective loss of central cholinergic neurons in Alzheimer's disease. *Lancet* **2**, 1403 (1976).
74. McGleenon, Dynan & Passmore. Acetylcholinesterase inhibitors in Alzheimer's disease: Acetylcholinesterase inhibitors in Alzheimer's disease. *Br. J. Clin. Pharmacol.* **48**, 471–480 (2001).
75. Donev, R., Kolev, M., Millet, B. & Thome, J. Neuronal death in Alzheimer's disease and therapeutic opportunities. *J. Cell. Mol. Med.* **13**, 4329–4348 (2009).
76. Niikura, T., Tajima, H. & Kita, Y. Neuronal Cell Death in Alzheimers Disease and a Neuroprotective Factor, Humanin. *Curr. Neuropharmacol.* **4**, 139–147 (2006).
77. Sugimoto, T. *et al.* Signal transduction pathways through TRK-A and TRK-B receptors in human neuroblastoma cells. *Jpn. J. Cancer Res. Gann* **92**, 152–160 (2001).
78. Kaplan, D. R. & Miller, F. D. Neurotrophin signal transduction in the nervous system. *Curr. Opin. Neurobiol.* **10**, 381–391 (2000).
79. Aksamitiene, E., Kiyatkin, A. & Kholodenko, B. N. Cross-talk between mitogenic Ras/MAPK and survival PI3K/Akt pathways: a fine balance. *Biochem. Soc. Trans.* **40**, 139–146 (2012).
80. McCubrey, J. A. *et al.* Ras/Raf/MEK/ERK and PI3K/PTEN/Akt/mTOR cascade inhibitors: how mutations can result in therapy resistance and how to overcome resistance. *Oncotarget* **3**, 1068–1111 (2012).
81. Castellano, E. & Downward, J. RAS Interaction with PI3K: More Than Just Another Effector Pathway. *Genes Cancer* **2**, 261–274 (2011).
82. Belka, C. & Budach, W. Anti-apoptotic Bcl-2 proteins: structure, function and relevance for radiation biology. *Int. J. Radiat. Biol.* **78**, 643–658 (2002).

83. Qian, J., Zou, Y., Rahman, J. S. M., Lu, B. & Massion, P. P. Synergy between phosphatidylinositol 3-kinase/Akt pathway and Bcl-xL in the control of apoptosis in adenocarcinoma cells of the lung. *Mol. Cancer Ther.* **8**, 101–109 (2009).
84. Saini, H. S., Gorse, K. M., Boxer, L. M. & Sato-Bigbee, C. Neurotrophin-3 and a CREB-mediated signaling pathway regulate Bcl-2 expression in oligodendrocyte progenitor cells. *J. Neurochem.* **89**, 951–961 (2004).
85. Chang, F. *et al.* Signal transduction mediated by the Ras/Raf/MEK/ERK pathway from cytokine receptors to transcription factors: potential targeting for therapeutic intervention. *Leukemia* **17**, 1263–1293 (2003).
86. Finkbeiner, S. CREB Couples Neurotrophin Signals to Survival Messages. *Neuron* **25**, 11–14 (2000).
87. Finkbeiner, S. *et al.* CREB: a major mediator of neuronal neurotrophin responses. *Neuron* **19**, 1031–1047 (1997).
88. McCubrey, J. A. *et al.* Roles of the Raf/MEK/ERK pathway in cell growth, malignant transformation and drug resistance. *Biochim. Biophys. Acta BBA - Mol. Cell Res.* **1773**, 1263–1284 (2007).
89. Shonai, T. *et al.* MEK/ERK pathway protects ionizing radiation-induced loss of mitochondrial membrane potential and cell death in lymphocytic leukemia cells. *Cell Death Differ.* **9**, 963–971 (2002).
90. McCubrey, J. A. *et al.* in *Apoptosis, Cell Signaling, and Human Diseases* (ed. Srivastava, R.) 101–134 (Humana Press, 2007).
91. Koliatsos, V. E. *et al.* Mouse nerve growth factor prevents degeneration of axotomized basal forebrain cholinergic neurons in the monkey. *J. Neurosci. Off. J. Soc. Neurosci.* **10**, 3801–3813 (1990).
92. Koliatsos, V. E. *et al.* Human nerve growth factor prevents degeneration of basal forebrain cholinergic neurons in primates. *Ann. Neurol.* **30**, 831–840 (1991).
93. Tuszynski, M. H., Sang U, H., Yoshida, K. & Gage, F. H. Recombinant human nerve growth factor infusions prevent cholinergic neuronal degeneration in the adult primate brain. *Ann. Neurol.* **30**, 625–636 (1991).
94. Friden, P. M. *et al.* Blood-brain barrier penetration and in vivo activity of an NGF conjugate. *Science* **259**, 373–377 (1993).

95. Kordower, J. H. *et al.* Intravenous administration of a transferrin receptor antibody-nerve growth factor conjugate prevents the degeneration of cholinergic striatal neurons in a model of Huntington disease. *Proc. Natl. Acad. Sci. U. S. A.* **91**, 9077–9080 (1994).
96. Kordower, J. H. *et al.* The aged monkey basal forebrain: rescue and sprouting of axotomized basal forebrain neurons after grafts of encapsulated cells secreting human nerve growth factor. *Proc. Natl. Acad. Sci. U. S. A.* **91**, 10898–10902 (1994).
97. Rosenberg, M. B. *et al.* Grafting genetically modified cells to the damaged brain: restorative effects of NGF expression. *Science* **242**, 1575–1578 (1988).
98. Barnett, J. *et al.* Human beta nerve growth factor obtained from a baculovirus expression system has potent in vitro and in vivo neurotrophic activity. *Exp. Neurol.* **110**, 11–24 (1990).
99. Tuszynski, M. H. *et al.* A phase 1 clinical trial of nerve growth factor gene therapy for Alzheimer disease. *Nat. Med.* **11**, 551–555 (2005).
100. Rafii, M. S. *et al.* A phase 1 study of stereotactic gene delivery of AAV2-NGF for Alzheimer's disease. *Alzheimers Dement. J. Alzheimers Assoc.* (2014). doi:10.1016/j.jalz.2013.09.004
101. Kita, T. *et al.* Scabronines B, C, D, E and F, novel diterpenoids showing stimulating activity of nerve growth factor-synthesis, from the mushroom *Sarcodon scabrosus*. *Tetrahedron* **54**, 11877–11886 (1998).
102. Kawagishi, H. *et al.* Erinacines E, F, and G, stimulators of nerve growth factor (NGF)-synthesis, from the mycelia of *Herichium erinaceum*. *Tetrahedron Lett.* **37**, 7399–7402 (1996).
103. Mori, K. *et al.* Nerve growth factor-inducing activity of *Herichium erinaceum* in 1321N1 human astrocytoma cells. *Biol. Pharm. Bull.* **31**, 1727–1732 (2008).
104. Dixon, E. *et al.* Bacteria-induced static batch fungal fermentation of the diterpenoid cyathin A3, a small-molecule inducer of nerve growth factor. *J. Ind. Microbiol. Biotechnol.* **38**, 607–615 (2010).
105. Obara, Y., Kobayashi, H., Ohta, T., Ohizumi, Y. & Nakahata, N. Scabronine G-methylester enhances secretion of neurotrophic factors mediated by an activation of protein kinase C-zeta. *Mol. Pharmacol.* **59**, 1287–1297 (2001).
106. Counts, S. E. & Mufson, E. J. Noradrenaline activation of neurotrophic pathways protects against neuronal amyloid toxicity. *J. Neurochem.* **113**, 649–660 (2010).

107. Apte, S. P. & Ugwu, S. O. in *Development of Vaccines* (eds. Singh, M. & Srivastava, I. K.) 399–414 (John Wiley & Sons, Inc., 2011).
108. Stein, G. H. T98G: an anchorage-independent human tumor cell line that exhibits stationary phase G1 arrest in vitro. *J. Cell. Physiol.* **99**, 43–54 (1979).
109. Emmett, C. J., McNeeley, P. A. & Johnson, R. M. Evaluation of human astrocytoma and glioblastoma cell lines for nerve growth factor release. *Neurochem. Int.* **30**, 465–474 (1997).
110. Wion, D., Mac Grogan, D., Houlgatte, R. & Brachet, P. Phorbol 12-myristate 13-acetate (PMA) increases the expression of the nerve growth factor (NGF) gene in mouse L-929 fibroblasts. *FEBS Lett.* **262**, 42–44 (1990).
111. Zhu, Y. & Kriegelstein, J. β 2-Adrenoceptor Agonist Clenbuterol Causes NGF Expression and Neuroprotection. *CNS Drug Rev.* **5**, 347–364 (2006).
112. Lu, B., Yokoyama, M., Dreyfus, C. & Black, I. NGF Gene Expression in Actively Growing Brain Glia. *J. Neurosci.* **11**, 318–326 (1991).
113. Furukawa, S. & Furukawa, Y. Nerve growth factor synthesis and its regulatory mechanisms: an approach to therapeutic induction of nerve growth factor synthesis. *Cerebrovasc. Brain Metab. Rev.* **2**, 328–344 (1990).
114. Mowla, S. J. *et al.* Differential sorting of nerve growth factor and brain-derived neurotrophic factor in hippocampal neurons. *J. Neurosci. Off. J. Soc. Neurosci.* **19**, 2069–2080 (1999).
115. Edwards, R. H. *et al.* Processing and secretion of nerve growth factor: expression in mammalian cells with a vaccinia virus vector. *Mol. Cell. Biol.* **8**, 2456–2464 (1988).
116. Pernot, F., Dorandeu, F., Beaup, C. & Peinnequin, A. Selection of reference genes for real-time quantitative reverse transcription-polymerase chain reaction in hippocampal structure in a murine model of temporal lobe epilepsy with focal seizures. *J. Neurosci. Res.* NA–NA (2009). doi:10.1002/jnr.22282
117. TrueORF cDNA Clones, Lenti Particles, and PrecisionShuttle Vector System Application Guide.
118. Hung, J. & Medicus, R. Designing & Validating Real-Time PCR Primers: Systematic Guidelines. *Pathways* (2008).
119. Karcher, S. J. *Molecular biology: a project approach.* (Academic Press, 1995).

120. Wold, W. S. M. *Adenoviruses, ad vectors, quantitation and animal models*. (Humana Press, 2007).
121. Riaz, S., Malcangio, M., Miller, M. & Tomlinson, D. R. A vitamin D(3) derivative (CB1093) induces nerve growth factor and prevents neurotrophic deficits in streptozotocin-diabetic rats. *Diabetologia* **42**, 1308–1313 (1999).
122. Zhou, H.-C. *et al.* Activation of 2-adrenoceptor enhances synaptic potentiation and behavioral memory via cAMP-PKA signaling in the medial prefrontal cortex of rats. *Learn. Mem.* **20**, 274–284 (2013).
123. El-Osta, M. A., Idkowiak-Baldys, J. & Hannun, Y. A. Delayed Phosphorylation of Classical Protein Kinase C (PKC) Substrates Requires PKC Internalization and Formation of the Pericentron in a Phospholipase D (PLD)-dependent Manner. *J. Biol. Chem.* **286**, 19340–19353 (2011).
124. Mosior, M. & Newton, A. C. Mechanism of interaction of protein kinase C with phorbol esters. Reversibility and nature of membrane association. *J. Biol. Chem.* **270**, 25526–25533 (1995).
125. Hirai, S. -i. Protein Kinase C delta Activates the MEK-ERK Pathway in a Manner Independent of Ras and Dependent on Raf. *J. Biol. Chem.* **271**, 23512–23519 (1996).
126. Hu, X. *et al.* Src kinase up-regulates the ERK cascade through inactivation of protein phosphatase 2A following cerebral ischemia. *BMC Neurosci.* **10**, 74 (2009).
127. Boglári, G. & Szeberényi, J. Nuclear translocation of p90Rsk and phosphorylation of CREB is induced by ionomycin in a Ras-independent manner in PC12 cells. *Acta Biol. Hung.* **53**, 325–334 (2002).
128. Huang, J. & Manning, B. D. The TSC1-TSC2 complex: a molecular switchboard controlling cell growth. *Biochem. J.* **412**, 179–190 (2008).
129. Julien, L.-A., Carriere, A., Moreau, J. & Roux, P. P. mTORC1-activated S6K1 phosphorylates Rictor on threonine 1135 and regulates mTORC2 signaling. *Mol. Cell. Biol.* **30**, 908–921 (2010).
130. Ordway, G. A., O'Donnell, J. M. & Frazer, A. Effects of clenbuterol on central beta-1 and beta-2 adrenergic receptors of the rat. *J. Pharmacol. Exp. Ther.* **241**, 187–195 (1987).

131. Cheng, X., Ma, Y., Moore, M., Hemmings, B. A. & Taylor, S. S. Phosphorylation and activation of cAMP-dependent protein kinase by phosphoinositide-dependent protein kinase. *Proc. Natl. Acad. Sci. U. S. A.* **95**, 9849–9854 (1998).
132. Cauthron, R. D., Carter, K. B., Liauw, S. & Steinberg, R. A. Physiological phosphorylation of protein kinase A at Thr-197 is by a protein kinase A kinase. *Mol. Cell. Biol.* **18**, 1416–1423 (1998).
133. Obara, Y., Labudda, K., Dillon, T. J. & Stork, P. J. S. PKA phosphorylation of Src mediates Rap1 activation in NGF and cAMP signaling in PC12 cells. *J. Cell Sci.* **117**, 6085–6094 (2004).
134. Vuchak, L. A., Tsygankova, O. M., Prendergast, G. V. & Meinkoth, J. L. Protein Kinase A and B-Raf Mediate Extracellular Signal-Regulated Kinase Activation by Thyrotropin. *Mol. Pharmacol.* **76**, 1123–1129 (2009).
135. Dessauer, C. W., Scully, T. T. & Gilman, A. G. Interactions of forskolin and ATP with the cytosolic domains of mammalian adenylyl cyclase. *J. Biol. Chem.* **272**, 22272–22277 (1997).
136. Tang, W. J. & Gilman, A. G. Construction of a soluble adenylyl cyclase activated by Gs alpha and forskolin. *Science* **268**, 1769–1772 (1995).
137. Anderson, R. J., Breckon, R. & Colston, D. Regulation by forskolin of cyclic AMP phosphodiesterase and protein kinase C activity in LLC-PK1 cells. *Biochem. J.* **279** (Pt 1), 23–27 (1991).
138. GolinHarris International. New therapies for the prevention and treatment of Alzheimer's disease identified. *ScienceDaily* (2011).
139. Deming, D. *et al.* ZM336372, A Raf-1 Activator, Causes Suppression of Proliferation in a Human Hepatocellular Carcinoma Cell Line. *J. Gastrointest. Surg.* **12**, 852–857 (2008).
140. Duncia, J. V. *et al.* MEK inhibitors: the chemistry and biological activity of U0126, its analogs, and cyclization products. *Bioorg. Med. Chem. Lett.* **8**, 2839–2844 (1998).
141. Ohori, M. *et al.* Identification of a selective ERK inhibitor and structural determination of the inhibitor-ERK2 complex. *Biochem. Biophys. Res. Commun.* **336**, 357–363 (2005).
142. Sapkota, G. P. *et al.* BI-D1870 is a specific inhibitor of the p90 RSK (ribosomal S6 kinase) isoforms in vitro and in vivo. *Biochem. J.* **401**, 29 (2007).

143. Thakur, J. K., Yadav, A. & Yadav, G. Molecular recognition by the KIX domain and its role in gene regulation. *Nucleic Acids Res.* **42**, 2112–2125 (2014).

Biography

Justin B. Davis graduated from Hampton Roads Academy, Newport News, Virginia, in 2006. He received his Bachelor of Science from the University of North Carolina at Chapel Hill in 2010 and his Master of Science from George Mason University in 2011. Since enrolling in the doctoral program, Justin has served as a Graduate Teaching Assistant and Graduate Research Assistant at George Mason University.